WIND TUNNEL WALL EFFECTS IN V/STOL MODEL TESTING

Final Report
covering the period
1 October 1965 - 31 March 1967
under
NASA Grant NGR-47-005-040

Principal Investigator

G. B. Matthews

Research Laboratories for the Engineering Sciences

University of Virginia

Charlottesville

Report No. AEEP-4036-102-68U

July 1968

WIND TUNNEL WALL EFFECTS IN V/STOL MODEL TESTING

Final Report
covering the period
1 October 1965 - 31 March 1967
under
NASA Grant NGR-47-005-040

Principal Investigator

G. B. Matthews

Department of Aerospace Engineering and Engineering Physics
RESEARCH LABORATORIES FOR THE ENGINEERING SCIENCES
SCHOOL OF ENGINEERING AND APPLIED SCIENCE
UNIVERSITY OF VIRGINIA
CHARLOTTESVILLE, VIRGINIA

Report No. AEEP-4036-102-68U
July 1968

Copy No._____

Preface

This report, issued as a final report under NASA Grant NGR-47-005-040, represents the progress achieved during the period from October 1965 through March 1967 on a long-range continuing program in V/STOL aerodynamics being carried out in the Department of Aerospace Engineering and Engineering Physics at the University of Virginia.

The initial effort in these studies was performed by Mr. David L. I. Kirkpatrick as a Master's degree thesis under the author's direction during the academic year 1961-62. This unsponsored work was primarily of a theoretical nature, with some applications to existing data. The author's interest in wind tunnel wall corrections for high lift configurations continued through the summers of 1963 and 1964 as a part-time effort at Langley Research Center in cooperation with the Full Scale Research Division. An attempt was made to apply Kirkpatrick's slipstream analysis to some existing wind tunnel data; and a technical note describing these results, co-authored with R. J. Margason, is pending.

From October 1965 until the present, research has been carried out on the interaction of high-lift slipstreams and wind tunnel free stream flows as the critical phenomenon controlling the validity of any mathematical model of V/STOL correction factors. As a direct result of the aforementioned NASA support of this program, a small-scale, open-circuit tunnel facility was modified and improved for flow visualization studies of jets, and a master's degree thesis treating jet interaction phenomena was completed by Mr. W. G. S. Hardy, under the author's supervision. At the same time, the design of a partially-constructed large subsonic wind tunnel was completed with the expectation of performing quantitative experiments on larger size jets over a wider range of free stream speeds. Following the conclusion of this grant, a small University-supported effort continued with one master's degree candidate and one undergraduate student, both under the author's direction. Additional jet velocity decays were studied, and initial photographs of jet cross sections were obtained. The latter will appear as a graduate thesis during the current academic year.

The bulk of this report is contained in Mr. Hardy's (1967) thesis, which appears as an ~~appendix~~ Removed and to which frequent reference is made. Several of the recommendations made by Mr. Hardy have already been followed, and the conclusions presented in this report incorporate these more recent changes.

TABLE OF CONTENTS

LIST OF FIGURES

LIST OF SYMBOLS

C_D	Drag coefficient
D	Diameter of circular nozzle orifice
D_E	Equivalent diameter of slot
f	Momentum factor
v_C	Centerline velocity of free jet
v_E	Equivalent velocity of free jet
v_F	Free-stream velocity
v_J	Equivalent velocity of a jet immersed in a moving stream
v_{J_o}	Initial jet velocity
v_P	Jet profile velocity
y_E	Half-width of equivalent jet
y_J	Half-width of curved jet
y_5	Half-width of free jet at $v_P = (1/2)v_C$
x, y, z	Spatial coordinates of free jet and curved jet
ξ	Curvilinear coordinate for free jet
θ	Total jet inclination
$d\theta_M$	Change in θ due to mixing
$d\theta_D$	Change in θ due to drag

I. Introduction

A. Background

The use of wind tunnels and scale models to obtain aerodynamic data which may be applied to full-size vehicles in flight has long been accepted by the aerospace community. The prohibitively high costs of constructing and testing full-scale configurations have made this alternative impractical and have emphasized the importance of performing reliable experiments in controlled-flow facilities at a reduced geometric scale. However, corrections must be made to data obtained in these facilities to account for both the smaller scale and the influence of the test section walls. Although scaling laws based on dynamic similarity are well-proven and universally employed, no such reliable rules are currently available to predict wind tunnel wall effects in all the flight regimes of importance in aeronautics.

The extreme distortion of the main flow of a tunnel in the presence of high-lift model slipstreams, such as those representative of V/STOL behavior in transition from hover to high speed flight, is sufficiently well-documented (Appendix References 6 and 13) to warrant extensive study of these wall effects as well as the primary phenomena which contribute to them. A generalized theoretical method for deriving these correction factors has been developed by several investigators over the past two decades. An initial attempt to predict the ground effect on a lifting rotor was made in 1941 at the Georgia Institute of Technology*(1). This was followed by an extensive series of papers by H. H. Heyson of the Langley Research Center in which the ground effect theory was refined and applied to the first calculations of wind tunnel wall effects in helicopter testing (2, 3). Later extensions to other classes of V/STOL configurations were also published by Heyson, supplemented by tables of calculated correction factors (4).

The essential characteristic of all these early theoretical models is their mathematical representation of the downwash, or wake, from the lifting vehicle as a series of potential flow components in the form of distributed

*Numbers in parentheses correspond to references at the end of the report.

vortices or doublets. The model chosen by Heyson consists of a constant-strength, straight line wake skewed at an angle to the vertical determined by the net thrust and lift generated at the vehicle. A first attempt to represent the actual curvature of the wake and to express the change in mass flow within the wake resulting from mixing and entrainment of free stream air was presented by D. L. I. Kirkpatrick in a master's degree thesis at the University of Virginia (Appendix Reference 11). These models are compared by Hardy in Figure I.1 of the Appendix and are described in detail in Appendix Section I.

B. Purpose of Research Program

The overall purpose of this research program is to gain a thorough understanding of the flow field in the vicinity of a high-lift model and on the boundaries of the wind tunnel test section so as to enable one to predict the influence of the finite walls on the model force and moment measurements. As a consequence of some initial attempts to apply both Heyson's straight wake analysis and Kirkpatrick's curved one to empirical data on a V/STOL configuration, it was concluded that at relatively high slipstream-to-freestream velocity ratios with the slipstream normal to the free stream, the additional complexity of Kirkpatrick's curved slipstream model is not justified for the purpose of correcting lift, drag and angle of attack data at the lifting surface location. However, the wall correction factors for predicting the free-flight equivalent of pitching moments and local angles of flow inclination at points downstream from the lifting surface are very severely influenced by the curvature assumed in the mathematical model of the wake. On V/STOL models with tail surfaces, the differences between straight and curved wake analyses may be so great as to actually predict a change in the direction of pitching moment in the two cases from pitch up to pitch down.

This evidence of the extreme importance of properly representing the slipstream in a theoretical model of the flow field established the short-range purpose of the research task reported herein, i.e., to study the interaction between a jet and a cross section with the goal of being able to predict the curvature of this mixing jet from the simplest possible information concerning the jet and the free stream.

There is no doubt that complete knowledge of the slipstream-freestream interaction can only come about through a more thorough understanding of the basic nature of turbulent transport phenomena and accompanying measurements of the micro-structure of the mixing, distorting jet. Nevertheless, a gross representation of this mixing based upon reasonable mathematical approximations, mean values of flow parameters, and simple geometric shapes may be sufficient to provide a workable theoretical model for describing effectively the wake curvature and growth. Such a model would then become the basis for predictions of the influence of the wake on the flow field throughout the tunnel as well as the effects of the presence of finite test section walls. Further, the insight gained into the relative importance of both aerodynamic and geometric jet characteristics on the mixing process may well focus attention on the critical parameters of the process and thereby establish realistic goals for further research.

II. Analytical Studies

A. Review of Theoretical Models

In the Appendix to this report (Sections I and II-A), Hardy has reviewed briefly the available literature on theoretical representations of the mixing jet. In addition to the work of Ehrick, Ackerberg and Pai, Heyson, and Kirkpatrick (Appendix References 1, 5, 6, 11) reported therein, the more recent treatments of Chang (5), Epstein (6), and Pratt and Baines (7) are deserving of attention.

These analyses are based primarily upon a macroscopic examination of the interacting flows rather than a detailed picture of the microstructure of localized turbulent mixing. Consequently, all follow the same generalized pattern as that reported herein in that they postulate a hypothetical model of the transfer of mass and momentum either along the jet, or across its boundaries. In none of these models is this transfer directly attributed in a mathematical way to either laminar or turbulent shear stresses. The replacement of the actual viscous behavior by an artificial, but essentially irrotational, process thus allows one to treat the slipstream and free stream as a combination of potential flow elements whose strengths are determined by the postulated mixing or related momentum exchange.

The mathematical model chosen here is a similar attempt to account for what is fundamentally a dissipative, viscous phenomenon through the introduction of empirical or semi-empirical information based upon the similarity of behavior observed in a large number of jet flows. Hardy has presented Kirkpatrick's original semi-empirical model as well as his own revisions in some detail in the Appendix (Sections II-B through D), and it will be only briefly summarized here.

B. Revised Jet Analysis

1. Momentum Considerations

The essence of both Kirkpatrick's and Hardy's contributions to jet interaction analysis lies in the postulate that momentum transfer from the higher speed jet into the lower speed free stream occurs in the cross-flow

situation in a manner similar to the dissipation of a free jet into quiescent air. However, the driving mechanism causing this gradual, but predictable, velocity decay is not merely the jet dynamic pressure but rather the difference between this pressure and that of the free stream component which is parallel to the local jet centerline.

In the simpler case of coaxial stream mixing, this assumption reduces to a decay which is dependent on the differences in the squares of the velocities of the two parallel streams, a model which agrees substantially with the detailed experiments reported by Warren (Appendix Reference 17). When the streams are not parallel, the components of free stream flow are illustrated as $v_F \sin\theta$ and $v_F \cos\theta$ in Appendix Figure 2.4. In this case $v_F \sin\theta$ flows parallel to the jet and is entrained through the aforementioned dynamic pressure difference. At the same time, however, this entrained flow carries with it an orthogonal component, $v_F \cos\theta$, which acts to change the direction of the mixed flow by increasing the deflection angle, θ.

A further condition bearing upon the representation of the mixing process arises from the virtual absence of external forces on the jet in a direction perpendicular to the free stream. Negligible weight of the air, nelgect of viscosity per se, and a nearly uniform transverse static pressure field lead to the reasonable assumption that the initial momentum component of the jet normal to the free stream will be conserved, providing no walls are close enough to disturb the static pressure. In the particular case studied here, the jet issues vertically into a horizontal stream; so the assumption is expressed as an invariance of vertical momentum during the addition of horizontal momentum. It must be noted that this conservation hypothesis does not imply a constant vertical velocity. In fact, the vertical component of the jet velocity must decrease as free stream mass flow is entrained, for the original vertical momentum must now be distributed over a larger mass flow.

2. Semi-Empirical Inputs

Recognizing that most of the free stream flow is not entrained by the jet but in fact passes around it, one identifies a second contribution to the curvature in the form of an equivalent bluff body drag. Kirkpatrick evaluated this drag force on the basis of an ever-expanding circular jet cross section. However, as Hardy has

pointed out in Appendix Section II-D-2, this cross section must be considered to be a more general shape, since jet nozzles are not always circular nor does any jet remain circular for a very long time as it is swept in the free stream direction. Visual observations by several investigators substantiated by pressure surveys by Jordinson (Appendix Reference 9) have indicated that a double-lobed kidney shape is quickly formed by the shear stresses acting on the jet periphery, and this shape is retained with gradual increase in width, for a great distance along the jet path. The drag coefficients chosen in the present study are thus representative of bluff semi-cylindrical shells, whereas Kirkpatrick's drag coefficient was that of a solid circular cylinder. The diameter of the circular cylinder was established by Kirkpatrick's postulate of conservation of vertical momentum and by a specified semi-empirical jet centerline decay curve. Hardy, on the other hand, has selected three empirical curves illustrating the spreading of the kidney-shaped cross section as they may be inferred from Jordinson's pressure profiles. This revision to the earlier theoretical model is shown in Appendix Figure 2.8.

One final, but very significant, revision of the theory is described in detail in Appendix II-D-3. This is the use of a more realistic representation of the jet velocity decay. Both the centerline decay curve and the highly-simplified momentum factor characterizing the velocity profile as introduced by Kirkpatrick were subjected to a more careful examination. Several numerical calculations indicated that this velocity decay expression was the most sensitive parameter contained in the curvature theory. As a result of this observation, a more sophisticated momentum factor and resultant equivalent velocity distribution were introduced into the theory following the methods of Warren (Appendix Reference 17). The details of this revised model are developed in Appendix Equations 2.16 through 2.29. It should be noted that the direct application of Warren's expressions requires that the core region of the jet be two-dimensional or axially symmetric in behavior and that similarity exist in the time average free jet velocity profiles, based on the width at the half-velocity point. If these conditions are not met (as they are not in a rectangular jet orifice), one may still employ the momentum factor and equivalent velocity concepts; but he must determine these at each axial station of the free jet by numerical or graphical integration of the measured velocity profile.

3. Numerical Calculation Scheme

A numerical integration procedure for the final jet curvature differential equation was developed using a Runge-Kutta scheme. This procedure was programmed in Algol for the University of Virginia Burroughs B5500 digital computer. Several combinations of the revisions described in the preceding section were calculated as a means of detecting the relative sensitivity of the final jet curvature to the input parameters. These results are described and presented by Hardy in Appendix, Section II-D-5. The general form of the jet angle equation is a combination of mixing and drag effects which are simply superimposed in their differential form, thus:

$$d\theta = \frac{d\theta_M(\theta,\ \xi/D)}{d(\xi/D)}\, d(\xi/D) + \frac{d\theta_D(\theta,\ \xi/D)}{d(\xi/D)}\, d(\xi/D),$$

with each term given by:

$$\frac{d\theta_M(\theta,\ \xi/D)}{d(\xi/D)} = \frac{-\dfrac{v_F v_{J_o}^2}{2v_J^3}\cos\theta\left[1-\left(\dfrac{v_F}{v_{J_o}}\right)^2\sin^2\theta\right]}{\left\{1-\dfrac{v_F}{v_J}\sin\theta+\left(\dfrac{v_F}{v_J}\right)^3\left[1-\left(\dfrac{v_E}{v_{J_o}}\right)^2\right]\sin\theta\cos^2\theta\right\}}\,\frac{d\left[\left(\dfrac{v_E}{v_{J_o}}\right)^2\right]}{d(\xi/D)}$$

and:

$$\frac{d\theta_D(\theta,\ \xi/D)}{d(\xi/D)} = \frac{4C_D}{\pi}\left(\frac{v_F}{v_{J_o}}\right)^2\left(\frac{y_J}{D}\right)\cos^3\theta,$$

where: $d\theta_M(\theta,\ \xi/D)$ = differential curvature caused by entrainment of free stream at the particular location $(\theta,\ \xi/D)$

$d\theta_D(\theta,\ \xi/D)$ = corresponding local differential curvature due to aerodynamic drag

ξ/D = non-dimensional downstream distance along jet curvature

v_F = free-stream velocity

v_{J_o} = initial jet velocity (assumed uniform)

v_J = local effective jet velocity based upon momentum flux averaged across jet profile

v_E = equivalent velocity of a free jet based upon average momentum flux issuing into quiescent air

C_D = assumed bluff-body drag coefficient

y_J = assumed (or empirically-determined) jet half-width at local station (ξ/D)

The application of this equation to predict local jet angle as a function of downstream distance requires the direct input of initial jet velocity, jet orifice diameter, free stream velocity and drag coefficient as constants for the entire process. In addition, the variation of jet width must be specified either functionally or tabularly as one proceeds downstream. In the present calculations, this distribution of y_J with increasing (ξ/D) was obtained from empirical data of Jordinson for a circular jet orifice; but it might well be appreciably different for square, rectangular, or elliptical nozzle exits.

Calculation of the local effective curved jet velocity, v_J, is a straightforward extension of the equivalent free jet velocity, v_E, based upon Kirkpatrick's postulates of the similarity of mixing mechanisms in free jets of non-parallel streams. This relation is given as Appendix Equation 2.2 and is repeated here:

$$\left(\frac{v_J}{v_{J_o}}\right)^2 = \left(\frac{v_F}{v_{J_o}}\right)^2 \sin^2\theta + \left(\frac{v_E}{v_{J_o}}\right)^2 \left[1 - \left(\frac{v_F}{v_{J_o}}\right)^2 \sin^2\theta\right].$$

The equivalent free jet velocity decay is, then, the primary empirical input to the entire curvature calculation. In the case of axisymmetric flow without swirl, this free jet behavior is very well described by Warren (Appendix Reference 17); although boundary layer effects within the jet nozzle may not be negligible in very small orifices or very long nozzles. Some applicable data on swirling jets issuing into quiescent air have been published by W. G. Rose (8); but no general similarity has been established for such flows, and one could certainly not expect them to behave in the manner described above. For non-swirling jets without axial symmetry, momentum profiles must be established

experimentally for each jet as it exhausts into free air in order that appropriate momentum factors and centerline decay curves may be generated as inputs to theoretical calculations.

The highly non-linear nature of the trigonometric functions and the initial velocity decays in the jet angle calculations require careful programming and integration interval selection; but the resulting curves are quite smooth and, in the cases calculated to date, produced rapid convergence toward each successive point in the Runge-Kutta scheme employed. The final transformation of coordinates from θ and ξ/D to x/D and z/D, representing distances downstream and cross stream, respectively, when referred to the tunnel flow direction is accomplished as noted in Appendix Section II-C-3 and repeated here for the K^{th} step of the integration.

$$\frac{x_K}{D} = \frac{x_{K-1}}{D} + \sin(\theta_{K-1} + d\theta_K)d(\xi/D)$$

$$\frac{z_K}{D} = \frac{z_{K-1}}{D} + \cos(\theta_{K-1} + d\theta_K)d(\xi/D)$$

Preparation of experimental data for input to the computer program is accomplished in several steps which are mentioned in various sections in the Appendix and are summarized as follows, with explanatory notes where required:

a. Determine the centerline velocity decay of the free jet at desired initial velocities (v_C/v_{J_o} vs. x/D)

b. Determine the free jet velocity profiles with sufficient precision to evaluate the half-velocity width and at enough axial locations to identify the core and the fully-developed flow regions (v_P/v_C vs. y/y_5)

(NOTE: If only paper studies of hypothetical jets are of interest, one may accept Warren's velocity decays and velocity profiles for the appropriate jet Mach number and temperature. However, for the purposes of predicting the curvature of a particular jet geometry, it is desirable to establish by some minimum experimental program the existence of gross similarity of profiles and the agreement with or departure from Warren's representative data.)

c. Locate the free jet width (y_E), by calculation from Warren's profile expressions or by extrapolation of experimental profiles to $v_P = 0$.

d. Determine the momentum factor, f, by graphical integration of area under the squared velocity profile curves, $(v_P/v_C)^2$ vs. $(y/y_5)^2$. Thus, by definition,

$$f = \frac{1}{(y_E/y_5)^2} \int_0^{y_E/y_5} \left(\frac{v_P}{v_C}\right)^2 d\left[\left(\frac{y}{y_5}\right)^2\right]$$

(NOTE: Within the core region of the free jet, the momentum factor decreases monotonically from an initial value of 1.0 to a lesser value which is characteristic of the establishment of similarity in velocity profiles, non-dimensionalized by the half-velocity width. The value of f remains constant for this fully-developed region and may be calculated in accordance with Warren's profile representations or determined graphically at one station within the similarity region.)

e. Construct the equivalent velocity decay curve for the free jet by calculating at each desired x/D location;

$$\frac{v_E}{v_{J_o}} = \frac{v_C}{v_{J_o}} \sqrt{f} \quad .$$

f. Express the equivalent velocity decay curve as a polynomial function in (x/D)

(NOTE: The present calculation procedure utilized a fifth-order polynomial expression and performed a least squares fit to the velocity decay curve. Any curve-fitting technique desired may be utilized and substituted for the "Procedure MIXCHANGE" portion of the program.)

g. Express the curved jet spreading characteristics as a function of downstream location (y_J/D vs. ξ/D) from empirical observations, pressure profiles or theory.

(NOTE: The present program utilizes a third-order polynomial least squares fit to each of three sets of Jordinson's pressure profiles corresponding to three different velocity ratios. Any alternative growth expressions could be substituted for the "REAL Y" and "HDRAG" portions of the program.)

h. Select an appropriate drag coefficient (c_D), and specify initial jet conditions of velocity and angle measured from the cross stream direction.

A print-out copy of the actual computer program used by Hardy in the calculations reported herein is presented as Figure 1.

C. Comparison With Existing Data

The overall objective of the theoretical and numerical analysis of a jet issuing into a cross-wind is, of course, to derive a tractable yet physically realistic model which may be used to predict with acceptable accuracy the behavior of an actual jet mixing with a free stream flow. The analysis presented herein does not purport to be new or all-inclusive, but rather a more detailed and, hopefully, more realistic version of the model originally proposed by Kirkpatrick. Consequently, the first group of comparisons presented in Appendix Section II-D-5 are those which illustrate the significance (or insignificance) of the three major revisions to the earlier theory, namely, (a) more accurate free jet velocity decay and spreading characteristics, (b) more realistic curved jet cross-sectional growth and shape, and (c) more consistent values of equivalent bluff-body drag coefficient. As Hardy has noted in Appendix Figures 2.11 through 2.13 and the discussion accompanying them, one may summarize these comparisons by establishing a relative order of importance of the revisions insofar as each one influences the curves of the jet centerline location. Thus, at all jet-to-freestream velocity ratios the most influential parameter is the equivalent free jet velocity decay function. Secondary to this, but of considerable importance at low velocity ratios, is the input representing the changing width of the curved jet. Finally, of least significance at all velocity ratios examined is the variation of drag coefficient within the reasonable limits normally associated with bluff bodies.

For any chosen velocity ratio, the direct comparison of theoretically-predicted jet location with experimentally determined jet curves is the ultimate test of the validity of the postulated mathematical model. However, the present model incorporates both theoretical and empirical functions and is therefore not truly

```
04:18 PM     APRIL 14, 1967    ****************     HARDY     AEROSPACE
  COMMENT THIS PROGRAM USES HARDY DRAG,
          HARDY EQUIVALENT VELOCITY DECAY,
          CD=1.16, [illegible]0, 1.25,
          FOR V=4, 6, 8, 10;
  BEGIN
      REAL TT, TO, RO, TD, TM, X, Z, L, OL, CD, V, A, B, C, D,
          DTOD, DT1D, DT2D, DT3D, DTD, DTOM, DT1M, DT2M, DT3M, DTM,
          TOTAL, DRAG, MIX, DD, DM;
  FORMAT ZERO (X7);
      FORMAT ID ("HARDY DRAG AND HARDY EQUIVALENT VELOCITY DECAY");
      FORMAT WHICH("V=", F4.1, X10, "CD=", F5.2, X10, "INITIAL"
          " ANGLE=", F5.2);
  FORMAT HEAD (    "L(ALONG JET)", X3, "X(DOWNSTREAM)", X3,
          "Z(VERTICAL)", X3, "TOTAL ANGLE", X3, "DRAG ANGLE",
          X3, "MIXING ANGLE", X7, "DD", X10, "DM");
  FORMAT DATA (X4, F5.1, X8, F10.5, X4, F10.5, X4, F10.5, X3, F10.5,
          X4, F10.5, X4, F10.5, X4, F10.5);
  COMMENT THIS PROCEDURE IS KIRKPATRICKS MIXING EXPRESSION;                MIX
      REAL PROCEDURE MIXCHANGE(L, TT);                                     MIX
      VALUE L, TT;                                                         MIX
      REAL L, TT;                                                          MIX
  BEGIN                                                                    MIX
      REAL VE, VJ, DVE, DENOM, NUM, X0, X1, X2, X3, X4, X5, X6;            MIX
      X0←.99197499;                                                        MIX
      X1←-.12724219;                                                       MIX
      X2←.003663777;                                                       MIX
      X3←.00037471904;                                                     MIX
      X4←-.000027540388;                                                   MIX
      X5←.000000504586;                                                    MIX
      X6←.0000;                                                            MIX
      VE←X0+X1×L+X2×L*2+X3×L*3+X4×L*4+X5×L*5+X6×L*6;                       MIX
      DVE←2×VE×(X1+2×X2×L+3×X3×L*2+4×X4×L*3+5×X5×L*4+6×X6×L*5);            MIX
      VJ ←SQRT((SIN(TT )/V)*2+VE *2-(VE ×SIN(TT )/V)*2);                   MIX
      DENOM←1-SIN(TT )/(V×VJ )+(SIN(TT )×COS(TT )*2/                       MIX
          (V×VJ )*3)×(1-VE *2);                                            MIX
      NUM←-.5×COS(TT )×(1-SIN(TT )*2/V*2)×DVE /(V×VJ *3);                  MIX
      MIXCHANGE←NUM/DENOM;                                                 MIX
  END MIXCHANGE;                                                           MIX
  COMMENT THIS PROCEDURE IS FOR HARDYS DRAG EXPRESSION;                    HDR
      REAL PROCEDURE HDRAG (L, TT);                                        HDR
      VALUE L, TT;                                                         HDR
      REAL L, TT;                                                          HDR
  BEGIN                                                                    HDR
      REAL Y, CD;                                                          HDR
      Y ←.5+A×L +B×L *2+C×L *3;                                            HDR
      CD←4×D/(3.14159265×V*2×COS(RO));                                     HDR
      HDRAG←CD×Y×(COS(TT))*3;                                              HDR
  END HDRAG;                                                               HDR
      FOR V←4, 6, 8, 10 DO
  BEGIN
      A←-.17889+2.80896/V+.09677/V*2;
      B←.0076889+.16385/V-1.55475/V*2;
      C←.00097944-.0209673/V+.088504/V*2;
      FOR D←1.16, 1.25 DO
  BEGIN
```

Figure I. ALGOL Program for Jet Curvature Calculations

```
      T0←0;
      R0←.01745329×T0;
      WRITE(LP[PAGE], ZERO);
      WRITE (LP, ID);
      WRITE (LP, WHICH, V, D, T0);
      WRITE (LP[DBL], HEAD);
      TT←R0;
      TD←R0;
      TM←R0;
      X←0;
      Z←0;
      DL←.1;
      FOR L←0 STEP .1 UNTIL 22.01 DO
BEGIN
      DT0D←HDRAG(L,TT);
      DT0M←MIXCHANGE(L,TT);
      DT1D←HDRAG(L+.5×DL, TT+.5×DL×(DT0D+DT0M));
      DT1M←MIXCHANGE(L+.5×DL, TT+.5×DL×(DT0D+DT0M));
      DT2D←HDRAG(L+.5×DL, TT+.5×DL×(DT1D+DT1M));
      DT2M←MIXCHANGE(L+.5×DL, TT+.5×DL×(DT1D+DT1M));
      DT3D←HDRAG(L+DL, TT+DL×(DT2D+DT2M));
      DT3M←MIXCHANGE(L+DL, TT+DL×(DT2D+DT2M));
      DTD←DL×(DT0D+2×DT1D+2×DT2D+DT3D)/6;
      DTM←DL×(DT0M+2×DT1M+2×DT2M+DT3M)/6;
      TT←TT+DTD+DTM;
      TD←TD+DTD;
      TM←TM+DTM;
      X←X+DL×SIN(TT);
      Z←Z+DL×COS(TT);
      TOTAL←57.29577×TT;
      DRAG←57.29577×TD;
      MIX←57.29577×TM;
      DM←57.29577×DTM;
      DD←57.29577×DTD;
      WRITE (LP,DATA, L, X, Z, TOTAL, DRAG, MIX, DD, DM);
END;
END;
END;
END.
COS IS SEGMENT NUMBER 0010,PRT ADDRESS IS 0077
SIN IS SEGMENT NUMBER 0011,PRT ADDRESS IS 0075
SQRT IS SEGMENT NUMBER 0012,PRT ADDRESS IS 0076
OUTPUT(W) IS SEGMENT NUMBER 0013,PRT ADDRESS IS 0104
BLOCK CONTROL IS SEGMENT NUMBER 0014,PRT ADDRESS IS 0005
ALGOL WRITE   IS SEGMENT NUMBER 0015,PRT ADDRESS IS 0014
ALGOL READ    IS SEGMENT NUMBER 0016,PRT ADDRESS IS 0015
ALGOL SELECT  IS SEGMENT NUMBER 0017,PRT ADDRESS IS 0016
NUMBER OF ERRORS DETECTED = 000. LAST ERROR ON CARD #          . COMPILATION TIME = 0024 SECONDS.
NUMBER OF SEQUENCE ERRORS COUNTED =  000. NUMBER OF SLOW WARNINGS = 000.
PRT SIZE=0071;TOTAL SEGMENT SIZE=00382 WORDS;DRUM STORAGE REQ.=00485 WORDS;NO. SEGS.=0018.
ESTIMATED CORE STORAGE REQUIREMENT = 01228 WORDS.
```

Figure 1 - Continued

independent from the experiments to which it is compared. In the absence of free jet decay data for the slipstream curvatures available in the literature, it is impossible to select the optimum inputs for the numerical calculations of the present model. Nevertheless, some qualitative comparisons may be justified as presented in the curves of Figures 2 and 3. The particular experiments chosen from the larger group shown in the Appendix (Figure 3.1) are those of Jordinson (Appendix Reference 9) because of the use of this pressure profiles to define the half-width of the theoretical jet, those of Margason (9) because of the absence of end plate effects at the jet orifice, and those of Keffer and Baines (Appendix Reference 10) because of the very large ratio of tunnel dimension to jet diameter. The theoretical model shown in both figures corresponds to curve (b) of Appendix Figures 2.13, i.e., case iii of Hardy's calculations, in which Warren's generalized velocity decay function is combined with Jordinson's half-width and a semi-cylindrical shell drag coefficient. In spite of the possible disparity between these theoretical conditions and the actual experimental ones, the predicted jet locations are quite close to those observed; and the calculated local slope is very nearly that reported by the experimenters, particularly at the higher velocity ratio.

The good agreement between theory and Margason's empirical fit to his data is particularly encouraging, since his is the only experiment free from end plate effects at the nozzle, a condition specified in all of Warren's results and therefore inherent in the free jet velocity decay expressions used in deriving the theoretical curves presented. Certainly one cannot contribute all the discrepancies between various experimental results to the presence or absence of a finite end plate, but its effects on free jet velocity decay and distortion of the cross section of the mixing curved jet are not predictable at the moment in any quantitative manner and consequently cannot be entirely discounted.

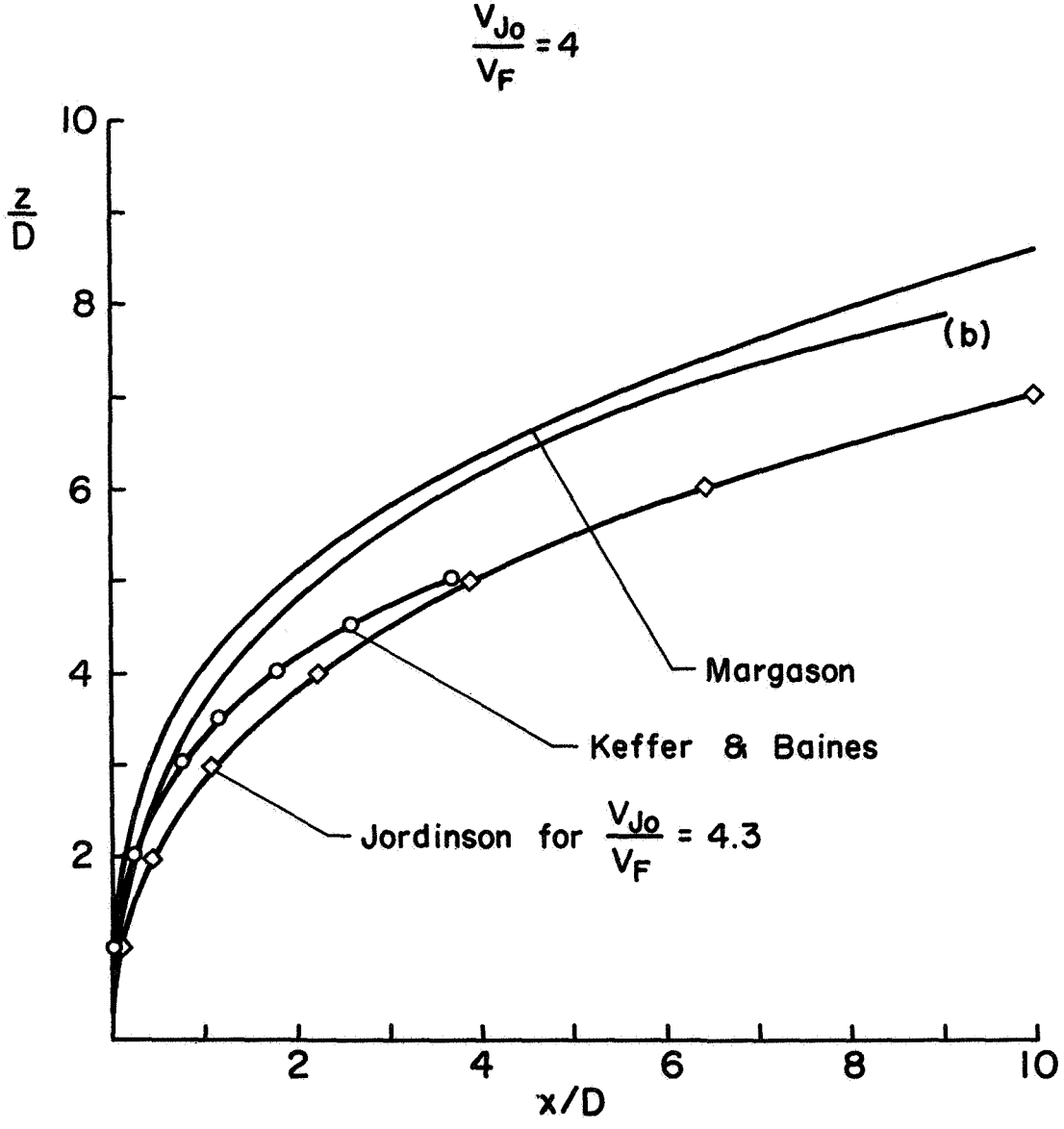

Figure 2. Comparison of Theoretical Model with Previous Experiments - Low Velocity Ratio

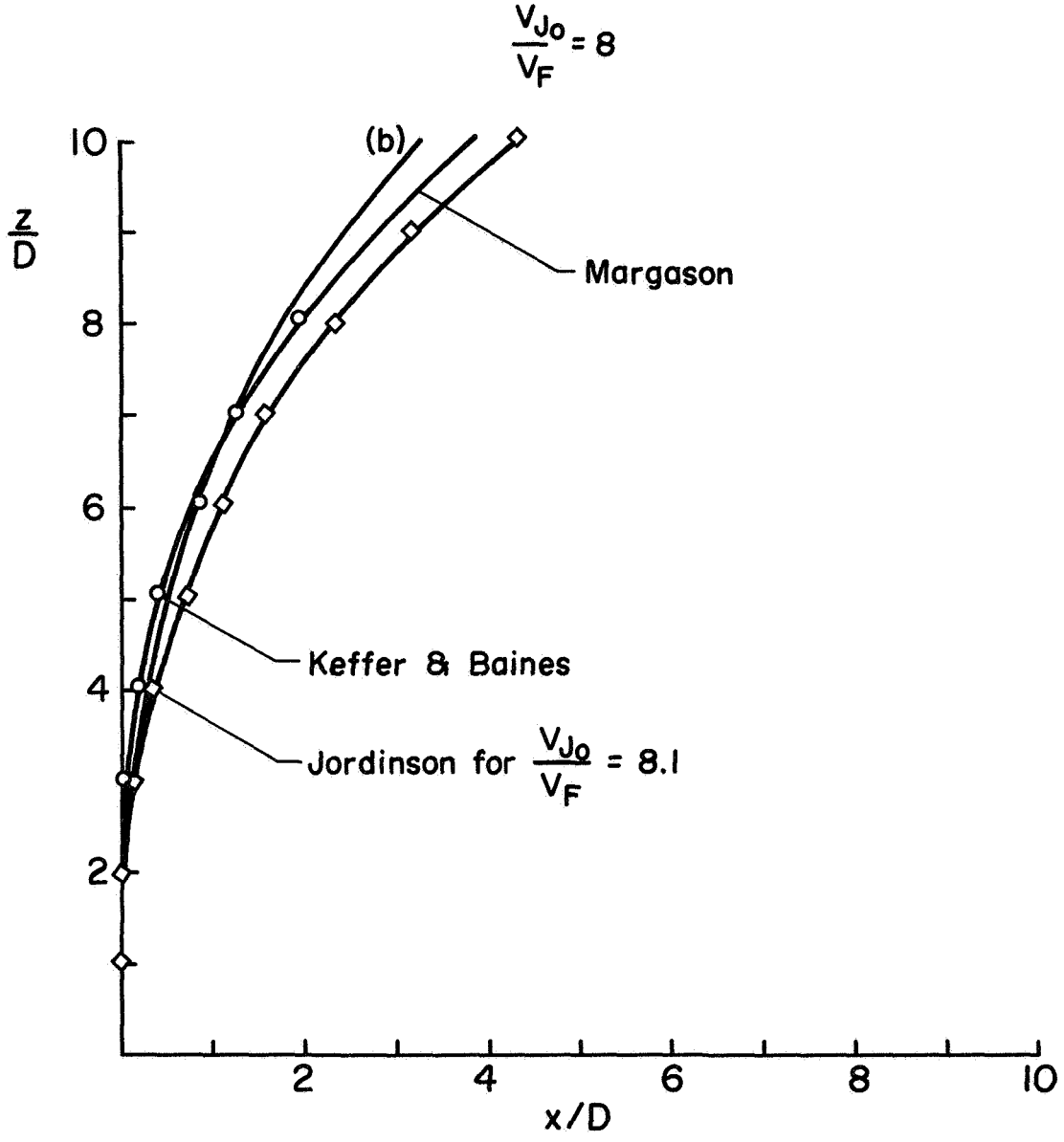

Figure 3. Comparison of Theoretical Model with Previous Experiments - High Velocity Ratio

III. Experimental Studies

A. Purpose of Experimental Program

As mentioned in the preceding section, the only valid test of both mixing and drag representations of the theoretical model is a comparison of its predictions of jet curvature with an experimentally observed jet whose characteristics when exhausting freely into quiescent air are used directly as the empirical inputs to the calculation procedure. The purpose of the experimental program reported herein is thus basically to supply a known free jet input and to determine the behavior of that same jet when issuing normal to a known cross flow.

Because of the rather sweeping assumptions in the model chosen to represent momentum and mass flow conservation and exchange, a longer range objective of the experimental phase of this research was to examine some specific aspects of the slipstream-freestream interaction process which might indicate the limitations of these theoretical assumptions. In particular, it was desired to examine the differences in both free jet and mixing jet developments between circular and rectangular orifices to observe the extent to which non-symmetry of the nozzle might effect equivalent velocity decays, downstream velocity profiles, and curvature in the cross-stream. Several such tests were made and are reported by Hardy in Appendix Sections II-D and III-F. As may be noted from these results, the differences in free jet behavior between the two nozzle geometries were significant and persisted for a large distance downstream. It became apparent from these tests that a new representation of jet width, equivalent velocity, and momentum factor would be necessary to provide acceptable inputs to the calculation program. No simple basis for establishing similarity of profiles was obvious, and the time available within the period of the grant was not sufficient to warrant a second major analytical development to represent a single new jet nozzle geometry. Consequently no attempt has been made to predict the curvature of the rectangular jet; the observed behavior has simply been reported for comparison with corresponding circular nozzle data.

An additional experimental program was planned and begun in an effort to clarify several questions concerning geometric influences on the mixing jet behavior. At the present time the effects of absolute magnitude of nozzle diameter on the spreading and distortion of the mixing jet are not known. Certainly one can partially account for differences in size by non-dimensionalizing on the basis of diameter. However, the conditions for dynamic similarity of two different sizes of turbulent jets must involve an equality of Reynolds' number based on an appropriate length scale; and the question of what length dimension is most meaningful, e.g., jet diameter, distance downstream, or distance along peripheral streamlines, has not been satisfactorily answered. It was felt that tests should be conducted on geometrically similar, larger scale jets in a large wind tunnel test section; and to this end, the design of a contraction section, motor drive system, and test section of the partially-built subsonic flow facility was pursued under this program.

Two other geometric uncertainties in jet mixing analyses must be clarified in larger scale facilities than those employed and described in Appendix Section III-D, and it was intended that the large subsonic tunnel be designed and constructed in such a way that it would be suitable for these tests. One of these unknowns is the effect of an end plate on the jet nozzle, as discussed in the preceding section. The second effect is that which originally led to the entire investigation of slipstream-free stream interaction, namely the influence of the wind tunnel walls on the flow field. Since one cannot move the jet nozzle away from the end-plate effect of a wind tunnel wall without necessarily moving it closer to the opposite wall in any closed test section, the identification of the individual influences can only be accomplished by examining the jet behavior in a large test section under controlled conditions similar to those already established in a smaller, but geometrically similar, section.

B. Description of Apparatus and Facilities

Considerable effort was expended by the principal investigator in the design and construction supervision of a variable-speed, variable-pitch propeller

drive system; a matching flow-straightener and diffuser section; a uniform outflow contraction nozzle; and a constant pressure, readily accessible test section for a large subsonic wind tunnel. Although this tunnel was not completed during the period of the grant, its development has since been continued with University support; and it is currently operating over a speed range from 20 to 120 feet per second. The characteristics of this closed-return facility are as follows:

Test Section: 3.5' x 5.0' x 6.0' long
Design Speed Range: 20-250 ft/sec
Drive System: 4-blade, variable-pitch fan (8-1/2 ft. diam.)
25 HP DC motor, 50-400 rpm
200 HP AC motor, 1175 rpm
Turbulence Level: 0.25% from 20-120 ft/sec at blade tip pitch angle = 25.2°
Balance System: 3-component electric beam balance
Contraction Ratio: 4.75

All the experiments reported in the Appendix were performed in an open-circuit, one-fifth scale pilot model of the large tunnel. This small, student-operated tunnel had been previously constructed for use as an undergraduate laboratory tool with a uniquely-designed contraction section intended to provide uniform flow with an area ratio of 5.0. As noted by Hardy, the actual flow distribution was surveyed and found to be uniform and axial to within one per cent of mean velocity and within one-half degree of the axis (the precision of the inclination sensor). This was felt to be sufficiently representative of the theoretical free stream conditions, so the only modifications which were made to the tunnel were the replacement of the original test section and improvements to the variable-speed drive reported by Hardy.

The uniformity of flow entering the test section warranted scaling the contractionnozzle design up to the large subsonic tunnel size. A pressure distribution along top and side contours was obtained; and the agreement with predicted gradients, after applying mass continuity corrections, was quite reasonable, exhibiting no areas of adverse gradients and no evidence of separation. The overall contraction section length for the large tunnel was decreased because of

the limited space available for the closed-return passage, and a revised contour was calculated retaining the local slopes of the small scale nozzle in those regions of minimum rate of change of pressure near the exit. Preliminary surveys of the large test section recently completed show no evident areas of flow separation or of extreme non-uniformity, although detailed flow inclination or vorticity measurements have not yet been obtained.

The jet nozzles, free jet expansion measurement instrumentation, and flow visualization equipment have been thoroughly described by Hardy in the Appendix, and no supplemental details appear necessary herein.

C. Results and Discussion

1. Free Jet Studies

Hardy has presented the centerline velocity decay and jet profiles for both axi-symmetric and slot jets in detail in Appendix Section III-F. The regular, predictable jet spreading and achievement of non-dimensionalized profile similarity in both geometries is evidence that both jets are "well-behaved," that is, that there is nearly uniform exit velocity at the nozzle plane with no indication of swirl or flow separation within the nozzle and that the exit flow is parallel to the nozzle axis with no curvature or angularity artificially introduced prior to exiting into the room.

The slot jet behaves initially as a combination of two-dimensional jets acting in planes perpendicular to each other. The interaction between the two distinct profiles continuously merges the characteristics of each into the other in a kind of intermediate zone of velocity decay, and finally a repeatable pattern of profile similarity appears which is akin to the fully-developed axi-symmetric jet. However, no simple basis for non-dimensionalizing a profile measured in an arbitrary plane containing the jet axis is apparent. Even the use of an equivalent diameter as introduced herein leads to some inconsistencies when comparing vertical and horizontal profiles which are gradually changing from a two-dimensional to a three-dimensional nature. One certainly cannot draw justifiable conclusions about the suitability of a theoretical descriptive model from these very limited data.

2. Jet Cross-Wind Studies

The jet cross-wind results show a definite improvement in the prediction of actual paths, although the theoretical paths depart from the measured locations by a dissapointingly large amount at the higher velocity ratios. As noted in Hardy's discussion, this discrepancy may arise from several possible sources. The fact that the initial slopes disagree so drastically indicates that the early portion of the velocity decay curve used as an input to the calculation procedure may be in error. This function must be extrapolated from downstream measurements at (x/D) ratios of about 1.0 to the nozzle exit plane; and there is a distinct possibility that the presence of a total pressure probe even a full diameter from the nozzle exit may have blocked the jet flow a non-negligible amount, leading to an erroneous shape of both the centerline velocity decay and the momentum factor curves in this critical region of high jet velocity.

Additional evidence supporting this postulate of the source of the discrepancy rather than an error in observation of the jet location comes from a comparison of Appendix Figure 3.12 with Figures 2.13 and 3.1. At velocity ratios of 6, 8, and 10, an overlay of figures 2.13 and 3.12 shows that an equivalent velocity decay based on Warren's jet predicts the initial slope of the experimental path quite well. Since Warren has presented a model of an entire class of jets, it should be expected that the decay curve of the free jet examined herein would agree closely with this general representation. An independent check on the probable reliability of the experimentally-determined location and curvature of the jets is made by overlaying Figure 3.1 on 3.12. At all velocity ratios tested, the current experimental curves lie very close to those of Keffer and Baines; so one cannot readily conclude that the identification of jet centerline by micro-densitometer is in error.

Examination of the velocity profiles at one diameter downstream in the free jet suggest that a measurable boundary layer effect is present at the nozzle exit and that the momentum factor at the exit plane is not unity. Consequently, the extrapolation of the calculated equivalent velocity decay by a least-squares fit to a specified end point of $v_E/v_{J_o} = 1.0$, as shown in Appendix Figure 3.11(b),

is subject to question. No quantitative data are available to provide justification for the selection of any more reasonable extrapolation, however; and the aforementioned blockage problems in so small a jet make the acquisition of velocity profiles at or near the exit extremely difficult and unreliable. A direct extrapolation disregarding the mathematical condition of uniform initial velocity certainly would lead to a decreased slope in the first two diameters downstream in Figure 3.11(b), but the extreme sensitivity of the calculations to this slope suggests that one might better choose to examine a larger jet in which probe blockage is not a severe problem or to examine this region in the existing jet with micro-size hot-wires or with more sophisticated non-interfering sensors such as laser optics. The modest program reported herein did not justify these additional efforts in instrumentation.

The technique of applying an optical micro-densitometer to the photographic negatives of the curved jet path led to new questions that can only be answered by additional experiments. One must arbitrarily define a jet centerline from the smoke density information obtained by some flow-visualization method, such as opaqueness of a film. The definition chosen herein is that the centerline is the locus of points of maximum smoke intensity of the traverses across the jet. A more rigorous choice, consistent with the theoretical model developed, would be the locus of points of maximum momentum flux or maximum axial velocity, assuming a symmetrical profile. However, until reasonably precise cross sections are determined for the mixing jet, one cannot interpret the smoke intensity information derived from a side view of the jet in terms of the local velocities internal to the section. The best compromise for the present study was therefore felt to be the assumption that the greatest concentration of mass flow could be treated as the location of the jet centerline.

IV. Conclusions and Recommendations

The basic objective of the current program as stated in the introduction has been achieved. A mathematical model of a curving, mixing jet as it interacts with a uniform cross-stream has been developed as an improvement and extension of earlier work by Heyson and Kirkpatrick. The essential contribution of this development to the longer range goal of complete understanding of jet mixing lies in its identification of important primary jet parameters insofar as they influence the mixing process. The experimental checks of this model support the results of numerical calculations in two ways: (a) the better agreement between prediction and reality indicates that the revised model definitely represents an improvement over previous theoretical descriptions, and (b) the departure of jet curvature in some of the experiments from predicted behavior is directly attributable to a variation from idealized performance of the most sensitive of the free jet parameters, i.e., velocity decay.

The significance of the contribution reported herein to the engineer who wishes to apply it in determining wind tunnel wall corrections, jet downwash effects, or even the spread of pollutants into a moving environment may be somewhat obscured by the minutiae of detailed derivations and discussions and should perhaps be stated more simply at this point. If one wishes to predict the centerline location, local curvature, or even local entrained mass flow of a non-swirling turbulent jet issuing into a uniform cross-stream, he may do so with reasonable confidence by examining the same jet as it issues freely into a quiescent environment. In the case of a jet which approximates ideal flow at the orifice, a previously-developed mathematical description of this free-jet behavior will suffice as an input to the calculations of the mixing jet. In the case of a new, untried nozzle design or one whose exit characteristics are known to depart appreciably from idealized conditions, one need only perform the relatively simple experiment of measuring velocity decay and velocity profiles in the freely-expanding jet rather than a complicated, difficult and often expensive series of experiments in the actual cross-flow mixing environment.

The recommendations made by Hardy in Appendix Section IV cannot be over-emphasized in the light of the results obtained and conclusions drawn in that section. Although the assumptions and approximations of the theory are fairly well justified by the comparisons of numerical and empirical results, a thorough understanding of the mixing process of non-parallel streams and its similarity to free-jet behavior requires a great deal of further investigation. One of the suggestions made by Hardy has been followed recently by Margason (9) and R. G. Williams (10) in which the influence of the end plate at the nozzle orifice is examined in both mixing and free jet situations. Although not a negligible effect, this end-plate blockage appears to be less significant than the effects of the actual velocity profile at the exit. A second recommendation of Hardy has been followed in a preliminary attempt to observe the mixing jet cross sections and the growth of the vortex "tails" at the edges of the jet by J. Schiller (11). A corresponding phenomenological model of this combination of entrainment and shear has been proposed by Pratt and Baines (7); and there appear to be serious discrepancies between this model and the observations, particularly with regard to direct penetration of the jet by cross-flow components of mass flux. Certainly this phase of the interaction problem must be clarified.

As Hardy has noted, no single approach toward the understanding and prediction of jet mixing in a free stream can be expected to be all-encompassing. Investigations of the local mechanisms of turbulent transport, the near-field influence of the jet on velocities and pressures in the free stream, the introduction of vorticity through viscous shear at the edges of the jet, the importance of asymmetry on jet curvature, and the general effects of jet swirl are recommended as potentially fruitful directions for further research.

V. Bibliography

1. Knight, Montgomery and Hefner, R. A., "Analysis of Ground Effect on the Lifting Airscrew," NACA TN No. 835, 1941.

2. Heyson, Harry H., "An Evaluation of Linearized Vortex Theory as Applied to Single and Multiple Rotors Hovering in and out of Ground Effect," NASA TN D-43, September 1959.

3. Heyson, Harry H., "Jet-Boundary Corrections for Lifting Rotors Centered in Rectangular Wind Tunnels," NASA TR-71, 1960.

4. Heyson, Harry H., "Tables of Interference Factors for Use in Correcting Data from VTOL Models in Wind Tunnels with 7 by 10 Proportions," NASA SP-3039, 1967.

5. Chang, H. C., "Rolling-Up of a Cylindrical Stream through a Cross-Wind," Ph.D. Dissertation, Göttingen University (West Germany), 1942 (in German).

6. Epstein, A., "The Curving of a Turbulent Circular Jet in a Free Transverse Flow," Technical Report of Institute of Thermophysics and Electron Physics, AN, ESSR, No. 2, 1966 (in Russian).

7. Pratt, B. D. and Baines, W. D., "Profiles of the Round Turbulent Jet in a Cross Flow," Journal of the Hydraulics Division, Proceedings of the American Society of Civil Engineers, November 1967.

8. Rose, W. G., "A Swirling Round Turbulent Jet," American Society of Mechanical Engineers, Paper No. 62-WA-59.

9. Margason, R. J., "The Path of a Jet Directed at Large Angles to a Subsonic Free Stream," NASA Langley Working Paper 590, May 1968.

10. Williams, R. G., "End Plate Effect on Free Jet Mixing," Undergraduate Thesis, School of Engineering and Applied Science, University of Virginia, May 1968.

11. Schiller, J., Unpublished Master's Thesis, University of Virginia, 1968 (in preparation).

NON-PARALLEL FLOW INTERACTIONS

A Thesis

Presented To

the Faculty of the School of Engineering and Applied Science

University of Virginia

NGR-47-005-040

In Partial Fulfillment

of the Requirements for the Degree

Master of Aerospace Engineering

---

by

William G. S. Hardy

June 1967

APPROVAL SHEET

This thesis is submitted in partial fulfillment of

the requirements for the degree of

Master of Aerospace Engineering

William G. S. Hardy

Approved:

G. B. Matthews,
Faculty Adviser

Dean, School of Engineering and
Applied Science

June 1967

ACKNOWLEDGEMENTS

The author wishes to thank Dr. George B. Matthews of the Department of Aerospace Engineering for the invaluable suggestions and criticisms which he made during the planning and writing of this thesis. The author is also grateful to Richard J. Margason of the Langley Research Center, Hampton, Virginia, for his suggestions and experimental data, and to Professor David C. Hazen of the James Forrestal Research Center, Princeton, New Jersey, for his technical assistance in preparing the flow visualization equipment used in this study.

TABLE OF CONTENTS

LIST OF FIGURES

CHAPTER I

INTRODUCTION

A. BACKGROUND

At the present time, the interaction between two distinct and non-paralled streams is a phenomenon which merits attention from the scientific community, not only because it is an interesting academic problem, but also because of its importance in the fields of mixing processes, industrial waste control, and V/STOL aircraft design. At the time of this writing, basic information concerning this type of interaction is wanting when compared to other problems in fluid dynamics. The following study grew out of an investigation of wind-tunnel wall corrections for tests of V/STOL models in the flight regime between vertical take off and conventional forward flight. It is desired in wind-tunnel tests to simulate free flight conditions. In order to do this, corrections which account for the presence of the tunnel walls must be applied to experimental measurements. A linearized theory has been developed and verified for conventional flight configurations. This theory is based on the assumption that disturbances to the test-section velocity field caused by the model's presence in the test-section are small and may be linearized. In the V/STOL trasition regime, the disturbances are no longer small and are quite non-linear. Thus the assumptions of the linearized theory are no longer valid.

Removing the effects of the presence of the test-section walls from measurements may be accomplished in two ways. The first

method is to withdraw the walls of the test-section to a point where their influences on the measured aerodynamic forces are negligible (e.g. by enlarging the test-section or by reducing the model size). This plan becomes prohibitive when the tunnel size becomes too large for economic operation or when the model becomes too small for precise measurements. The second method is to find an effective way to correct the measurements in order to compensate for the presence of the walls. This latter course of action is felt to hold more promise for the future since a complete theory can be applied to almost all tunnels.[1]

V/STOL wall correction theory has been developed in two stages. Initially a linearized theory was developed by Harry H. Heyson [6] of NASA, Langley Research Center, in which the wake of a V/STOL aircraft in transition is treated mathematically as a inclined, straight-line distribution of vertical and longitudinal doublets. The conventional theoretical techniques, e.g., image distribution methods, are then used to calculate wall correction factors. Heyson's wake, however, is inclined at an angle to the free stream determined by the lift and drag measurements to which the corrections are to be applied.

Realizing that the straight-line wake is physically incorrect, Kirkpatrick [11] set out to introduce a curved wake into Heyson's development. Kirkpatrick's study showed that the corrections calculated

[1] Olcott, J. W., "Survey of V/STOL Wind-Tunnel Wall Corrections and Test Techniques," Princeton University Dept. of Aero. Eng. Report No. 725, 1965.

employing a curved wake model varied significantly from those calculated using the straight-line wake model. This result suggests to the observer that the representation of the wake is of major importance in the wall correction analysis, and thus the present study was initiated to attempt to provide this representation. Figure 1.1 shows the types of wakes as described above.

It is not the purpose of this study to consider V/STOL wind-tunnel corrections per se. It is intended herein to examine the interaction of two streams similar to those found in V/STOL aerodynamics. An effort will be made to establish a simple analytical model of such wakes and to confirm experimentally the validity of the model. In doing so, it is felt that an insight into the overall V/STOL wall interference problem will be gained.

B. WAKE REPRESENTATION

No single representation of the wake (or slipstream) of V/STOL configurations could ever hope to cover all of the possible combinations of wings, rotors, fans, and jets that have been considered in such designs; but by understanding the simplest of these, inferences can be made about the others. The model chosen here is simply that of a jet of air injected normal to the wind or free stream direction. Such a jet model was originally suggested by Kirkpatrick. The present work, however, plans to incorporate into Kirkpatrick's model some features which are more closely correlated to the observed physical aspects of such flows.

(a)

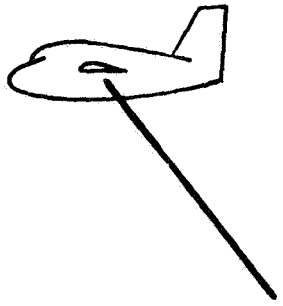

(b)

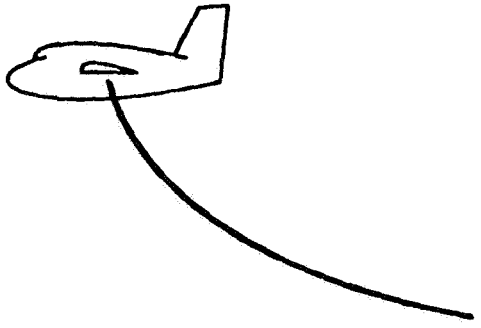

(c)

FIGURE 1.1 (a) Slipstream in forward flight
(b) Heyson's V/STOL wake representation
(c) Kirkpatrick's curved wake

Henceforth, no further mention will be made of the V/STOL problem. The aforementioned wake will now be referred to as the jet or slipstream and the wind as the cross-wind or free stream. Any mention of a free jet will hereafter refer to a jet discharging into quiescent air.

The following development will consider the interaction of two streams which are incompressible, and of equal density and temperature. However, the analysis can easily be expanded to include compressibility, differences in jet-free stream composition, and temperature effects. It is felt, however, that a basic understanding of the mechanisms of the interaction are far more important at this stage than including methods for handling all of the effects that might be encountered.

It has been shown that the presences of boundaries alter the flow in the jet [16]; however, the jet model developed herein will not include any attempt to compensate for the presence of walls. Experiments to verify the present analysis were performed in the confines of a wind-tunnel test section and for this reason must be considered with some reservation. However, the experiments were designed to reduce these effects to as great an extent as possible.[2] But, as is pointed out above, it is the aim of this study to gain an understanding of the primary variables which influence interaction and, in this way, to present a guide for future studies.

[2] See Chapter III

CHAPTER II

ANALYTICAL STUDIES

A. EXISTING THEORIES

It has been pointed out in the introduction that there is a minimum amount of information available on the subject of non-parallel flow interactions. The theories which have been presented on this subject do not agree about how to approach the subject analytically.

Fredric F. Ehrich of the Westinghouse Electric Corporation has presented a solution for the steady, incompressible, two-dimensional potential flow of equal velocity streams [5]. By transferring the flow to the hodograph plane he is able to represent the jet boundaries and the orifice boundaries by circles and radial lines, respectively. Then, by mapping and employing the Schwartz-Christoffel transformation, he is able to find the bounding streamlines of the jet in the physical plane. Although indicative of the existence of a solution, Ehrich's treatment is unable to arrive at any specific conclusions for the cases where the jets might be compressible or unequal in velocity. The use of potential flow methods, of course, precludes any consideration of viscous effects.

In a similar mathematical approach, Ackerberg and Pal [1] also consider a potential flow solution in two dimensions. This development is an improvement over Ehrich in that it includes the effects of streams of different densities and unequal velocity. Again, the analysis does not consider viscous or three dimensional flows.

B. INTRODUCTION TO INCOMPRESSIBLE JET CHARACTERISTICS

Before continuing with the discussion of non-parallel flows, a brief discussion of free jets and parallel flows is in order. Extensive work has been done in these fields, and some of the conclusions of these studies can be applied to the slipstream analysis.

Free-jet theory considers the jet to be divided into two regions shown in Figure 2.1a: a mixing or core region which extends three to four diameters downstream from the orifice, followed by a fully-developed flow region. Theory predicts and experiment verifies that aerodynamic similarity exists between jets provided their methods of generation are also similar. The centerline velocity, v_c , remains nearly constant in the core region, and then, in the developed region, it decays as some power of the axial distance as seen in Figure 2.1b. Within the confines of the jet itself, similarity exists between the velocity profiles normal to the centerline or line of symmetry (Figure 2.1c & 2.1d).

Free jets may be correlated to the flow situation which occurs when the jet is not issuing into quiescent air but instead issues into a stream moving parallel to it. In making this correlation, the concept of an equivalent velocity is introduced. This equivalent velocity, v_E , is defined as that uniform-profile velocity which provides the same momentum flux for the jet as the assumed or measured profile (see Figure 2.2). In other words the original jet with non-uniform velocity profiles is transformed into an equivalent jet with the same momentum flux as the original at all axial stations but with uniform velocity

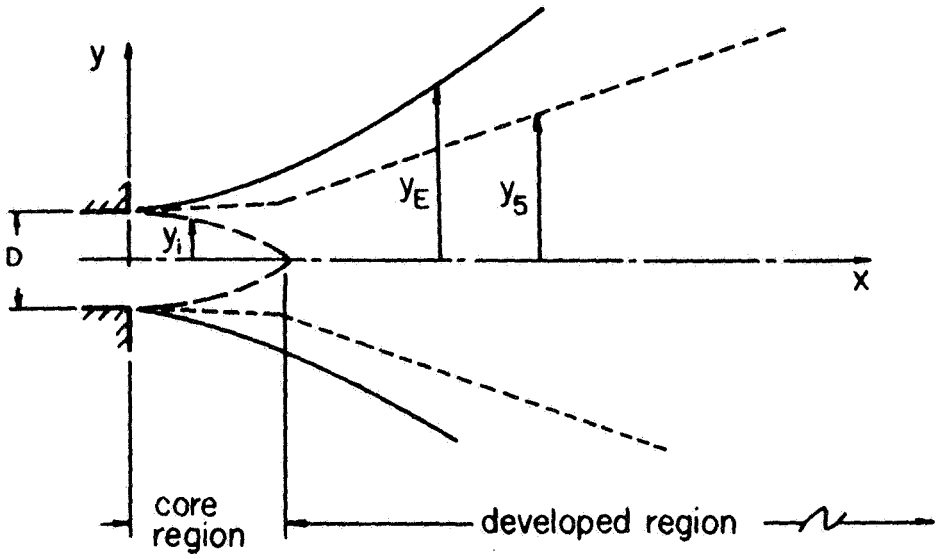

(a) Typical jet geometry

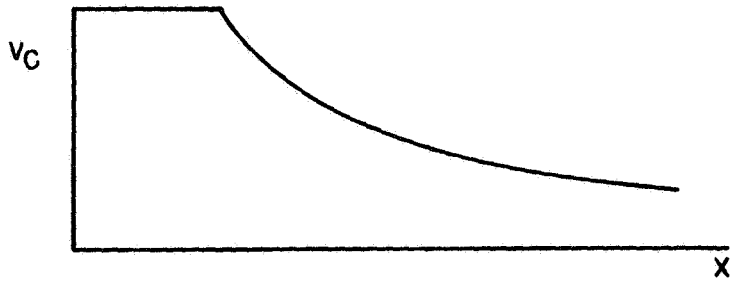

(b) Centerline velocity decay

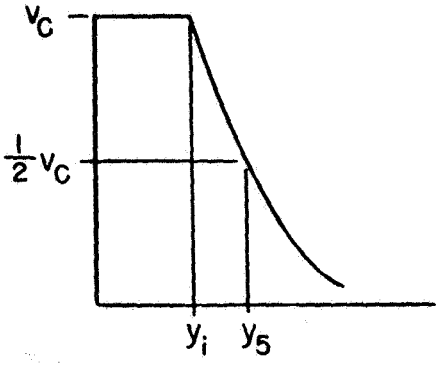

(c) Jet profile in core region

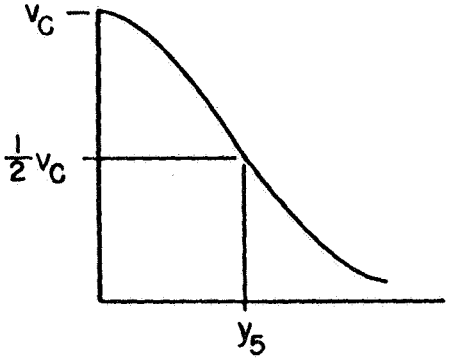

(d) Jet profile in developed region

FIGURE 2.1 - Axisymmetric Jet

profiles throughout. The equivalent velocity describes the decay of the equivalent jet and is a function of axial location. Once the equivalent velocity for the free jet, v_E, is known, the equivalent velocity for the same jet in a parallel stream may be determined by equation (2.1).

$$\frac{\rho_J v_J^2}{\rho_{J_o} v_{J_o}^2} = \frac{\rho_F v_F^2}{\rho_{J_o} v_{J_o}^2} + \frac{\rho_E v_E^2}{\rho_{J_o} v_{J_o}^2}\left(1 - \frac{\rho_F v_F^2}{\rho_{J_o} v_{J_o}^2}\right) \qquad (2.1)$$

The velocity v_J is the equivalent velocity of the jet in a parallel stream. It is not the actual measured velocity. The velocities v_{J_o} and v_F are the actual velocities of the jet at its orifice and of the parallel stream, respectively.

C. KIRKPATRICK'S JET ANALYSIS[3]

Kirkpatrick, in his analysis of a jet in a cross-wind, makes the simplifying assumptions that

$$\rho_{J_o} = \rho_J = \rho_E = \rho_F$$

He also relates the equivalent jet velocity of the curved jet to that of the free jet in much the same way as was done above for the jet in a parallel stream. By assuming that only the component of the free stream velocity which is parallel to the jet contributes to the change

---

[3] Kirkpatrick, D. L. I., "Wind-Tunnel Corrections for V/STOL Model Testing," Unpublished Thesis, University of Virginia, 1962, Chapter III.

in equivalent velocity, he expresses the equivalent velocity of a jet at an angle θ to the free stream as:

$$\left(\frac{v_J}{v_{J_o}}\right)^2 = \left(\frac{v_F}{v_{J_o}}\right)^2 \sin^2\theta + \left(\frac{v_E}{v_{J_o}}\right)^2 \left[1 - \left(\frac{v_F}{v_{J_o}}\right)^2 \sin^2\theta\right] \qquad (2.2)$$

where ($v_F \sin\theta$) is the component of the free stream parallel to the jet. Figure 2.3 shows the nomenclature used. Kirkpatrick attributes the bending of the jet to the action of two mechanisms: a net exchange of momentum in the wind direction between the free stream and the jet, and the action of an aerodynamic drag force akin to bluff-body drag on the slipstream cross-section.

1. Momentum Considerations

It is an established fact that a jet interacts with the medium into which it issues by the process of turbulent mixing, whether the medium is quiescent or not [17]. This mixing process is evidenced by a decay in the centerline velocity and by a spreading of the jet resulting in a decrease of the momentum of the jet. This momentum exchange between the jet and its surrounding medium is accounted for in (2.2). Realizing that the momentum losses have been accounted for, Kirkpatrick assumes that the vertical momentum of the jet is conserved when it issues into a horizontal, free stream. Referring to Figure 2.4 this assumption is stated by

$$\frac{d}{d\xi}\left[\dot{m}_J v_J \cos\theta\right] = 0 \qquad (2.3)$$

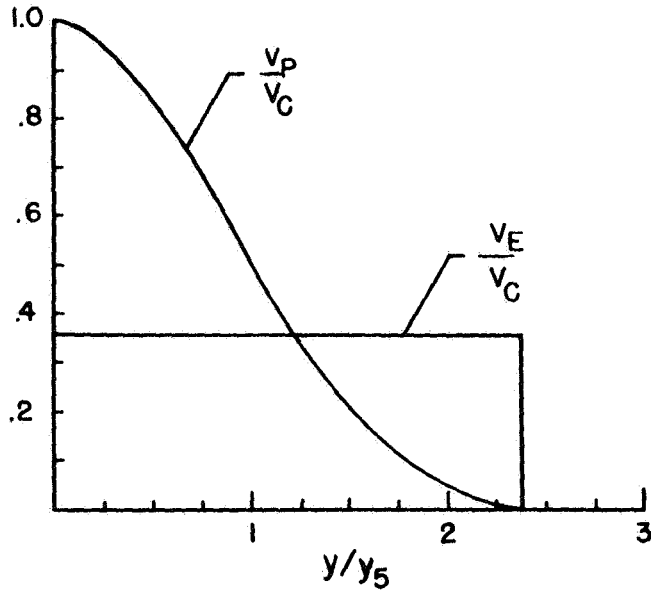

FIGURE 2.2 - Equivalent jet velocity

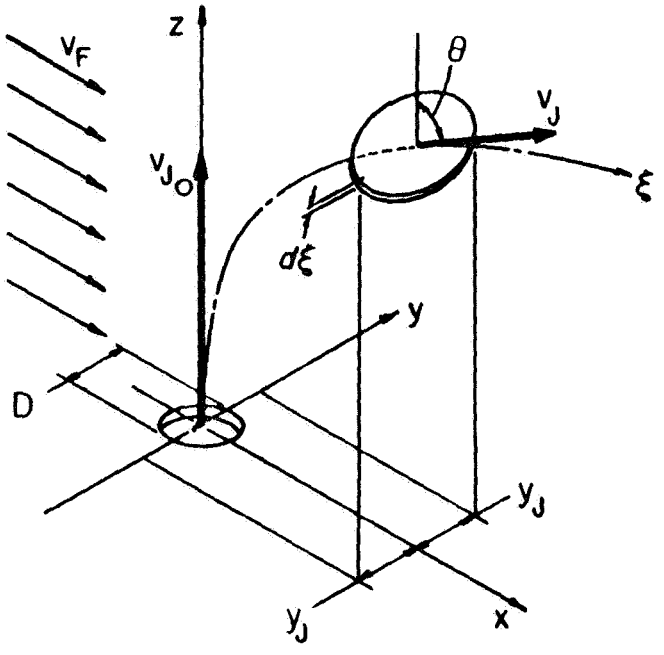

FIGURE 2.3 - Jet Nomenclature

By conserving the combined momentum flux of the jet and free stream normal to the jet path, he also demonstrates that

$$\frac{d\theta}{d\xi} = \frac{1}{\dot{m}_J v_J} \frac{d\dot{m}_J}{d\xi} v_F \cos\theta \tag{2.4}$$

Combining (2.2), (2.3), and (2.4), one arrives at Kirkpatrick's expression for the contribution of the momentum exchange between the free stream and jet to the curvature of the jet.

$$\frac{d\theta}{d(\xi/D)}\left\{1 - \frac{v_F}{v_J}\sin\theta + \left(\frac{v_F}{v_J}\right)^3\left[1 - \left(\frac{v_E}{v_{J_o}}\right)^2\right]\sin\theta\cos^2\theta\right\}$$
$$= -\frac{1}{2}\frac{v_F v_{J_o}^2}{v_J^3}\cos\theta\left[1 - \left(\frac{v_F}{v_{J_o}}\right)^2\sin^2\theta\right]\frac{d}{d(\xi/D)}\left[\frac{v_E}{v_{J_o}}\right]^2 \tag{2.5}$$

2. Aerodynamic Considerations

The mass of fluid contained in a length, $d\xi$, of the jet is

$$dm_J = \rho_J(\pi y_J^2 d\xi) \tag{2.6}$$

where ρ_J is constant and $y_J = y_J(\xi)$. The aerodynamic force normal to such a jet element is a drag force, which may be expressed as

$$dF_D = \left(\frac{1}{2}\rho_J v_n^2\right)(C_D)(2y_J d\xi). \tag{2.7}$$

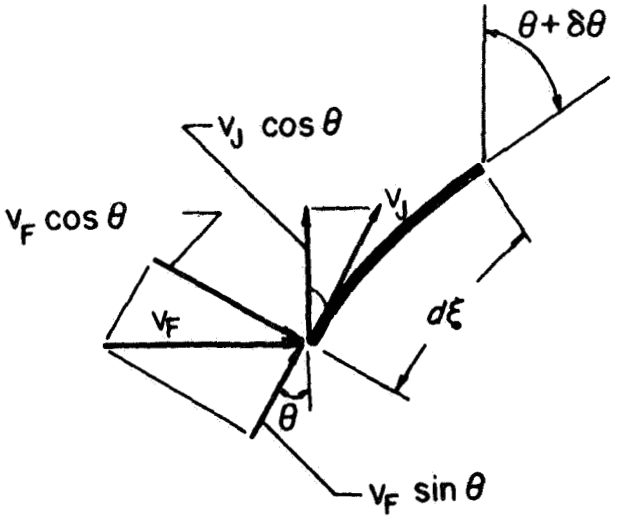

FIGURE 2.4 - Representation of a Jet element

Writing Newton's law for the mass of fluid

$$dF_c = \frac{dm_j}{R} v_j^2$$

where

$$v_j = \frac{d\xi}{dt} \qquad \text{and} \qquad d\xi = R\,d\theta .$$

Combining (2.6), (2.7), and (2.8),

$$dm_j\, v_j \frac{d\theta}{dt} = \rho_j y_j v_n^2 C_D\, d\xi$$

$$\therefore \quad \pi y_j^2 \rho_j v_j \frac{d\theta}{dt} d\xi = \rho_j y_j v_n^2 C_D\, d\xi$$

giving

$$\frac{d\theta}{d\xi} = \frac{C_D}{\pi y_j}\left(\frac{v_n}{v_j}\right)^2 = \frac{C_D}{\pi y_j}\left(\frac{v_F}{v_j}\right)^2 \cos^2\theta . \tag{2.9}$$

The assumption of conservation of momentum in the vertical direction supplies the condition that

$$d\dot{m}_{j_o}(v_{j_o}\cos\theta_o) = d\dot{m}_j(v_j\cos\theta)$$

where

$$d\dot{m}_{j_o} = \frac{\pi D^2}{4}\rho_{j_o} v_{j_o}$$

$$d\dot{m}_j = \pi y_j^2 \rho_j v_j \tag{2.10}$$

Combining these equations, one obtains

$$y_j = \frac{D}{2}\left(\frac{v_{j_o}}{v_j}\right)\left[\frac{\cos\theta_o}{\cos\theta}\right]^{\frac{1}{2}} ,$$

which, when substituted into (2.9), gives

$$\frac{d\theta}{d(\xi/D)} = \frac{2C_D}{\pi} \frac{v_F^2}{v_J v_{J_0}} \sqrt{\cos^5 \theta} \qquad (2.11)$$

where $\theta_0 = 0$ and $C_D = 1.25$ in Kirkpatrick's analysis.

3. Calculations

Using a Runge-Kutta scheme of integration, Kirkpatrick calculated the jet coordinates. Letting θ be the total angle of inclination, the differential equation describing the local jet angle is in the form

$$d\theta = \frac{d\theta_M(\theta, \xi/D)}{d(\xi/D)} d\left[\frac{\xi}{D}\right] + \frac{d\theta_D(\theta, \xi/D)}{d(\xi/D)} d\left[\frac{\xi}{D}\right].$$

This equation is non-linear, and thus care must be taken to use the current value of the local angle in the step-wise integration. The actual coordinates of the jet are then determined from

$$\frac{X_K}{D} = \frac{X_{K-1}}{D} + \sin(\theta_{K-1} + d\theta_K)\, d\left[\frac{\xi}{D}\right]$$

$$\frac{Z_K}{D} = \frac{Z_{K-1}}{D} + \cos(\theta_{K-1} + d\theta_K) d\left[\frac{\xi}{D}\right].$$

4. Remarks

Kirkpatrick has thus taken the results of free-jet and parallel-jet studies and has applied these results to the analysis of a jet in a cross-wind. The assumption that the velocity decay of a curved jet

may be correlated to the velocity decay of a free jet is of considerable practical significance, since free jets are relatively easy to investigate experimentally and are amenable to straightforward analysis. The centerline decay and the corresponding equivalent velocity decay used by Kirkpatrick are shown in Figure 2.5. The resulting jet paths are given in Figure 2.6.

Kirkpatrick concludes that the jet path is dependent on two parameters, the ratio of initial jet velocity to free stream velocity, and the initial angle of the jet with respect to the free stream.

D. REVISED ANALYSIS OF THE JET IN A CROSS-WIND

The conclusions of Kirkpatrick's analysis are significant but are not a complete evaluation of the problem. Also, several changes in the analysis are indicated when it is examined carefully.

1. The Momentum Analysis

Until quantitative measurements can be made to show otherwise, there is no compelling reason to question the assumption that the jet centerline velocity behaves according to equation (2.2). Therefore, the present analysis will use the results of Kirkpatrick's momentum considerations.

2. Structure of the Jet and the Drag Model

Experiments [9 & 10] have shown that the jet does not remain circular as implied by equation (2.10). After a distance of two or

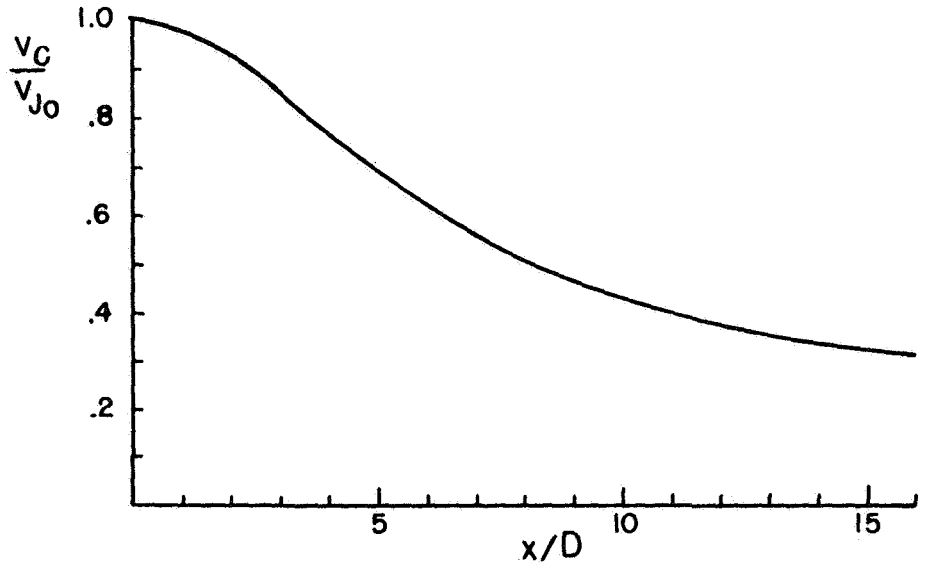

(a) Centerline velocity decay

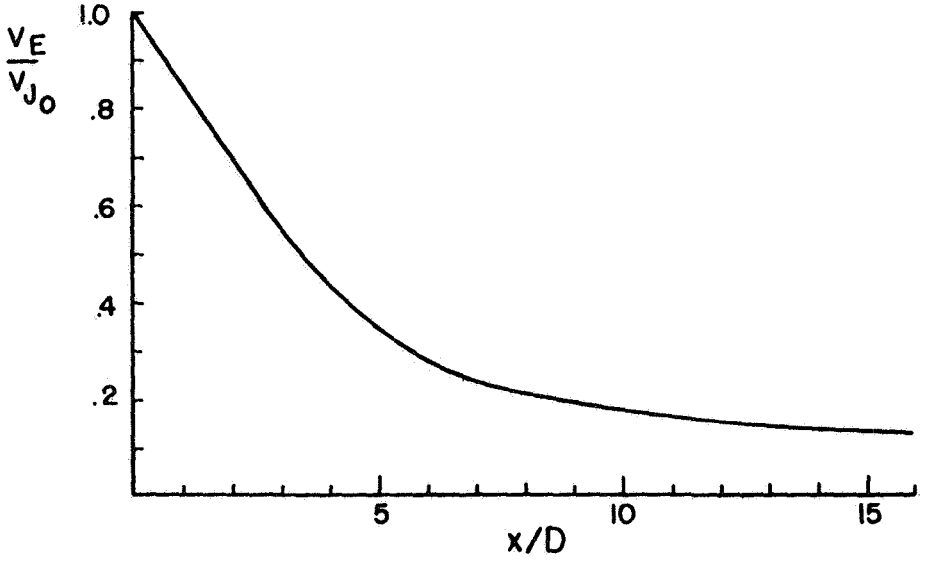

(b) Equivalent velocity decay

FIGURE 2.5 - Kirkpatrick's velocity decays

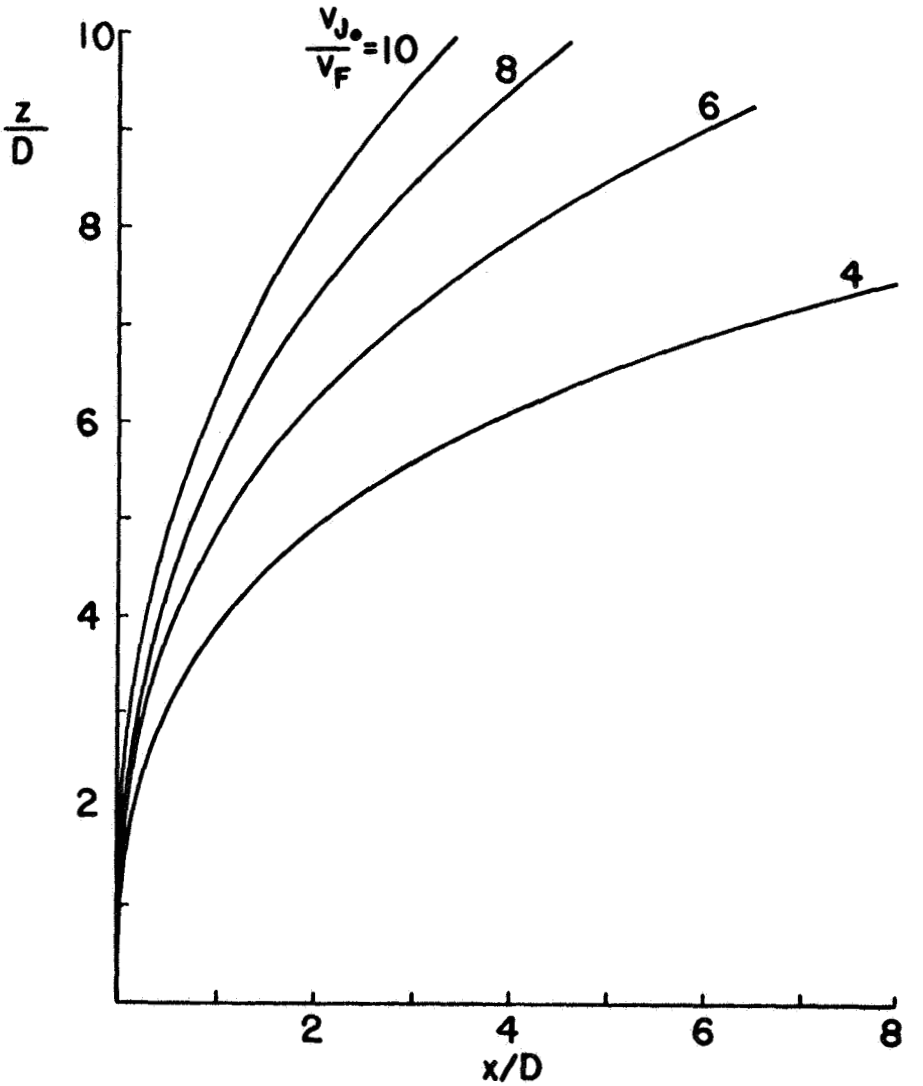

FIGURE 2.6 - Kirkpatrick's jet paths

three diameters along the centerline, the cross sectional shape of the jet, viewed normal to the centerline, assumes a kidney shape, as shown in Figure 2.7. This shape is maintained as the distance from the orifice is increased. Letting

$$S_J = S_J(\xi)$$

be the cross sectional area of the jet at ξ, then the mass of a jet element is given by

$$dm_J = \rho_J S_J \, d\xi ;$$

$$dF_D = \frac{1}{2} \rho_J v_n^2 C_D (2 y_J \, d\xi) , \tag{2.12}$$

and

$$\begin{aligned} dF_c &= \rho_J S_J \, d\xi \frac{d\theta}{dt} v_J \\ &= \rho_J S_J v_J^2 \, d\theta \end{aligned} \tag{2.13}$$

where y_J is the half-width of the jet. Equating (2.12) and (2.13) and simplifying,

$$\begin{aligned} \frac{d\theta}{d\xi} &= C_D \frac{y_J}{S_J} \left(\frac{v_n}{v_J}\right)^2 \\ &= C_D \frac{y_J}{S_J} \left(\frac{v_F}{v_J}\right)^2 \cos^2\theta . \end{aligned} \tag{2.14}$$

Conservation of momentum in the vertical direction gives the condition that

$$d\dot{m}_{J_o} v_{J_o} \cos\theta_o = d\dot{m}_J v_J \cos\theta$$

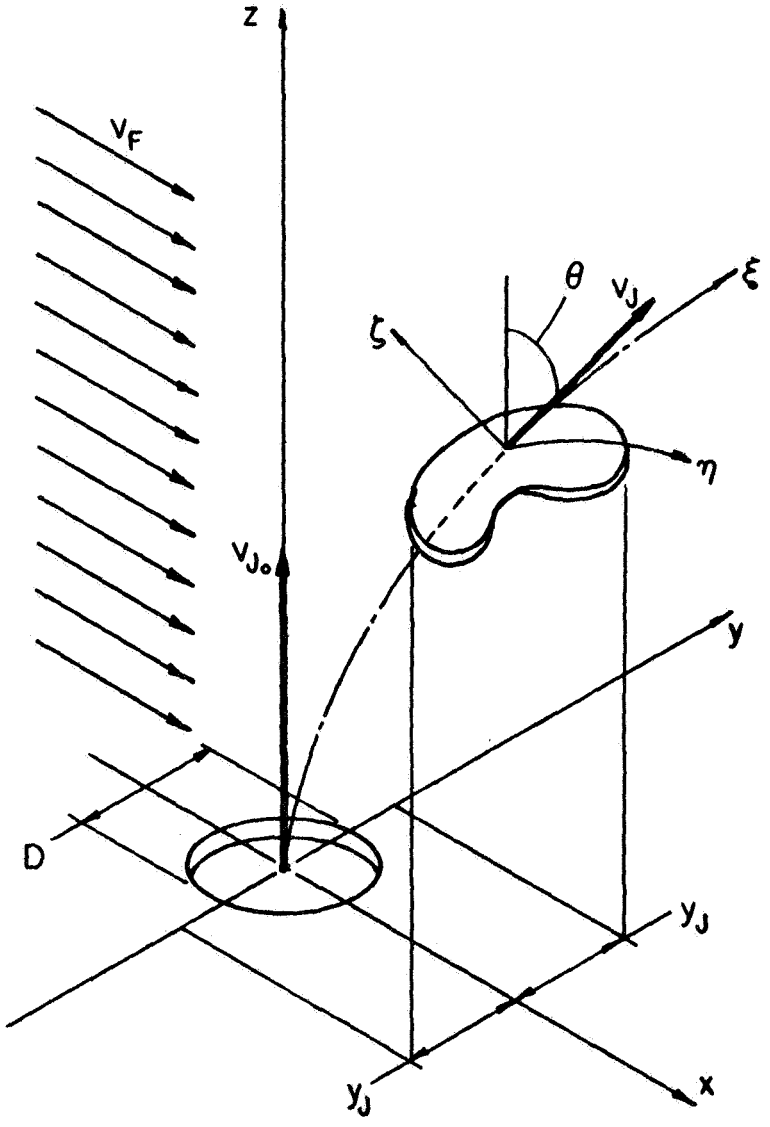

FIGURE 2.7 - Structure of a curved jet

where

$$d\dot{m}_{J_o} = \frac{\pi D^2}{4} \rho_{J_o} v_{J_o}$$

$$d\dot{m}_J = S_J \rho_J v_J$$

Combining and simplifying,

$$S_J = \left(\frac{v_{J_o}}{v_J}\right)^2 \frac{\pi D^2}{4} \frac{\cos\theta_o}{\cos\theta}$$

Substituting into (2.14) one finds the drag contribution to curvature to be

$$\frac{d\theta}{d(\xi/D)} = \frac{4C_D}{\pi} \left(\frac{v_F}{v_{J_o}}\right)^2 \left(\frac{y_J}{D}\right) \cos^3\theta \qquad (2.15)$$

A drag coefficient of 1.16 was chosen for this investigation, since this is an accepted empirical drag coefficient for a cylindrical semi-shell. Values for y_J/D were taken from experimental pressure distribution measurements [9], since no analysis is currently available to describe the growth or distortion of the kidney shape. A polynomial fit was made to the experimental jet width data as shown in Figure 2.8. Due to the lack of data at both the lower and the higher values of the initial jet-to-free-stream velocity ratio, this analysis is restricted to the range of v_{J_o}/v_F between four and ten.

3. Velocity Distribution & the Momentum Factor

Since both analyses depend upon the assumption that the free jet can be related to the curved jet, it seemed constructive to investigate free jet characteristics in more detail.

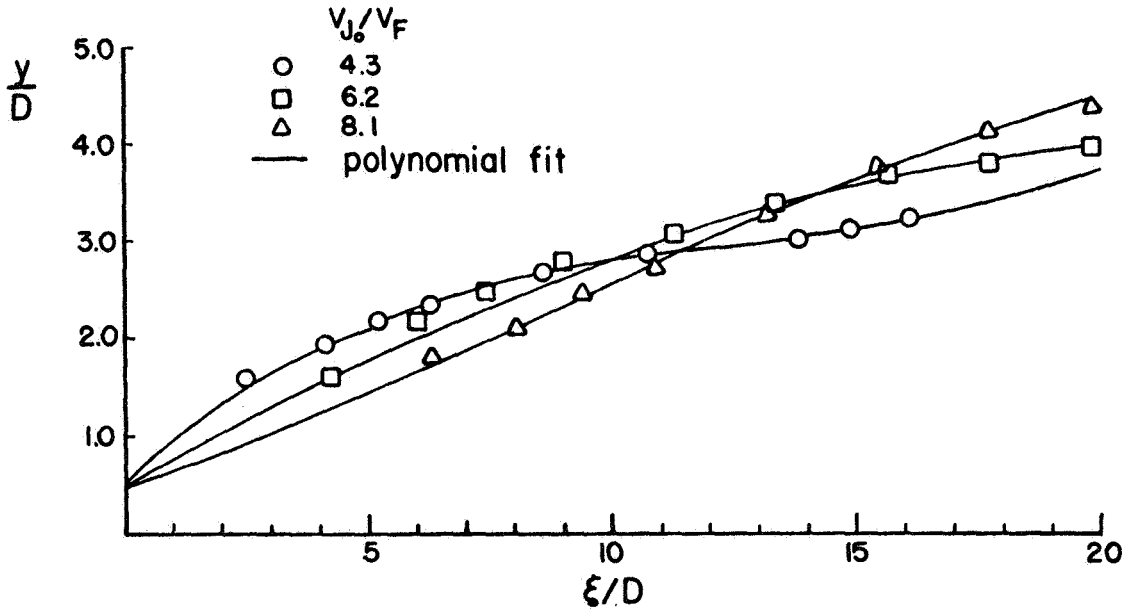

FIGURE 2.8 - Jet spreading

Kirkpatrick's analysis calls for a circular, axisymmetric, free jet, yet the centerline velocity decay which he introduced into his analysis is not that of such a jet. Nor is the equivalent velocity analysis consistent with other theoretical and experimental analyses of axially symmetric jets. One such analysis was carried out extensively by Warren [17], and the following is a summary of this work as well as an application of it to the determination of the equivalent velocity decay. The methods developed here can be extended to other types of jets, e.g., those issuing from non-circular orifices. However axisymmetric jets are more amenable to this treatment because of their symmetry and because of the existence of similarity within the jet itself, and therefore are considered here in order to present the methods involved in finding the equivalent jet characteristics.

As was noted in part B, free jets may be considered in two parts: the core region and the developed region. Centerline velocity decay in the core region is negligible. In the developed region, decay occurs in two stages; a characteristic decay, dependent on the jet orifice geometry, followed by an axisymmetric decay region. It is meant by axisymmetric decay that the centerline velocity decays as $1/X$ (Figure 2.9b)

At any axial, or X, location, Warren finds that the velocity profiles normal to the centerline may be given by the following expressions:

In the core region:

$$\frac{v_P}{v_c} = \begin{cases} 1.00 & (y \le y_i) \\ e^{-.6932\left[\frac{y^2 - y_i^2}{y_s^2 - y_i^2}\right]} & (y > y_i) \end{cases} \tag{2.16}$$

and in the developed region:

$$\frac{v_P}{v_c} = e^{-.6932\left(\frac{y}{y_s}\right)^2} \tag{2.17}$$

The parameters y_i (core width), y_s (width at which $v_P = \frac{1}{2} v_c$), and v_c (the centerline velocity) are functions of axial position and are calculated from the following equations:

In the core region,

$$\frac{v_c}{v_{J_o}} = 1.00$$

$$\left(\frac{y_i}{D}\right)^2 = \alpha - \beta\left(\frac{y_s}{D}\right)^2$$

$$K\frac{x}{D} = 1.8673\left\{\left(\frac{y_s}{D}\right)^2 + \left(\frac{y_i}{D}\right)^2 - \alpha^{\frac{1}{2}} \ln\left[\frac{\alpha^{\frac{1}{2}} + \left(\frac{y_i}{D}\right)}{\beta^{\frac{1}{2}}\left(\frac{y_s}{D}\right)}\right] - .4438\right\} \tag{2.18}$$

where $\alpha = .8972$, $\beta = 2.5887$, and $K = .0434$.

In the developed region,

$$\frac{v_c}{v_{J_o}} = \frac{.30629}{.03654 + K\frac{x}{D}} \tag{2.19}$$

$$\frac{y_s}{D} = \frac{.5887}{\left(\frac{v_c}{v_{J_o}}\right)}$$

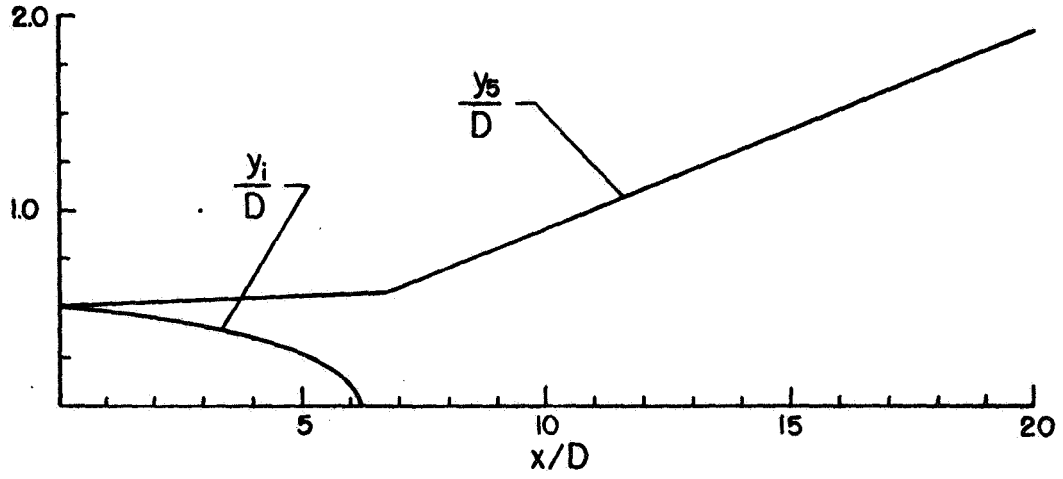

(a) Jet geometry

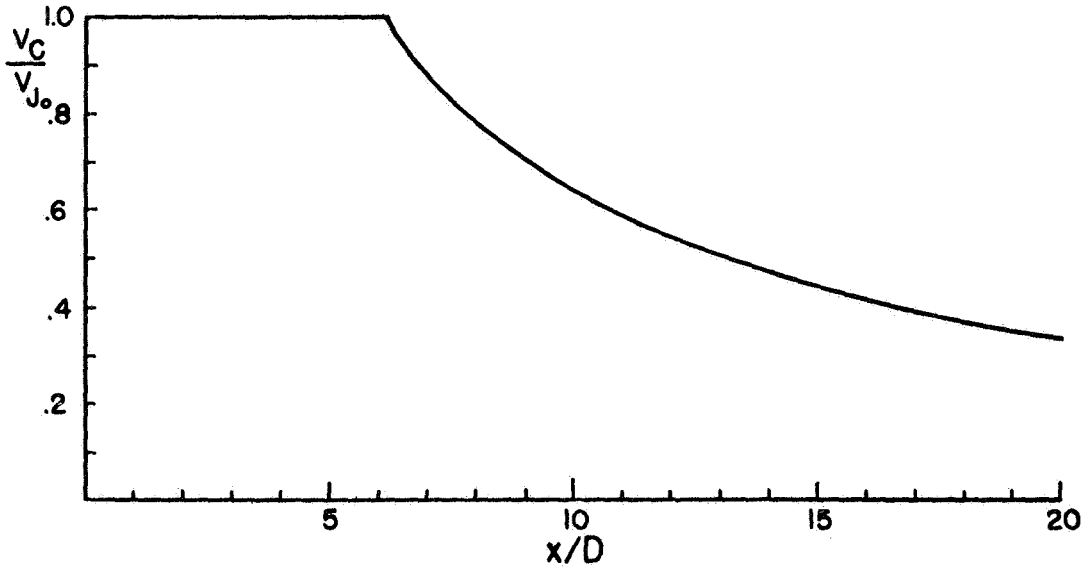

(b) Centerline velocity decay

FIGURE 2.9 - Warren's jet's characteristics

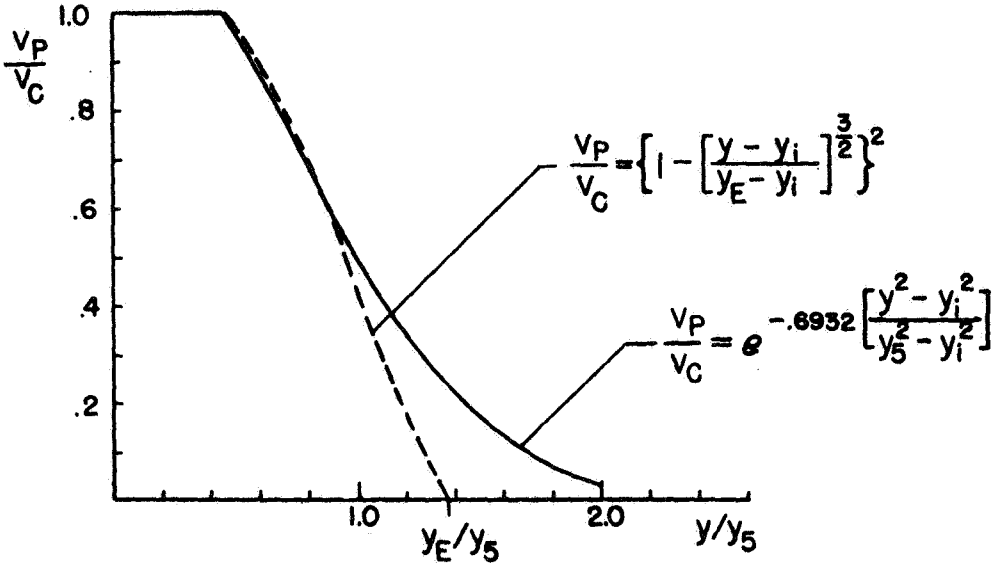

(c) Assumed jet profile in core region

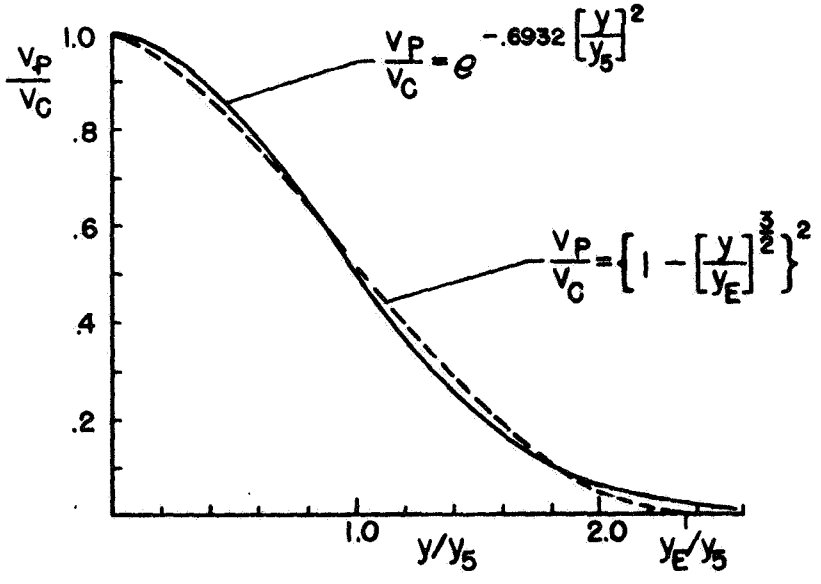

(d) Assumed jet profile in developed region

FIGURE 2.9 - Concluded

(For a detailed description of the derivation of these expressions, the reader is directed to Warren's thesis.) Figure 2.9 shows the properties of Warren's jet as described by these equations.

The equivalent velocity, v_E , has been described as that uniform profile velocity which passes the same momentum flux as does the actual jet, through a finite area of radius y_E . That is

$$\int_0^{y_E} \rho_j v_E \cdot v_E \, 2\pi y \, dy = \int_0^{\infty} \rho_j v_p \cdot v_p \cdot 2\pi y \, dy$$

$$\therefore \quad v_E^2 y_E^2 = \int_0^{\infty} v_p^2 \, dy^2 \tag{2.20}$$

One may define a momentum factor, f, such that:

$$f v_c^2 = v_E^2$$

Thus

$$f = \frac{1}{y_E^2} \int_0^{\infty} \left(\frac{v_p}{v_c}\right)^2 d y^2 \tag{2.21}$$

where v_p/v_c is given by equations (2.16) and (2.17). Alternative expressions for these velocity profiles are also given by Warren. In the core region,

$$\frac{v_p}{v_c} = \begin{cases} 1.00 & (y \le y_i) \\ \left[1 - \left(\frac{y - y_i}{y_E - y_i}\right)^{\frac{3}{2}}\right]^2 & (y > y_i) \end{cases} \tag{2.22}$$

and in the developed region,

$$\frac{v_p}{v_c} = \left[1 - \left(\frac{y}{y_E}\right)^{\frac{3}{2}}\right]^2 \tag{2.23}$$

Defining y_E as the radius at which the polynomial profiles (2.22) and (2.23) pass the same mass flux as (2.16) and (2.17), one may write

$$\int_o^\infty \rho_J [v_p]_{EXP} 2\pi y dy = \int_o^{y_E} \rho_J [v_p]_{POLY.} 2\pi y dy$$

$$\therefore \int_o^\infty [v_p]_{EXP} dy^2 = \int_o^{y_E} [v_p]_{POLY} dy^2 \qquad (2.24)$$

Making the proper substitutions into (2.24), integrating, and simplifying, it can be shown that the resulting equation for y_E in the core region is

$$y_E^2 + 1.5\, y_E y_i - (5.6101\, y_s^2 - 3.1101\, y_i^2) = 0 \qquad (2.25)$$

Substituting (2.18) into (2.25):

$$\left(\frac{y_E}{D}\right)^2 + 1.5\left(\frac{y_E}{D}\right)\left(\frac{y_i}{D}\right) - \left[1.9445 - 5.2773\left(\frac{y_i}{D}\right)^2\right] = 0$$

giving

$$\frac{y_E}{D} = -.75\,\frac{y_i}{D} + \sqrt{1.9445 - 4.7148\left(\frac{y_i}{D}\right)^2} \qquad (2.26)$$

Similarly, for the developed region,

$$\frac{y_E}{D} = 2.3686 \frac{y_5}{D} \tag{2.27}$$

Using (2.22) and (2.23) in (2.21), the momentum factor, f, may be found.

In the core region:

$$f = \left(\frac{y_i}{y_E}\right)^2 + .1335\left(\frac{y_E - y_i}{y_E}\right)^2 + .6532 \frac{y_i(y_E - y_i)}{y_E^2} \tag{2.28a}$$

and in the developed region

$$f = .1335 \tag{2.28b}$$

In the developed region, f is found to be a constant because of the close similarity between the jet velocity profiles in this region at successive downstream locations in this region. That is, the jet profiles can expressed as a single function of y/y_5 . In the core region, however, the profiles are dependent on the core width, y_i , as well as y/y_5 . Knowing f, the equivalent velocity can be found by:

$$\frac{v_E}{v_{J_o}} = \frac{v_c}{v_{J_o}} \sqrt{f} \tag{2.29}$$

The equivalent velocity decay for Warren's jet was calculated and is shown in Figure 2.10. A fifth order least squares polynomial fit was made to the calculated decay for use in the analysis and is shown in Figure 2.10.

4. Calculations

A Runge-Kutta integration scheme was used to calculate the jet paths. The basic procedure used by Kirkpatrick was adapted to the revised analysis described above with the end result being the x/D and z/D coordinates of the jet centerline.

5. Remarks

Kirkpatrick concluded that the jet path is dependent only upon the initial jet angle and the ratio of initial jet velocity to free stream velocity. It is felt as a result of the present investigation that, although this simple dependence may be true for one particular jet, the most important consideration in the general case is the ratio of the local equivalent jet velocity (2.2) to the component of the free stream velocity parallel to the jet. Of secondary importance is the method of representing the aerodynamic forces on the jet. Of still lesser importance is the selection of a proper drag coefficient for any given method. To demonstrate these results several cases were considered and their resulting jet paths calculated.

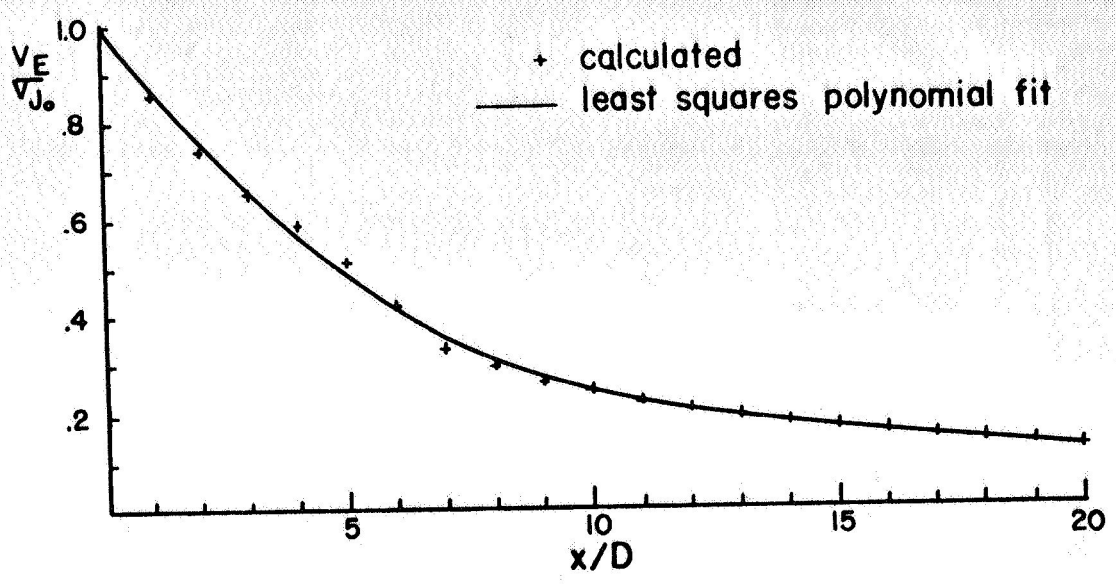

FIGURE 2.10 - Equivalent velocity decay for Warren's jet

Case i. Varying the drag model (Figure 2.11).

Using the revised drag analysis and the equivalent velocity decay chosen by Kirkpatrick (Figure 2.5b), the jet paths were found. Comparing these paths to Kirkpatrick's original results, it appears that Kirkpatrick underestimated drag at the lower velocity ratios, and overestimated it for the higher velocity ratios. Note, however, that at the higher velocity ratios the drag model does not seem as important.

Case ii. Varying drag coefficient (Figure 2.12).

Using the revised analysis, including in it the equivalent velocity calculated for Warren's jet, the jet paths were determined. By changing the drag coefficient from that of bluff solid to that of a cylindrical semi-shell, it was found that the path coordinates were not affected to a large extent. Therefore it was decided that a further revision of the analysis to account for the change from circular to kidney-shaped cross sections by varying the drag coefficient along the length of the jet would not be worth while.

Case iii. Effects of equivalent velocity decay (Figure 2.13)

Again using the revised analysis with a drag coefficient of 1.16, jet paths were found for three different equivalent velocity decays:

(a) Kirkpatrick's equivalent velocity (Figure 2.5b)

(b) Equivalent velocity decay for Warren's jet (Figure 2.10)

(c) The centerline velocity decay of Figure 2.5a.

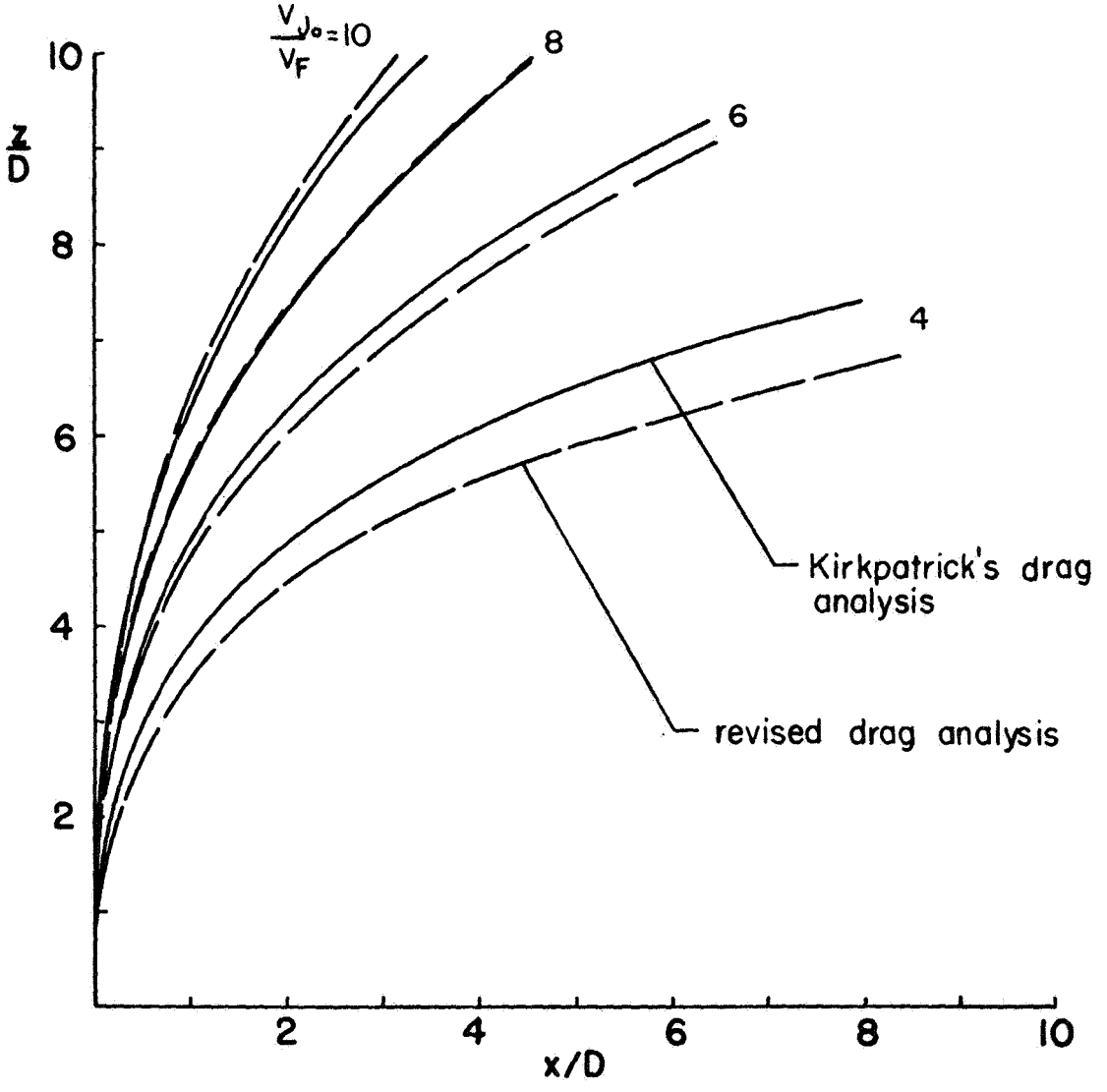

FIGURE 2.11 - Effects of the drag model. (Case i.)

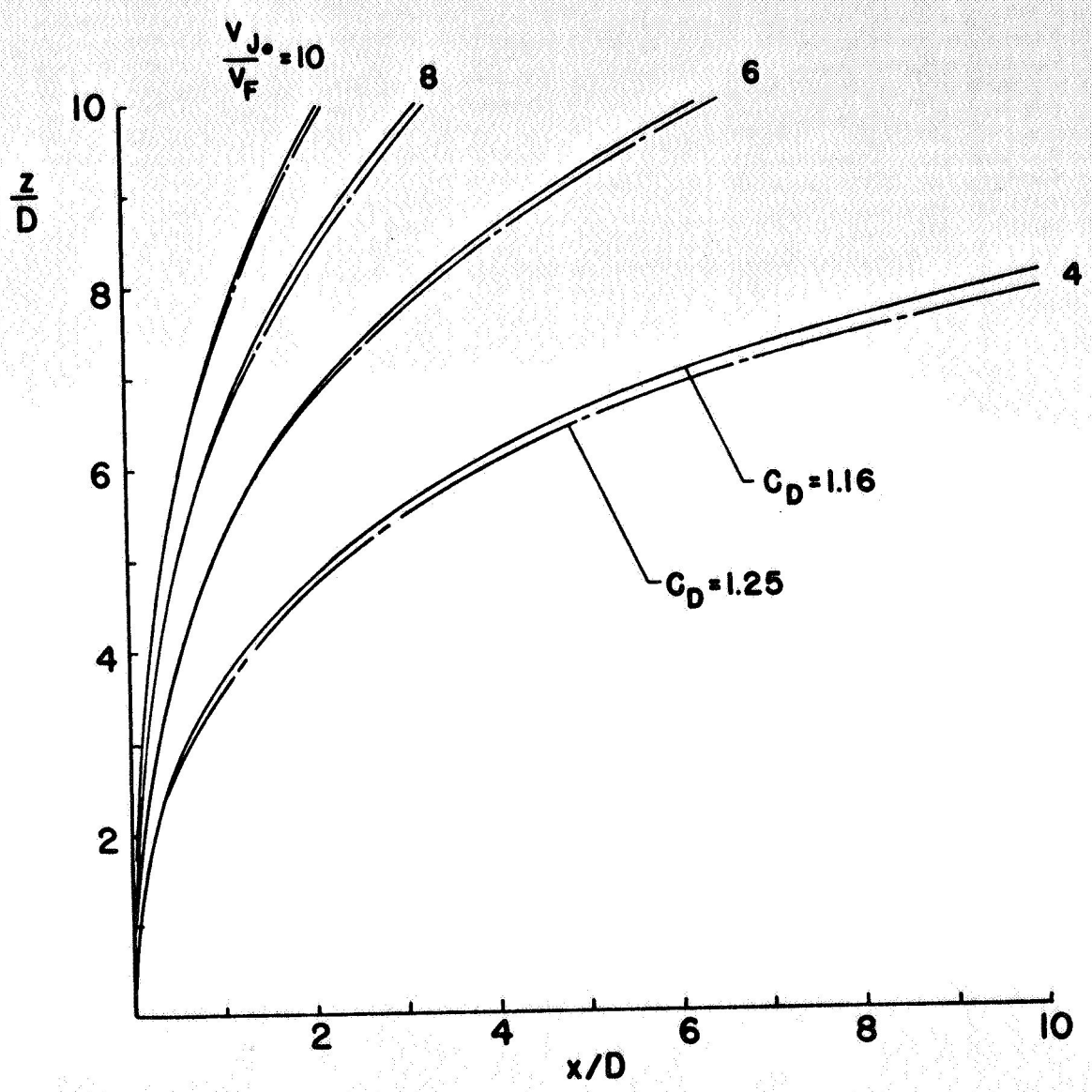

FIGURE 2.12 - Effect of drag coefficient using revised analysis. (Case ii.)

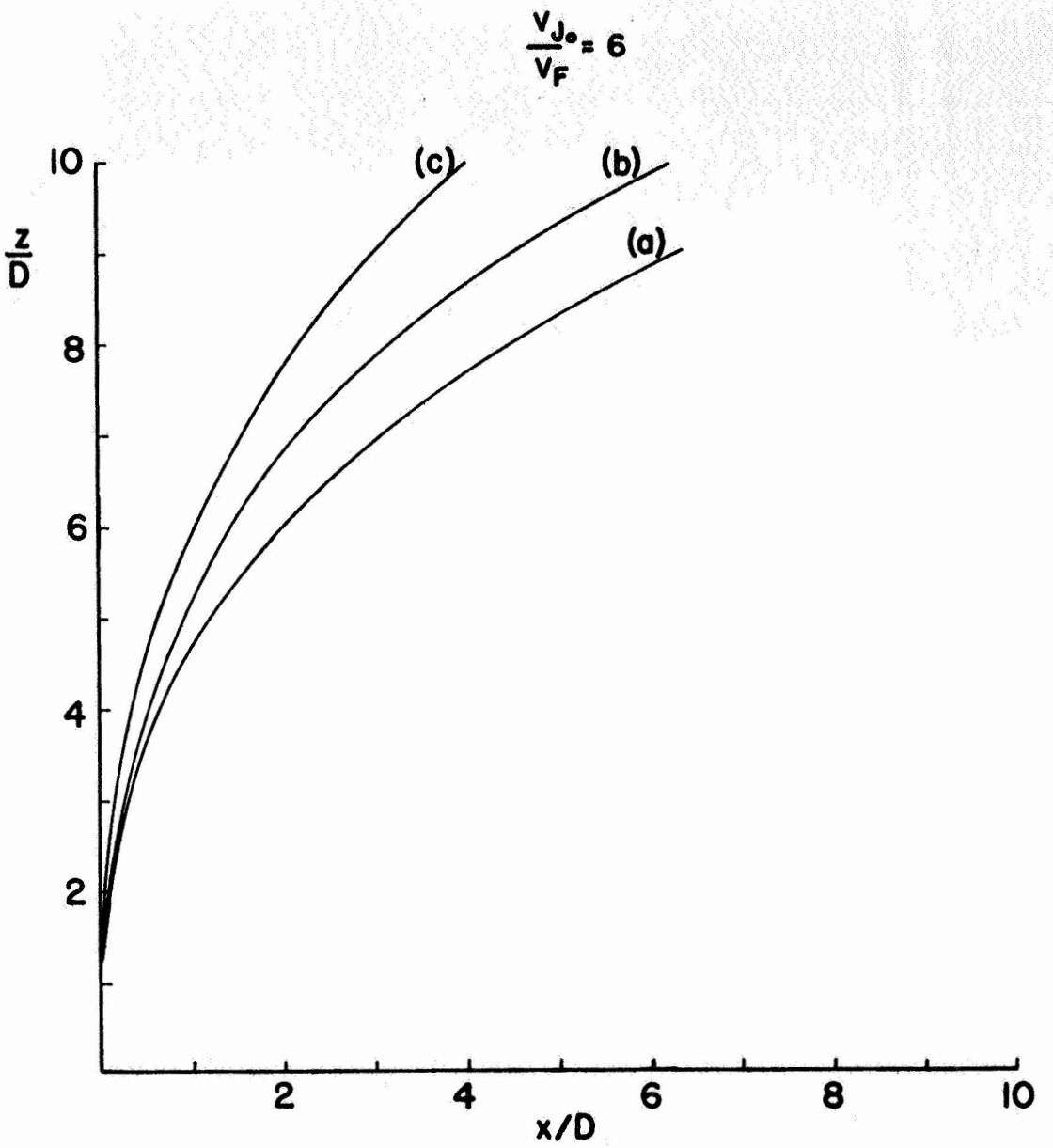

FIGURE 2.13 - Continued

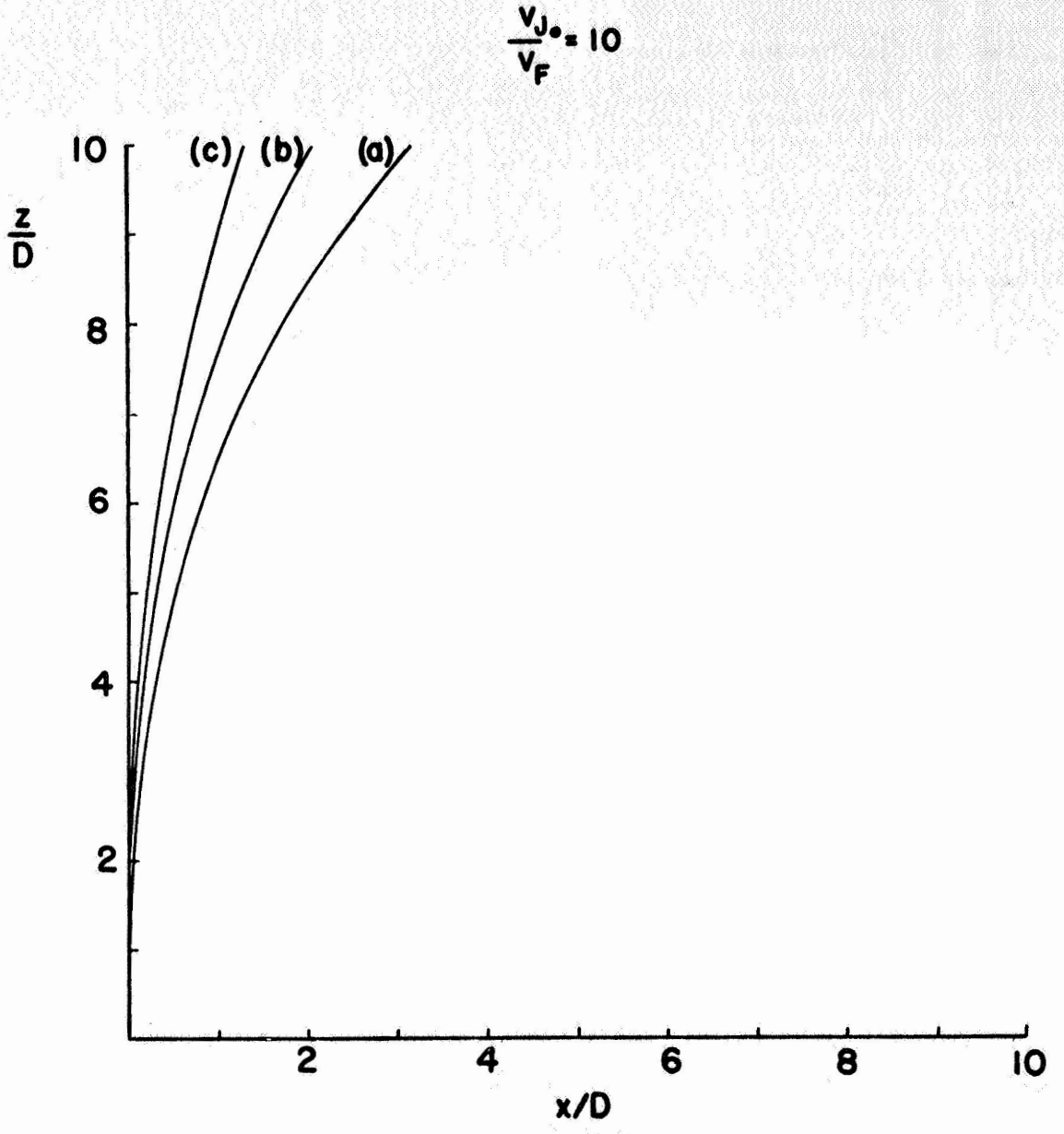

FIGURE 2.13 - Concluded

The importance of the equivalent velocity decay at all velocity ratios is clearly evident. This rate of decay is the most important single parameter contributing to the jet curvature. Curve (a) represents the fastest rate of decay and thus is effected by the cross-wind sooner than the others, whereas curve (c) has the slowest rate and therefore is not effected as much.

6. Discussion

This analysis of the jet in a crosswind indicates that the characteristic manner in which each jet distributes its initial momentum is the most influential factor in determining the jet curvature. As a result of this analysis one may expect jets having different spreading and decay characteristics to follow different paths even though their initial inclination, velocity, and free stream environments are identical.

The effect of turbulent mixing is, of course, to reduce the local momentum of the jet by spreading it over a larger area, thereby causing a decay in the dynamic pressure at the centerline as well as across the width of the jet. Therefore, a jet which is characterized by early mixing can be expected to penetrate into the cross-wind less than one which has delayed mixing.

A mathematical method for treating an axisymmetric jet has been presented above. This method may be expanded to treat jets of different geometries provided sufficient experimental velocity decay

and profile data, comparable to Warren's work, are available on which the extension can be based. Lack of existing experimental information dictates that sufficient tests be made on the free jet to determine the momentum factor and equivalent velocity by methods similar to those presented herein.

Once sufficient information concerning the free jet is on hand, it is felt that the present analysis offers the best available method for predicting jet paths. To demonstrate this point and to illustrate the methods involved, an experimental program has been undertaken as described in the subsequent sections.

CHAPTER III

EXPERIMENTAL STUDIES

A. PREVIOUS EXPERIMENTAL STUDIES

The calculations made in Chapter II were first compared to previous experimental observations of jet-crosswind interactions in order to estimate the accuracy of the analytical model. In reviewing the experimental observations, it was found that among the several investigators there was a wide spread of the jet paths observed at any one velocity ratio, v_{J_o}/v_F. However, in light of the conclusions of the analysis, this lack of correlation between various experiments is not surprising. That is, no two jet paths will be the same unless all of the free jet characteristics which produced them are identical. No attempt was made among the various studies to match the experimental conditions which generated the jets.

A secondary cause of the difference in the observed paths is the effect of the tunnel walls. Storm [16] has shown that the walls do have some effect on the jet path. The results of the previous experimental studies of jet-crosswind interactions are presented in Figure 3.1. Table 3.1 presents basic information relative to the jet studies.

Margason, Storm, and Callaghan and Ruggeri all give their results in the form of empirical equations. These are, respectively,

$$\frac{x}{D} = \frac{\frac{z}{D}}{4\left(\frac{v_{J_o}}{v_F}\right)^2 \cos^2\theta_o} + \frac{z}{D}\tan\theta_o \qquad (3.1)$$

TABLE 3.1

Investigator	Jet Location	Test Section	Jet Diameter
Margason	mid-stream	7'× 10'	1"
Storm [16]	wall	30" hexagon	.55"
Jordinson [9]	wall	5'× 1'	.50", 1.00"
Keffer and Baines [10]	wall	4'× 10'	.375"
Callaghan and Ruggeri [3]	wall	2"× 12"	.25", .375", .50", .625"

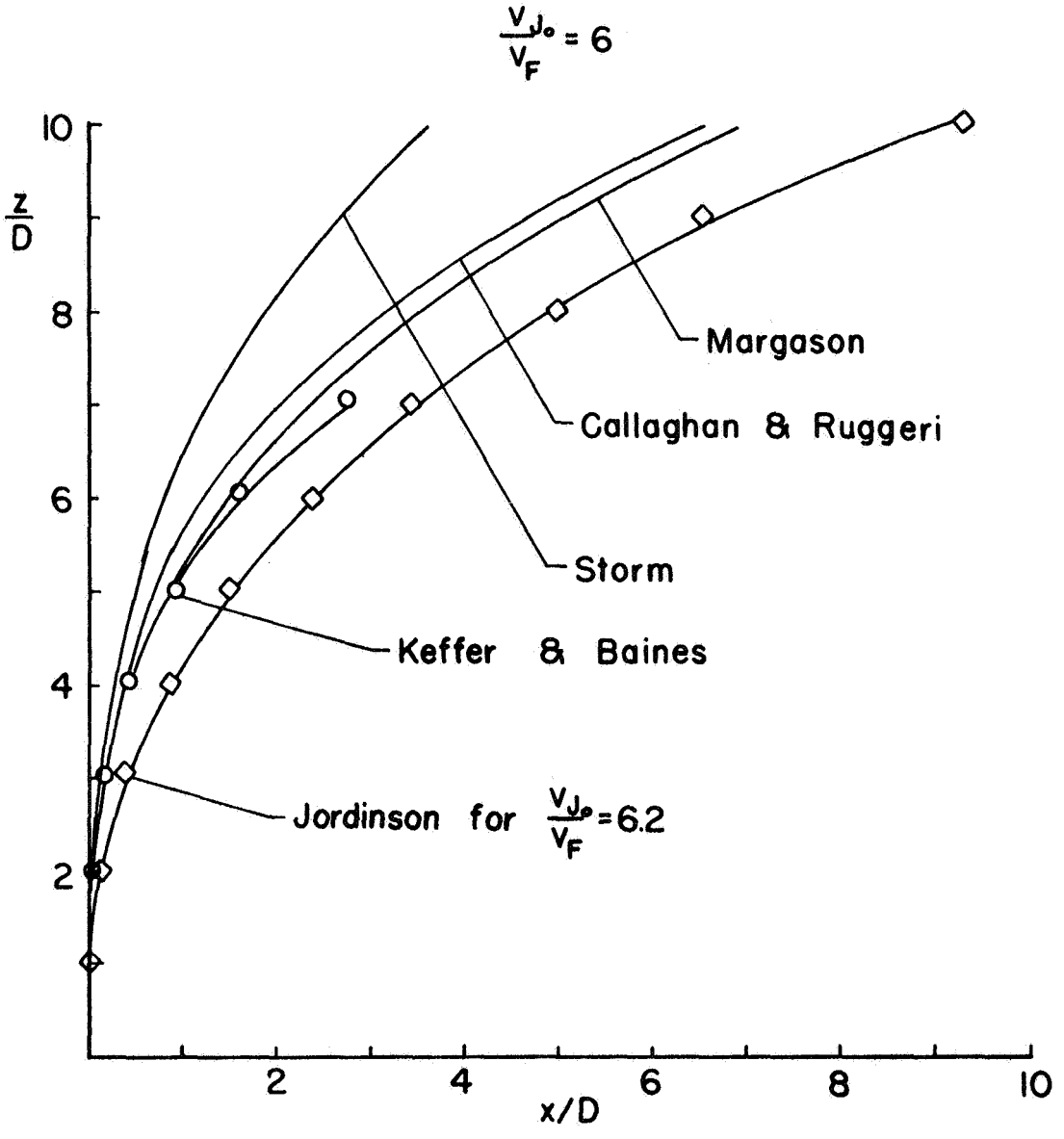

FIGURE 3.1 - Continued

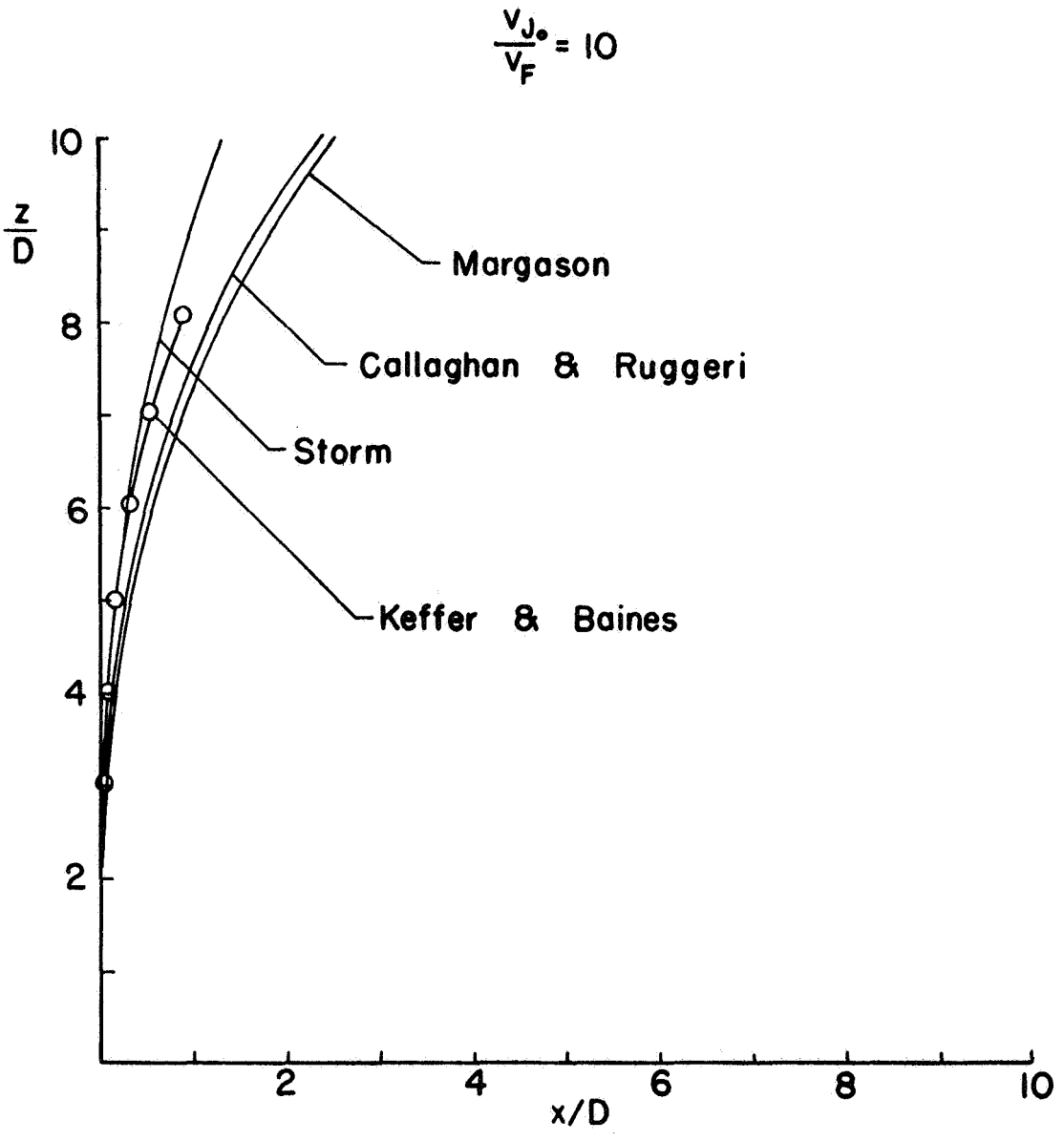

FIGURE 3.1 - Concluded

$$\frac{x}{D} = \frac{0.13}{\left(\frac{U_{J_o}}{U_F}\right)^2}\left(\frac{z}{D}\right)^3 \tag{3.2}$$

$$\left(\frac{z}{D}\right)^{1.65} = 2.91\left(\frac{U_{J_o}}{U_F}\right)\left(\frac{x}{D}\right)^{\frac{1}{2}} \tag{3.3}$$

B. PURPOSES OF THE PROGRAM

Since past experimental studies did not give sufficient information to check the analysis in Chapter II, an experimental program was undertaken in the present study with the following primary objectives in mind:

i. Determine the free jet characteristics of two distinct jets and apply, where possible, the free jet analysis described in Chapter II.

ii. Determine the dependence of the jet path curvature on the free jet centerline velocity decay.

iii. Determine the dependence of the jet path on the initial conditions of the test (the ratio of initial jet velocity to the free stream velocity).

iv. Provide an experimental check on the semi-empirical analysis developed in Section II. D.

In the remainder of this chapter is presented a review of the tests that were made, a description of the apparatus, an evaluation of the data, and a discussion of the results of the study. A comparison between the experimental results and the analysis is then made.

C. THE EXPERIMENTAL PROGRAM

Using total head measurements, a careful study was made of two different geometry jets issuing into quiescent air. Measurements were made in the incompressible range of jet velocities. Centerline velocity decay curves were obtained for several initial jet velocities to determine the effect of this parameter on the decay process. Profiles of the jet, normal to the centerline, were measured for a single initial jet velocity at many axial stations downstream from the orifice. In this way, the spreading characteristics were found, and the existence of similarity within the jets was examined.

Experimental data, in one case, were subjected to a rigorous application of the free jet analysis to determine the equivalent jet's characteristics heretofore described. This was accomplished by both a mathematical treatment and a graphical integration of the jet momentum profiles.

The jets were then introduced into a crosswind inside a wind-tunnel test section. Using flow visualization techniques, kerosene smoke was injected into the jet slipstream, and photographs were taken of both jets under the same initial conditions. The ratio of initial jet velocity to free stream velocity was changed by varying the former while keeping the latter constant. The jet paths were obtained from the photograph negatives by analyzing them with a micro-densitometer, and the effects of the velocity ratio on the jet path were determined.

By comparing the free-jet centerline velocity decay curves and the curved-jet paths of the two jets, the dependence of this path upon the free-jet centerline decay was determined.

Finally, using the calculated equivalent jet velocity, a comparison of the experiments and the analysis was made.

D. DESCRIPTION OF APPARATUS

1. Nozzle Design

The desire to investigate the effects of the centerline velocity decay on the curved-jet path required that two nozzles be designed which had significant differences in their free-jet characteristics. Another design consideration arose from the plan to apply the theoretical free-jet analysis to at least one of the jets. It was also desired to have nearly uniform and parallel flow at the orifice. Finally, it was desired that the two nozzles be designed to have the same exit area.

Using the observations of Higgins and Wainwright [8], it was concluded that the orifice geometry of the jets must be strikingly different to achieve notable differences in jet characteristics. To facilitate analysis, it was decided to construct one jet nozzle with a circular orifice; and, in order to minimize the wind-tunnel wall effects[4],

---

[4] See Chapter I.

the orifice was restricted to one-quarter of an inch in diameter. Comparing the jet characteristics of the various nozzle configurations investigated by Higgins and Wainwright, a rectangular slot nozzle of aspect ratio near five was noted to have significantly different characteristics from those of a circular nozzle. To maintain the same cross-sectional area at the slotted orifice as was present in the circular nozzle, the rectangular nozzle dimensions were selected to be one-tenth of an inch wide and four-hundred and ninety-one thousandths of an inch long, giving an aspect ratio near five.

The contraction section of the circular nozzle consisted of an axisymmetric contour designed to minimize skin friction and separation losses within the nozzle. The rectangular nozzle's contraction consisted of a horizontal two-dimensional contour followed by a vertical two-dimensional contour. Thus the fabrication of the nozzle was facilitated. It was hoped that by careful design, three-dimensional effects i.e., non-uniformities of the velocity in the corners, would be minimized. The nozzles were made from maple, sanded smooth, and the grain filled with a sanding sealer. Brass extensions were added to provide a method for introducing the jet into the windtunnel test section. Figure 3.2 presents the final nozzle designs.

Both nozzles were made to fit onto a 2.75"-I.D. plenum chamber. A fine mesh screen was placed before the contraction to reduce the turbulence intensity of the flow and to achieve a more nearly uniform

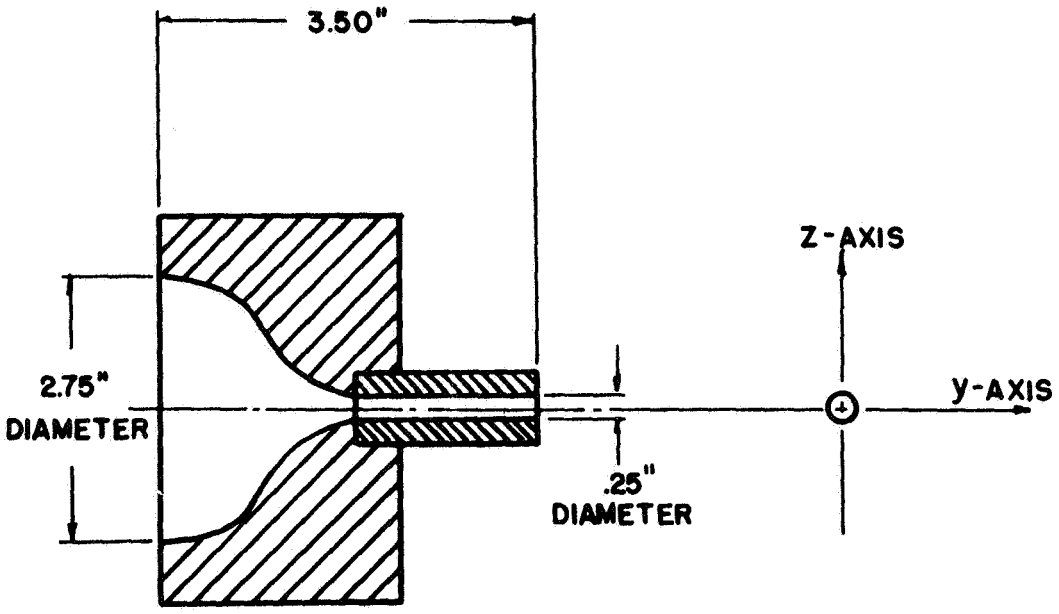

(a) Circular nozzle

FIGURE 3.2 - Nozzle configuration

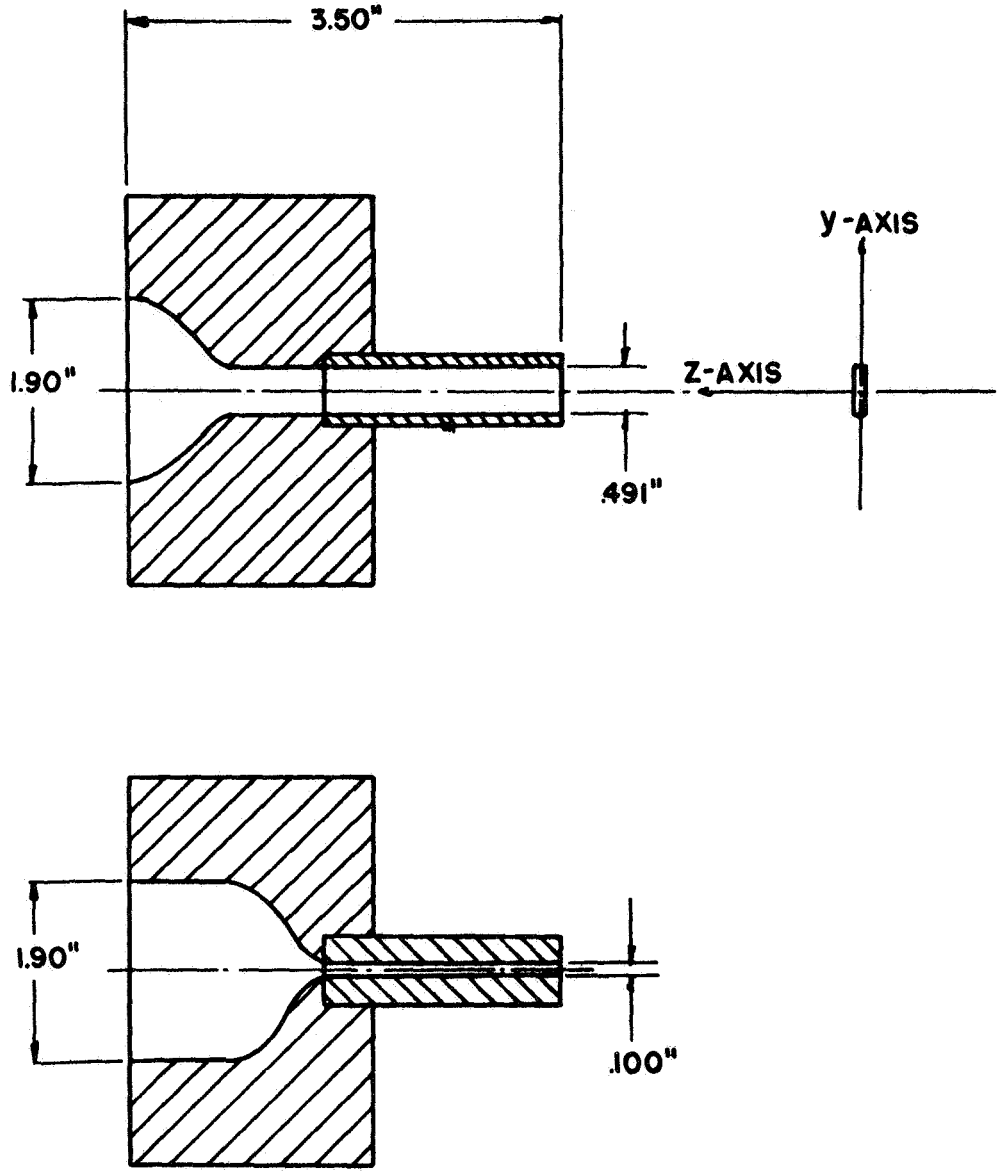

(b) Rectangular slot nozzle

FIGURE 3.2 - Concluded

distribution of the velocity. The plenum pressure was monitored during all tests to achieve the desired exit velocity from the nozzle. Figure 3.3 shows the plenum configuration.

The air supply to the plenum consisted of a 1000-cubic foot, high pressure storage tank which is a part of the University of Virginia's existing facilities. The plenum pressure was controlled by a Binks Air Pressure Regulator which maintained a constant downstream pressure.

2. The Wind-Tunnel

Investigations of jet-crosswind interactions were made in the University of Virgia 8.25-by-12-inch test section Pilot Wind-Tunnel shown in Figure 3.4. The flow in the test section was calibrated and found to be uniform to within 1% of the mean velocity. At the entrance of the test section, the boundary layer is approximately .15-inches thick, growing to a thickness of .30 inches at the exit. To reduce the effects of the tunnel boundary layer at the nozzle orifice, a one-eighth-inch thick boundary layer plate was placed in the test section at a height of three-quarters of an inch from the floor.

The plenum-nozzle assembly was attached beneath the test section, with the nozzle extension protruding through the tunnel floor and flush with the top surface of the boundary layer plate. The nozzle orifice was placed equidistant from the test section side walls and six inches downstream from the leading edge of the plate.

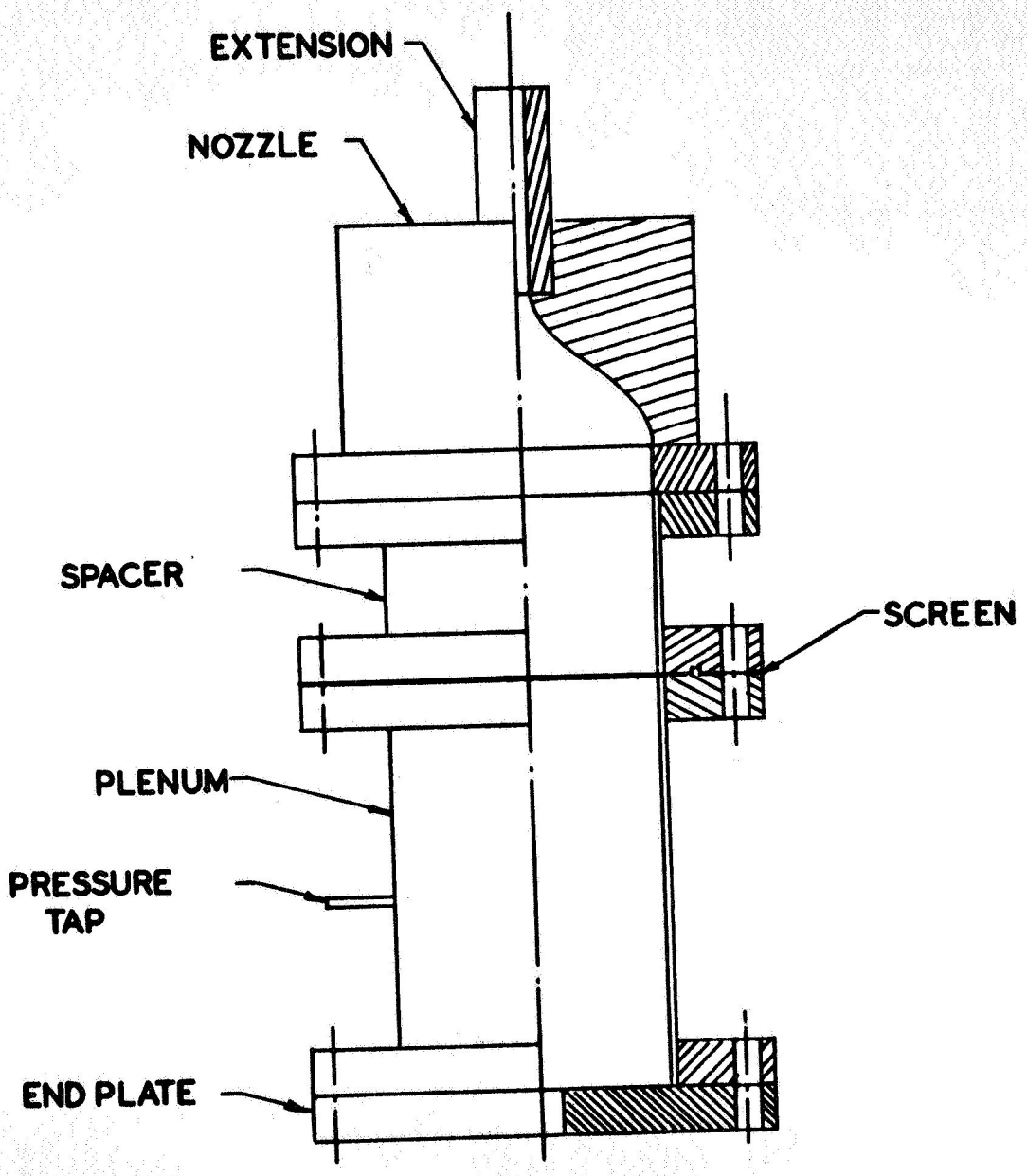

FIGURE 3.3 - Plenum configuration

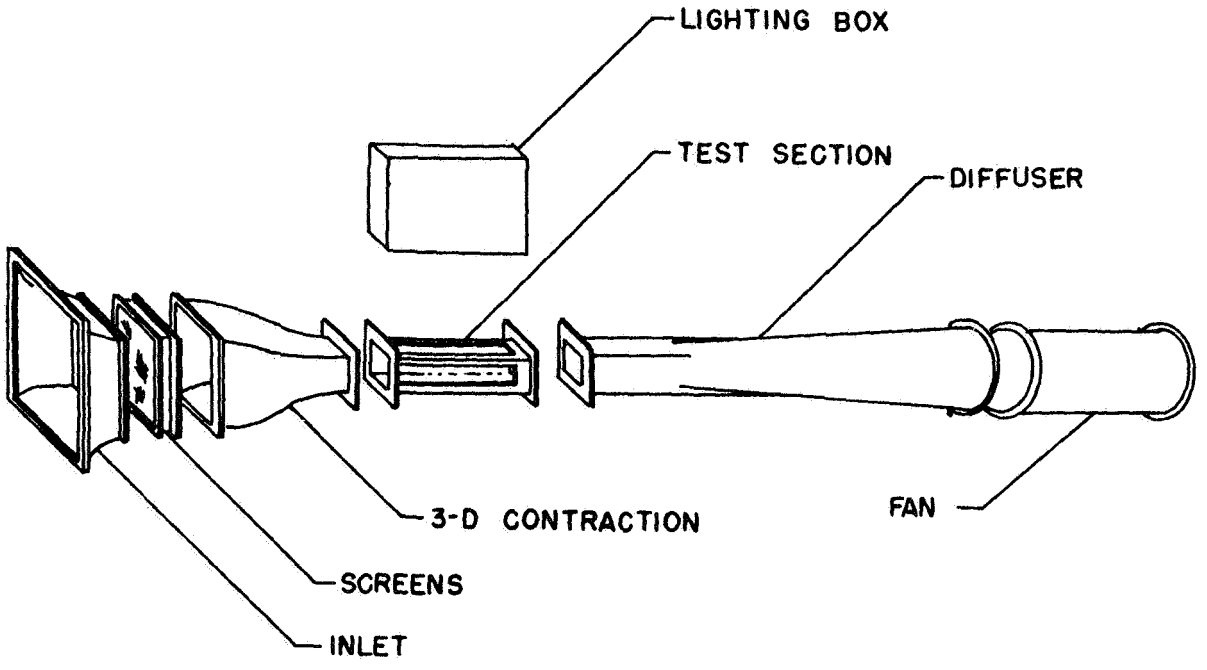

FIGURE 3.4 - University of Virginia Pilot Tunnel

3. The Smoke Generator

The flow visualization techniques employed in the jet crosswind experiments required the use of a smoke generator. The generator which was used was designed at the James Forrestal Research Center of Princeton University and has been used there in several flow visualization tunnels. The particular generator used herein was build at the University of Virginia.

The generator operates by boiling kerosene in a long, electrically-heated column. The resulting vapor is cooled to remove any condensate, and the remainder is a dense, white smoke which is both cool and dry. Kerosene smoke is superior to most other types of chemical vapors used in flow visualization because it is relatively clean, easy to produce and usually does not alter the phenomenon under investigation.

The odor produced by the smoke is non-toxic and is not disagreeable, although prolonged inhalation should be avoided. Care must be taken to prevent ignition of the smoke, even though there have been no reports to date of explosions using this type of equipment despite exposure to flame and electrical sparks.

Figure 3.5 provides an illustration of the smoke generator. The smoke is returned to the tank where the condensate is removed. It is then delivered to the desired location by 3/8-inch Tygon plastic tubing.

In the present experiments, the generator was placed directly into the air supply line to the plenum chamber. A back pressure had

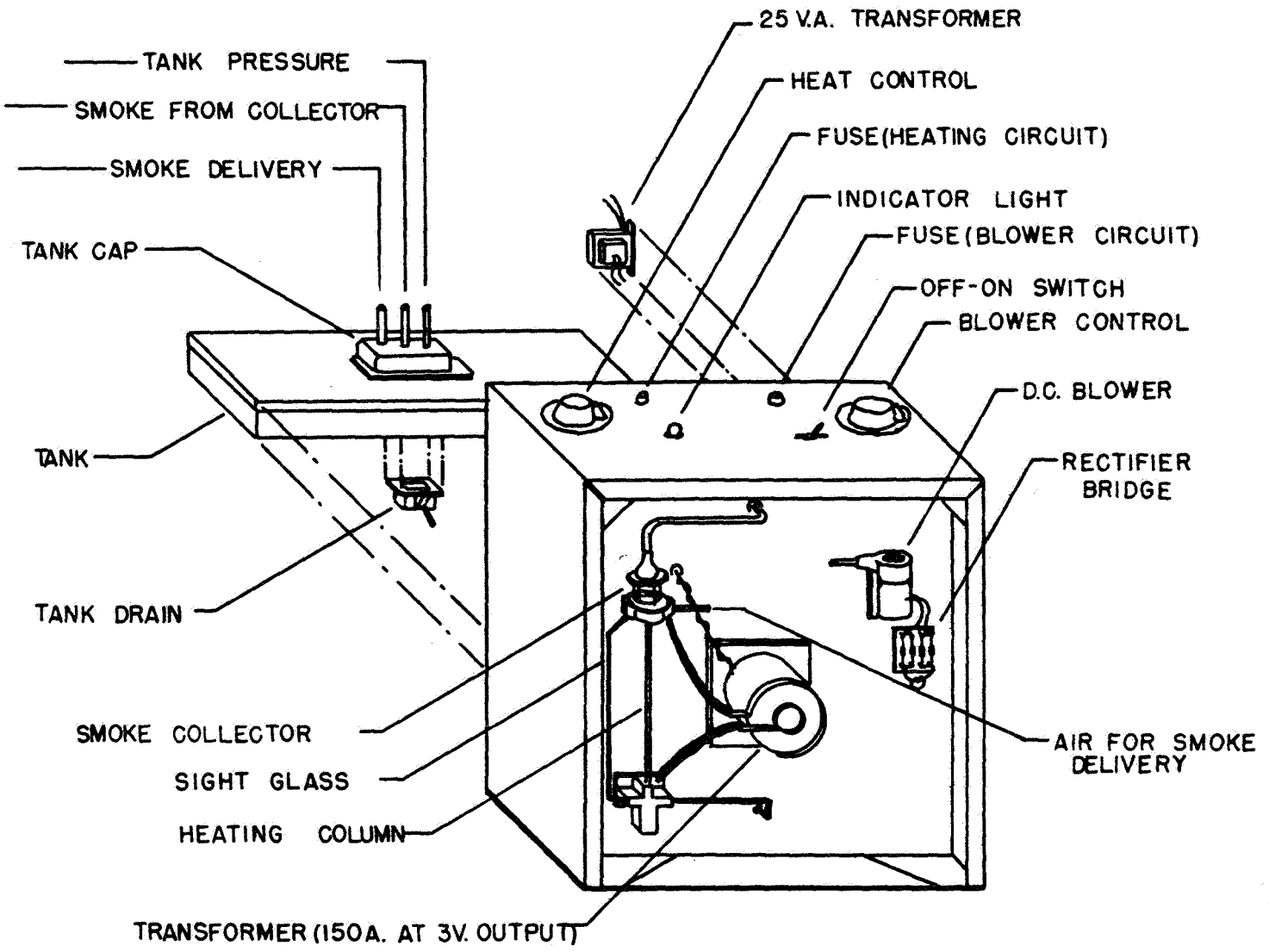

FIGURE 3.5 - Smoke generator

to be maintained on the kerosene storage tank to insure sufficient Kerosene in the heating column. Figure 3.6 presents a schematic diagram of the experimental setup used in the jet path studies.

4. Photographic Equipment

All photographs were taken using a Polaroid MP-3 Land camera with a 127mm focal length lens. The use of Type 55 P/N Polaroid Land film provided on-the-spot positive pictures along with negatives for future quantitative use.

The test section was illuminated by two 650-watt motion picture lights. The interior of the test section was painted glossy black in order to obtain sufficient contrast between the smoke and its background.

5. Measuring and Recording Devices

The primary pressure indicator was a Datametrics, Inc., Type 1012 Barocel electronic manometer with a Type 511-12 pressure transducer. This system was capable of measuring pressure differences as small as one one-hundredth of a millimeter of mercury.

During the free-jet studies, pressures were recorded on a Sanborn Model 322 Dual Channel D. C. Recorder. The test section pressure was indicated by a United Sensor Corp. inclined water manometer which was accurate to within two-thousandths of an inch of water.

The uncertainties of measuring static pressures in free jets required that all dynamic pressure measurements be made using the

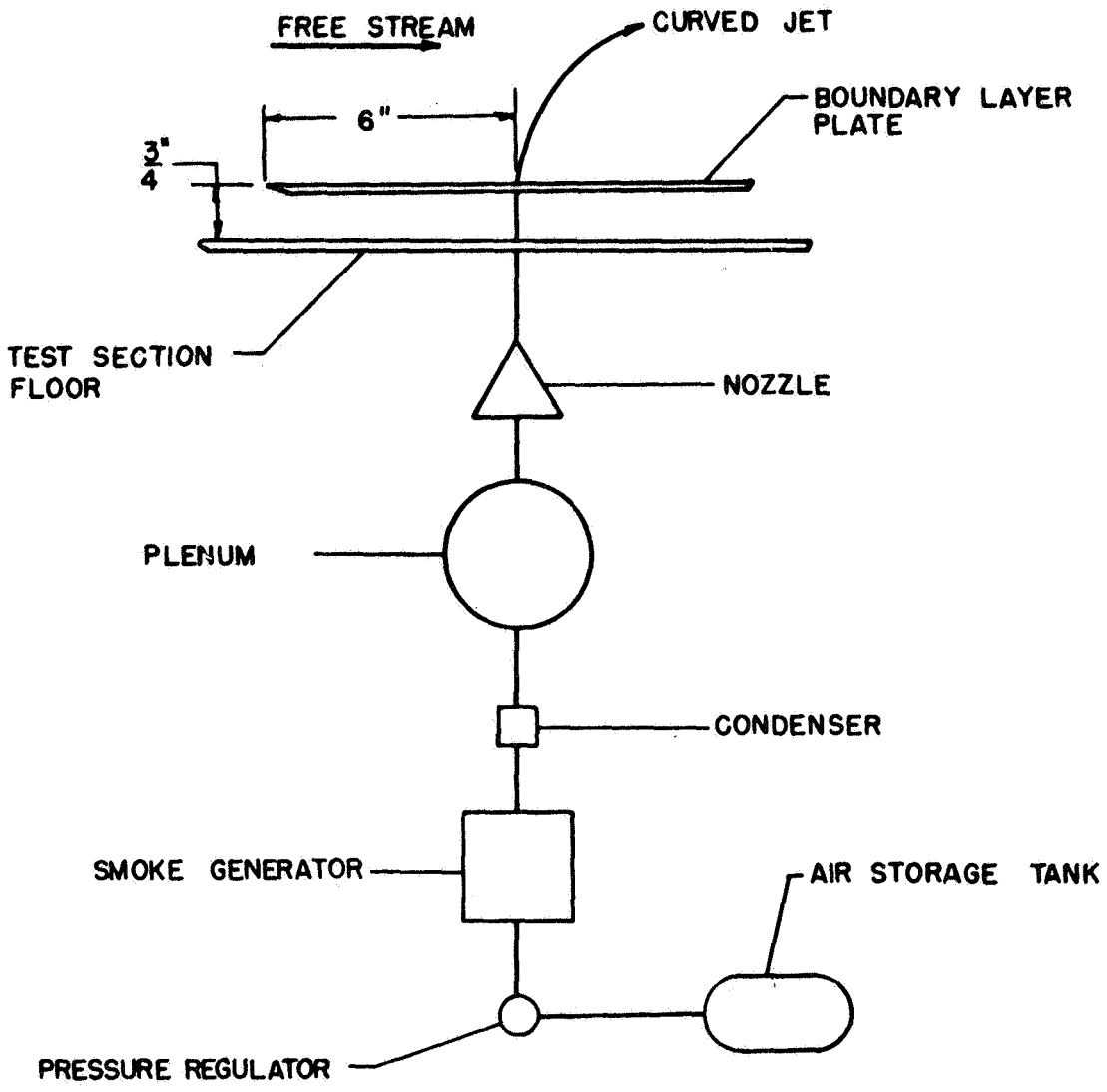

FIGURE 3.6 - Schematic diagram

differential pressure between the jet total pressure and ambient room pressure.[5] The total pressure in the jet was measured using a Kiel tube.

The photographic plates (negatives) were analyzed using a micro-densitomer. This instrument is basically a constant intensity point light source which is passed through the plate and focused on a sensitive photometer or photo cell. The photometer's output is a voltage which is proportional to the intensity of the light reaching it. This instrument is thus capable of determining the optical density of the grain on the plate. The plates were traversed across the instrument's source beam and thus the density distribution of the grain on the plate was measured. The densitometer also recorded the density distribution, thereby providing a permanent record. Using the densitometer it was possible to determine the locus of points of maximum smoke density (minimum light intensity) along the jet to a precision of five thousandths of an inch.

E. VALIDITY OF RESULTS

Using the measuring devices described above it was possible to determine pressures to within 1% accuracy except in regions near ambient pressures, when errors increased to as much as 5%. At near ambient pressures, large pulsations in pressure were observed

---

[5] Static pressures in free jets have been found to differ only slightly from the ambient pressure [17].

which have been attributed to turbulent fluctuations. In all those cases not near ambient pressures, the optimum range of the electric monometer was chosen to give the most accurate readings (in general, to 1% accuracy). Care was taken to calibrate all pressure indicating and recording devices before each test. All tests were found to be repeatable within the precision of the measuring devices.

The micro-densitometer was not used to give absolute quantitative information concerning the smoke density in the jet. Instead it was employed merely to indicate the position of the maximum smoke density. To this end it is quite accurate. Estimated uncertainty in the data obtained from this device is 1%. It must be noted, however, that inspite of this excellent instrument sensitivity, another uncertainty arises from the criterion for selecting the jet centerline location. It was decided to interpret the points of maximum smoke density as representing the location of the centerline. There is no method for placing a quantitative value on this uncertainty until detailed pressure measurements have been made within the jet slipstream. Until such measurements are made, all that can be stated quantitatively is that the data describing the jet paths herein are consistent with each other to within 1%.

F. RESULTS AND DISCUSSION

1. Free-Jet Studies

The coordinate systems utilized in the free-jet studies are shown in Figure 3.7. Figure 3.8 shows the centerline velocity decay curves

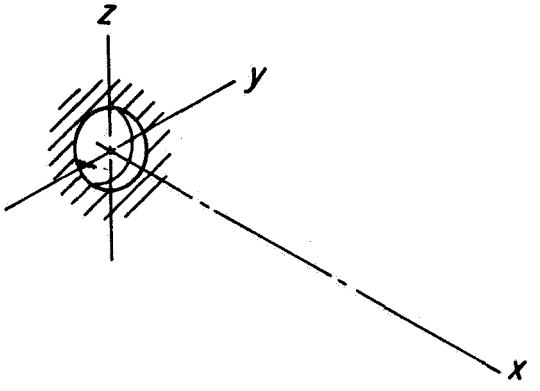

(a) Circular nozzle

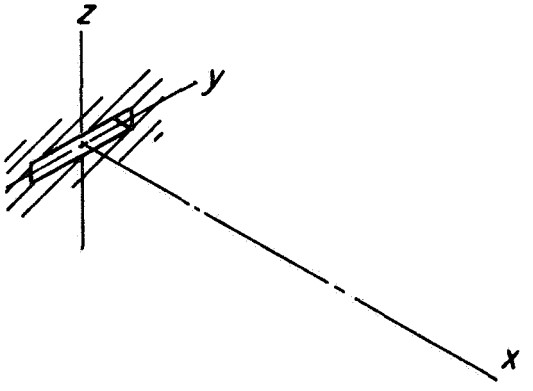

(b) Rectangular nozzle

FIGURE 3.7 - Free jet coordinate system

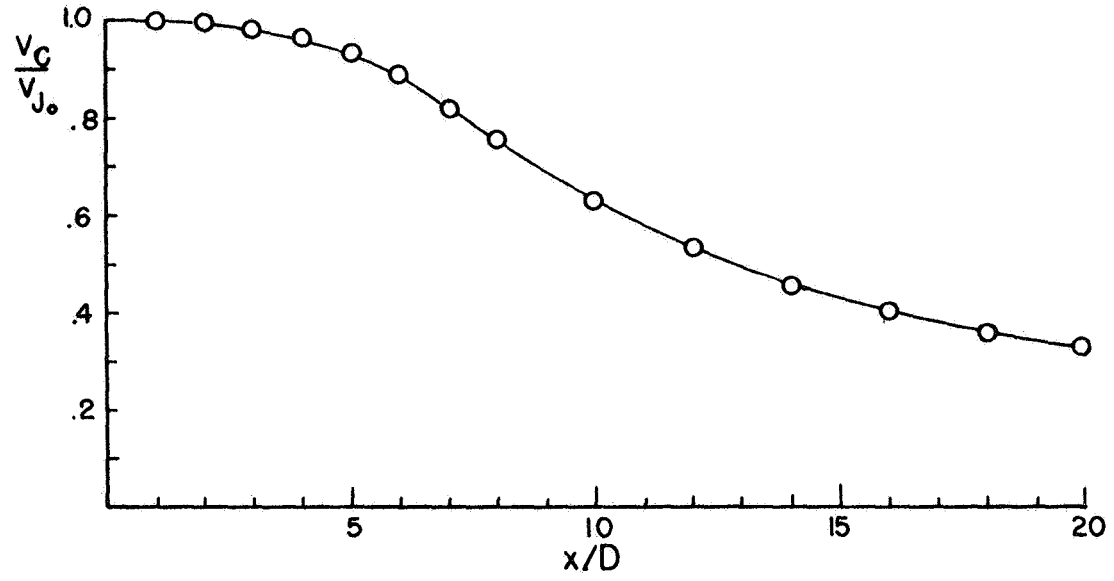

(a) Circular nozzle

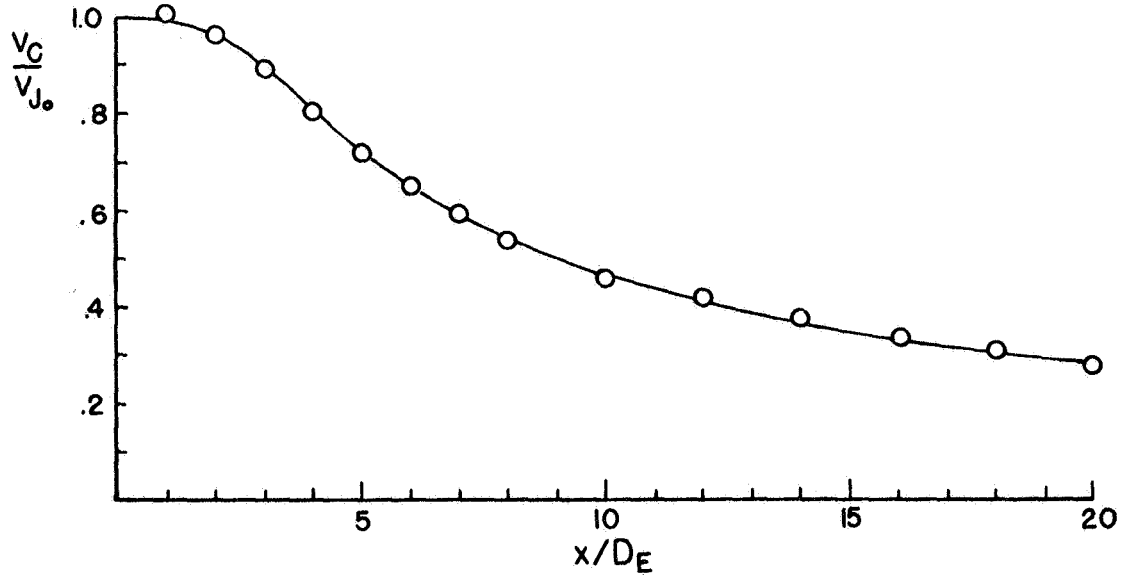

(b) Rectangular slot nozzle

FIGURE 3.8 - Measured centerline velocities

obtained for both nozzles. The effect of initial jet velocity, v_{j_o}, on the centerline velocity was seen to give a slightly more rapid decay at the lower velocities. At the higher velocities, a change in v_{j_o} has less effect. Since most jet-crosswind studies were made with high values of v_{j_o}, it was decided that the centerline velocity decay could be represented by one curve with the same overall characteristics for the entire velocity range. Comparison of the decay curves for the two jets shows that the rectangular nozzle has a decay notably earliest and slightly faster than the circular one. This result is consistent with Higgen's and Wainwright's [8] observations.

Figure 3.9 shows the spreading characteristics of the two jets. D and D_E are both one-quarter of an inch (D_E is the equivalent diameter of a circle having the same orifice area as the slot). It is interesting to note that the rectangular nozzle spreads much faster than the circular nozzle and that the spreading in the z-direction occurs faster than in the y-direction; i.e., spreading is not uniform in all directions. From these curves one may conclude that the mixing processes of the two nozzles are quite different. In the case of the slot nozzle the mixing causes an early degradation of the centerline velocity.

Figure 3.10 shows the velocity profiles of the jets at several axial stations. Note that after six diameters downstream, the circular nozzle profiles exhibit a close similarity to one another. This was

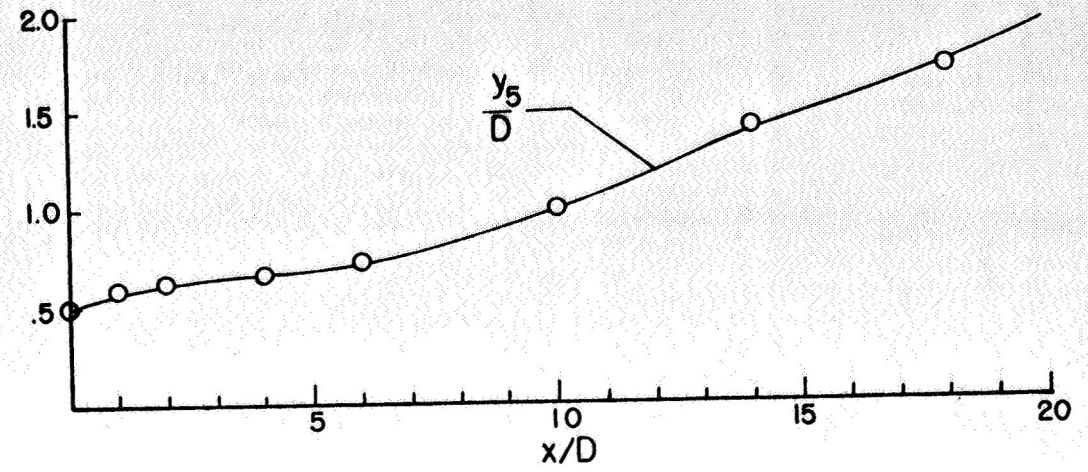

(a) Circular nozzle

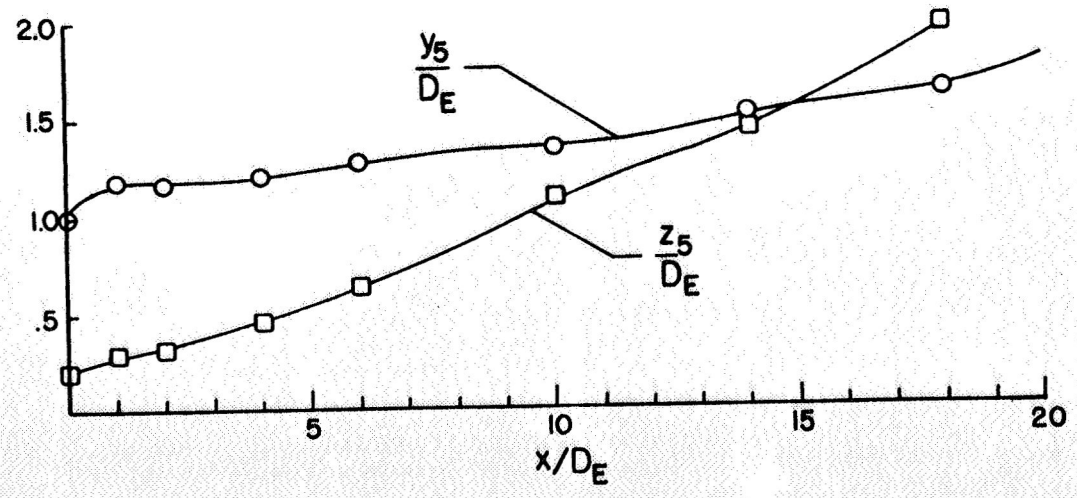

(b) Rectangular slot nozzle

FIGURE 3.9 - Jet spreading characteristics

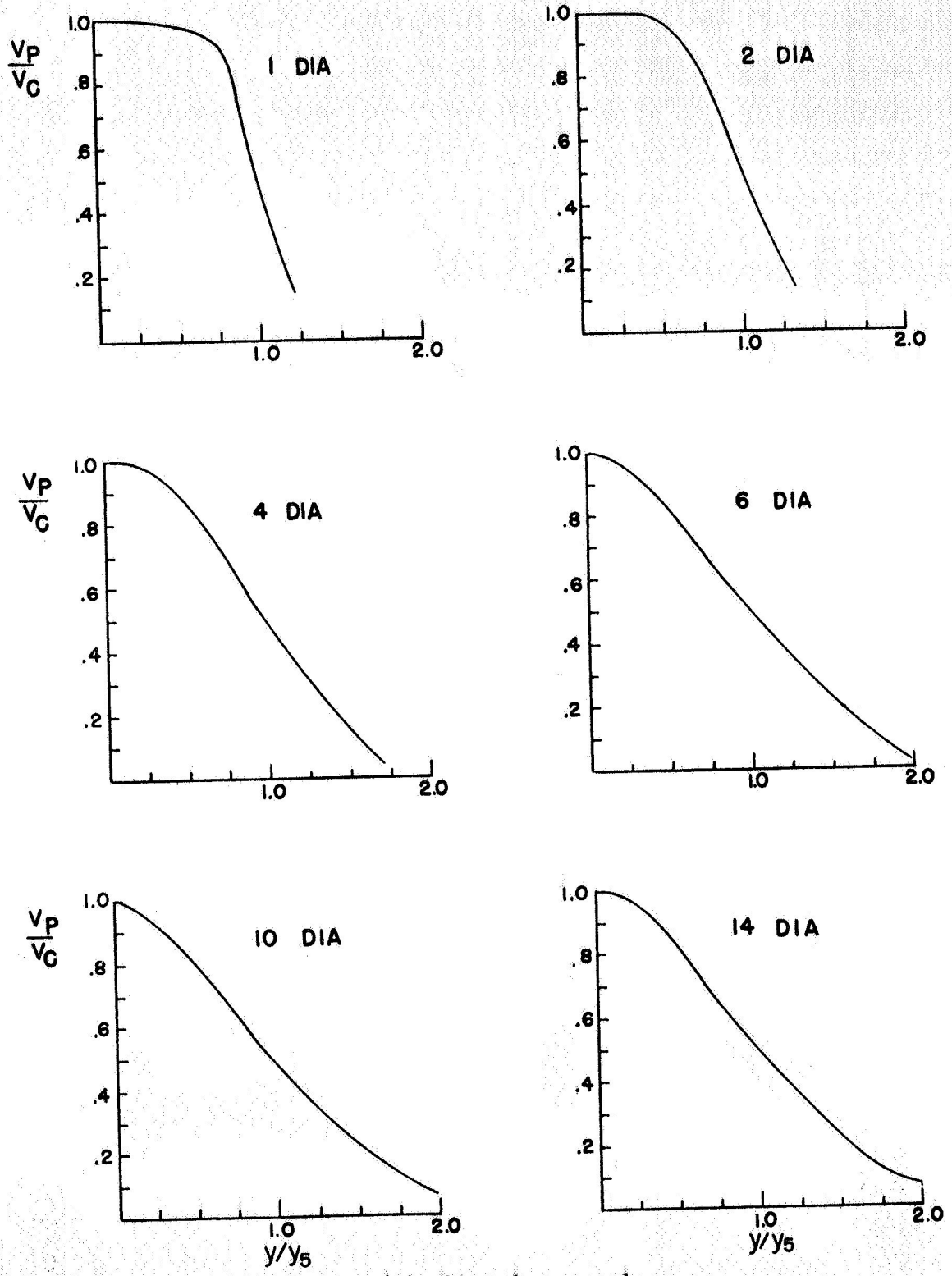

(a) Circular nozzle

FIGURE 3.10 - Jet profiles

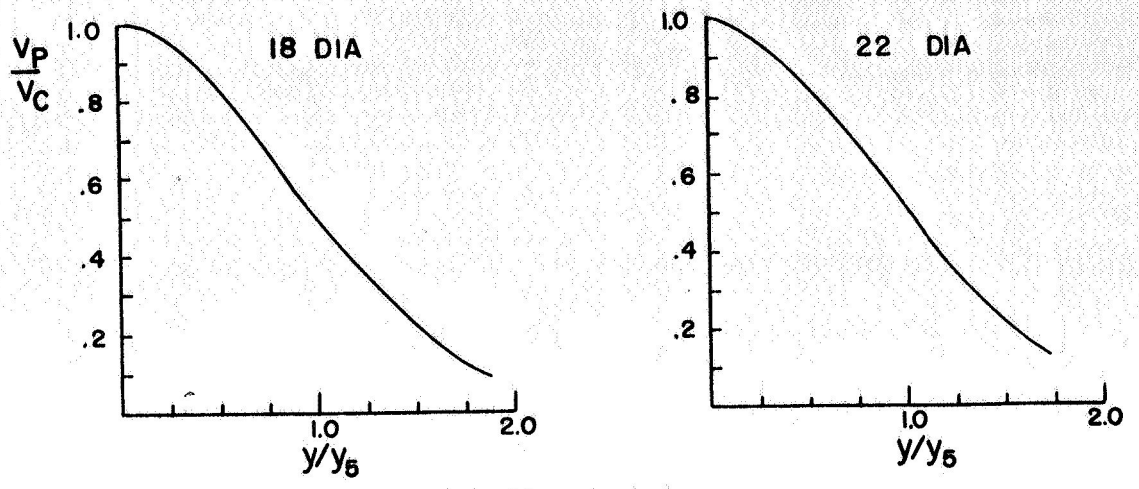

(a) Concluded

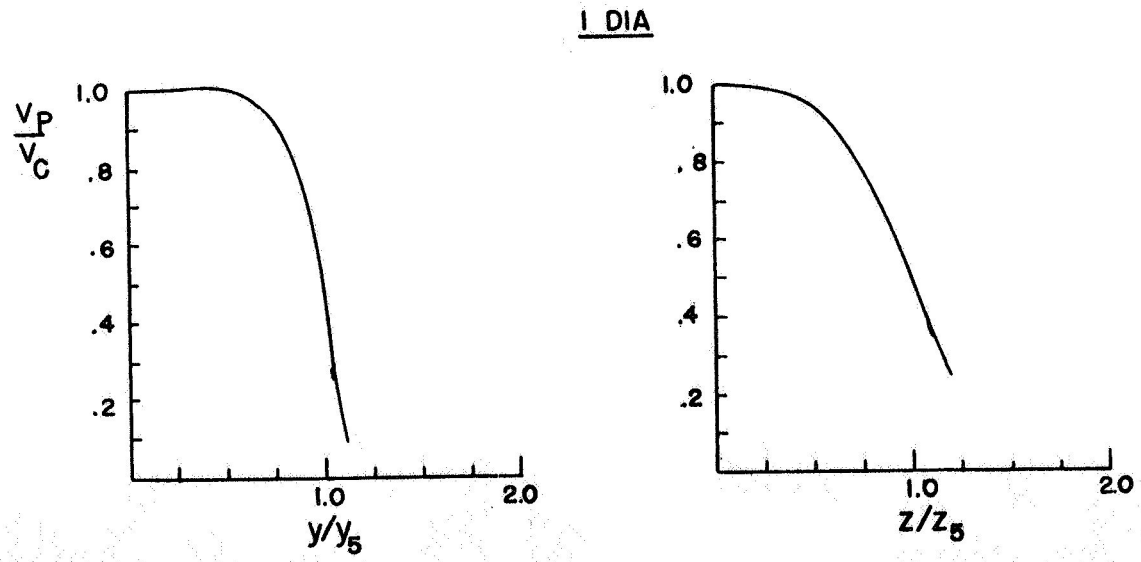

(b) Rectangular slot nozzle

FIGURE 3.10 - Continued

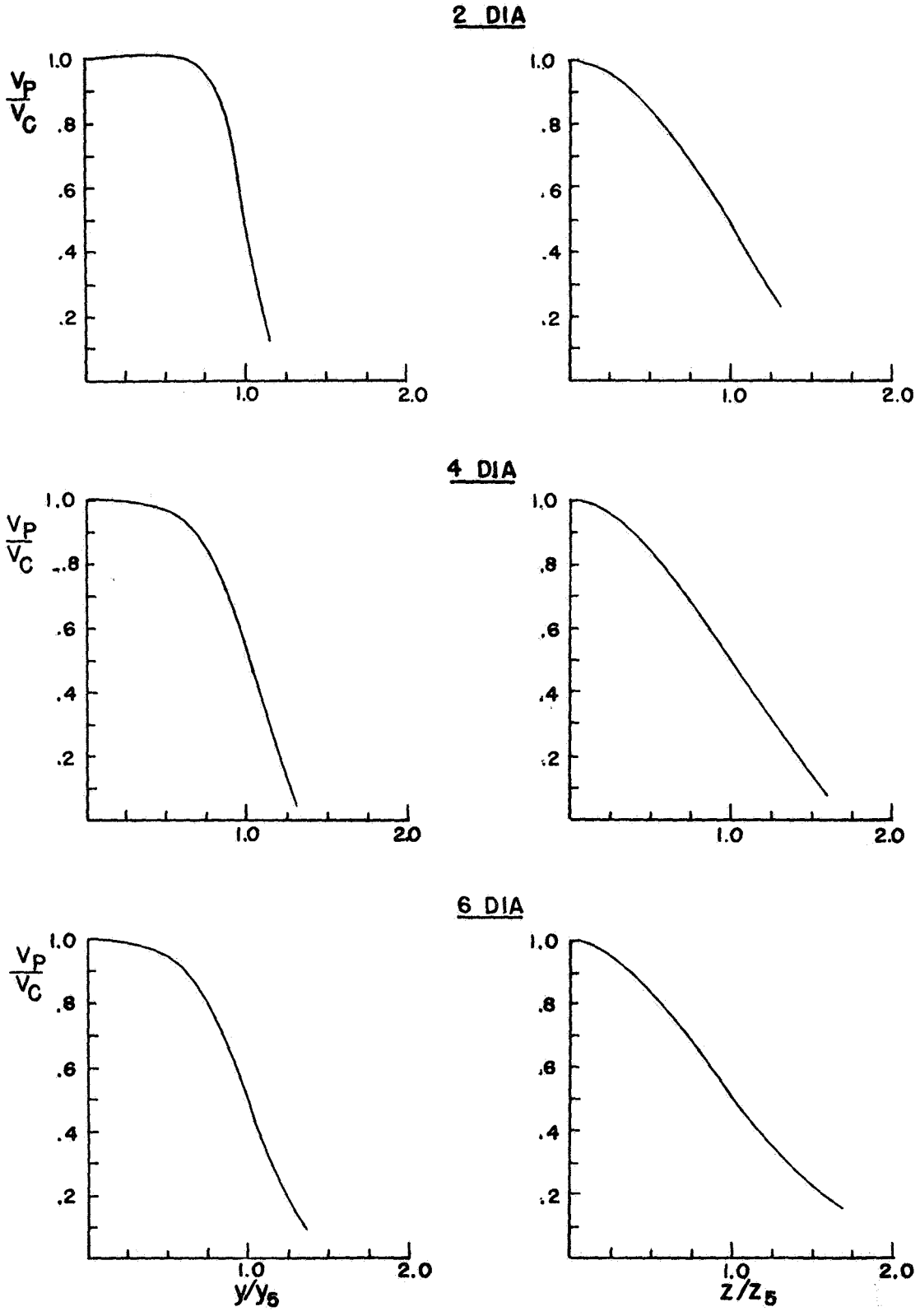

FIGURE 3.10b - Continued

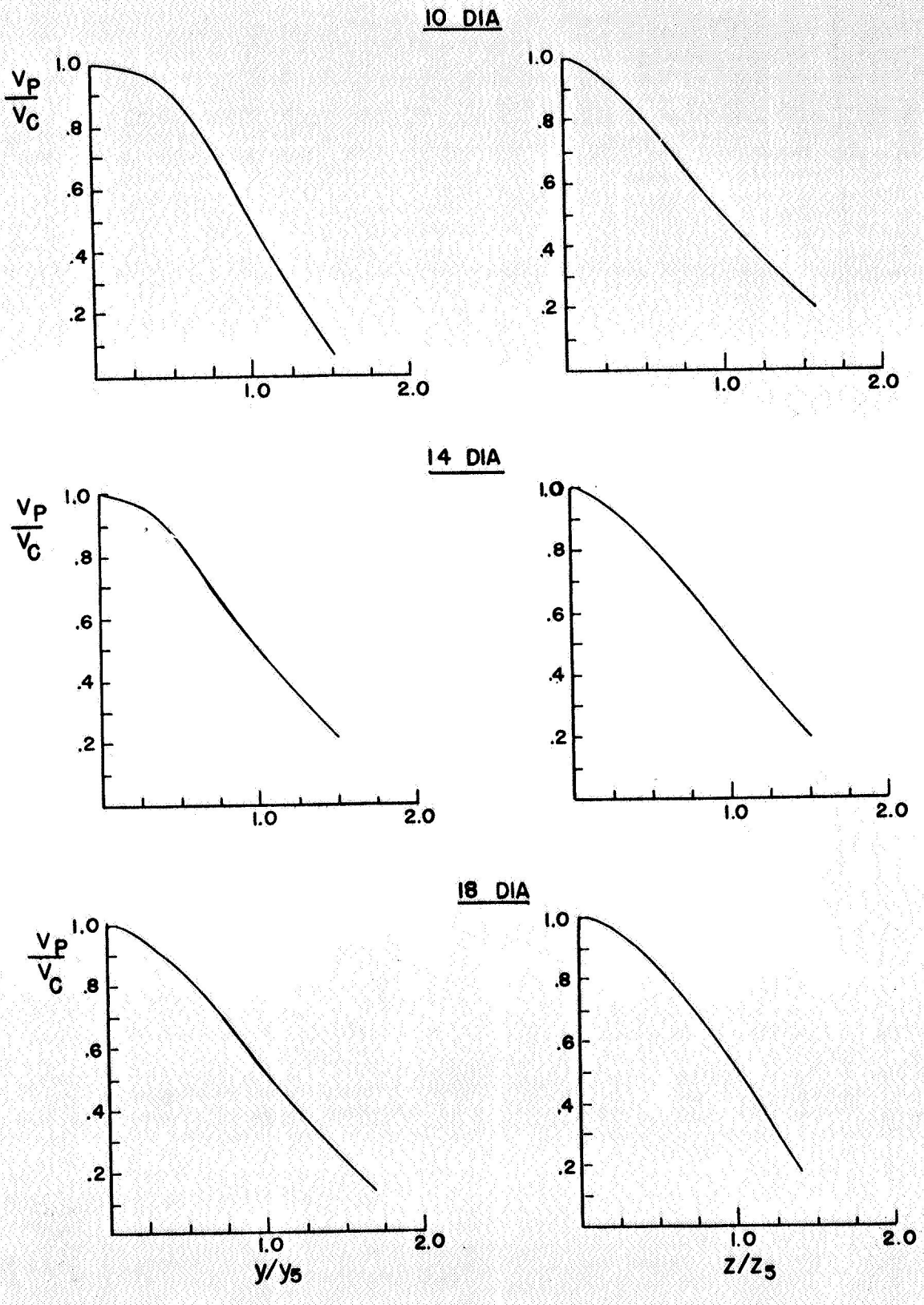

FIGURE 3.10b - Concluded

observed by Warren [17] as characteristic of axisymmetric jets. The slot nozzle, however, does not behave in this manner. This may be related to the three-dimensionality of the mixing process represented in Fugure 3.8b.

Non-axisymmetric jets decay in two stages after the core: a characteristic decay followed by an axisymmetric decay. The spreading of the slot-jet in the z-direction reaches an axisymmetric state (i.e., spreading at the rate of an axisymmetric jet) three to four diameters downstream from the orifice; whereas in the y-direction, the spreading does not reach an axisymmetric state until sixteen diameters. These results are reflected in the profiles. The z-profiles are similar to each other after only four diameters. The y-profiles do not become similar until after sixteen diameters. These profiles are also similar to the downstream developed profiles of the axisymmetric jet. Thus the three-dimensional mixing process tends to transform the asymmetric jet into an axisymmetric state.

The so-called equivalent jet described in the mathematical model of Chapter II was constructed for the circular nozzle by finding the momentum factor, f, through graphical methods. [The momentum factor was also calculated using the equations in Section II.D.3; however, it was felt that the graphical methods, e.g., use of a planimeter to find the area under the $(v_p/v_c)^2$ vs. $(y/y_5)^2$ curve, provided a better treatment of the data.] The characteristics of the equivalent jet are shown in Figure 3.11.

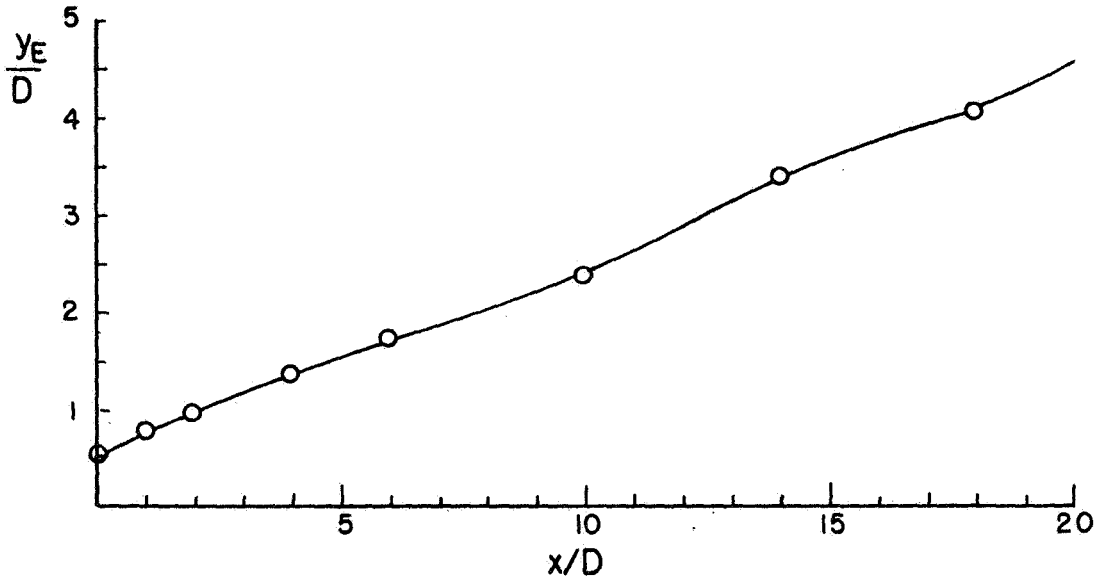

(a) Equivalent jet width

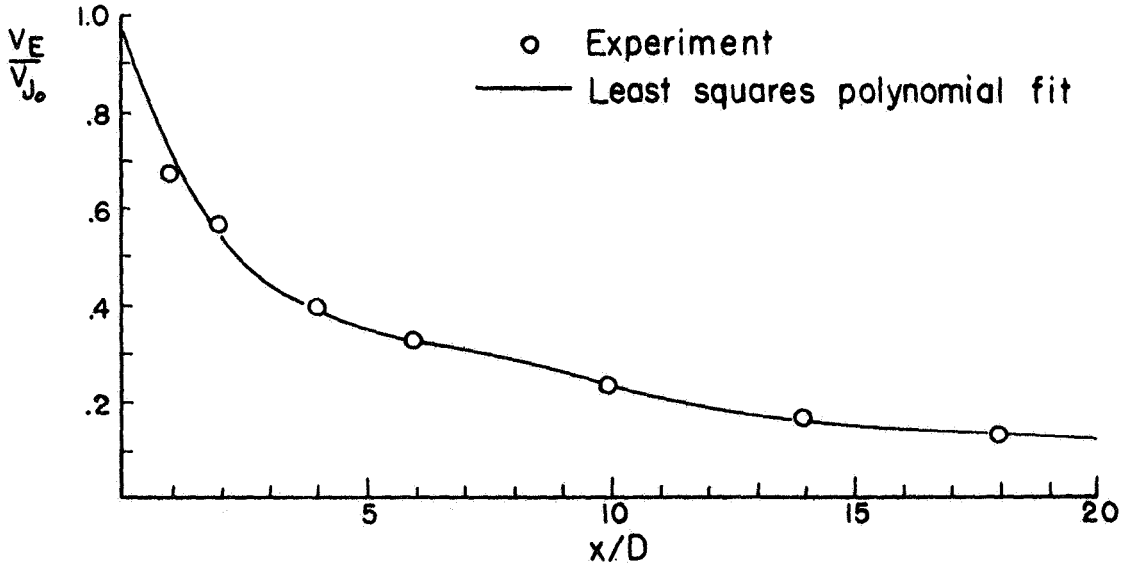

(b) Equivalent velocity decay

FIGURE 3.11 - Circular nozzle equivalent jet

2. Jet-Cross-wind Studies

Recalling the conclusions of Chapter II, it has been noted that the free-jet centerline velocity decay and geometry(i. e., the manner in which the jet spreads) are the primary considerations for determining the path of a jet in a cross-wind. The experimental studies of the jet support this conclusion. Figure 3. 12 shows the results of these studies. The slotted jet, characterized by early decay and rapid spreading, penetrates a lesser distance than does the circular jet at corresponding initial jet-to-free-stream velocity ratios.

A change in the velocity ratio, however, has the same effect on both jets. Increasing the initial jet velocity increases the jet's penetration into the free stream. This was predicted by Kirkpatrick and has been verified in previous studies.[6]

Of further interest is the ability of the mathematical analysis in Chapter II to predict the jet path. Introducing the equivalent jet corresponding to the circular nozzle into the analysis, the paths for this jet were calculated. The calculated paths are shown in Figure 3. 12a as dashed lines. The agreement between the calculated paths and those found from analysis of the photographic negatives at first glance may not appear very good, especially at the higher velocity ratios and near the orifice. However, the results must not be taken as discouraging. When the experimentally determined paths are compared to Kirkpatrick's paths (Figure 3. 13), it can be seen that the

[6] Section A of this Chapter

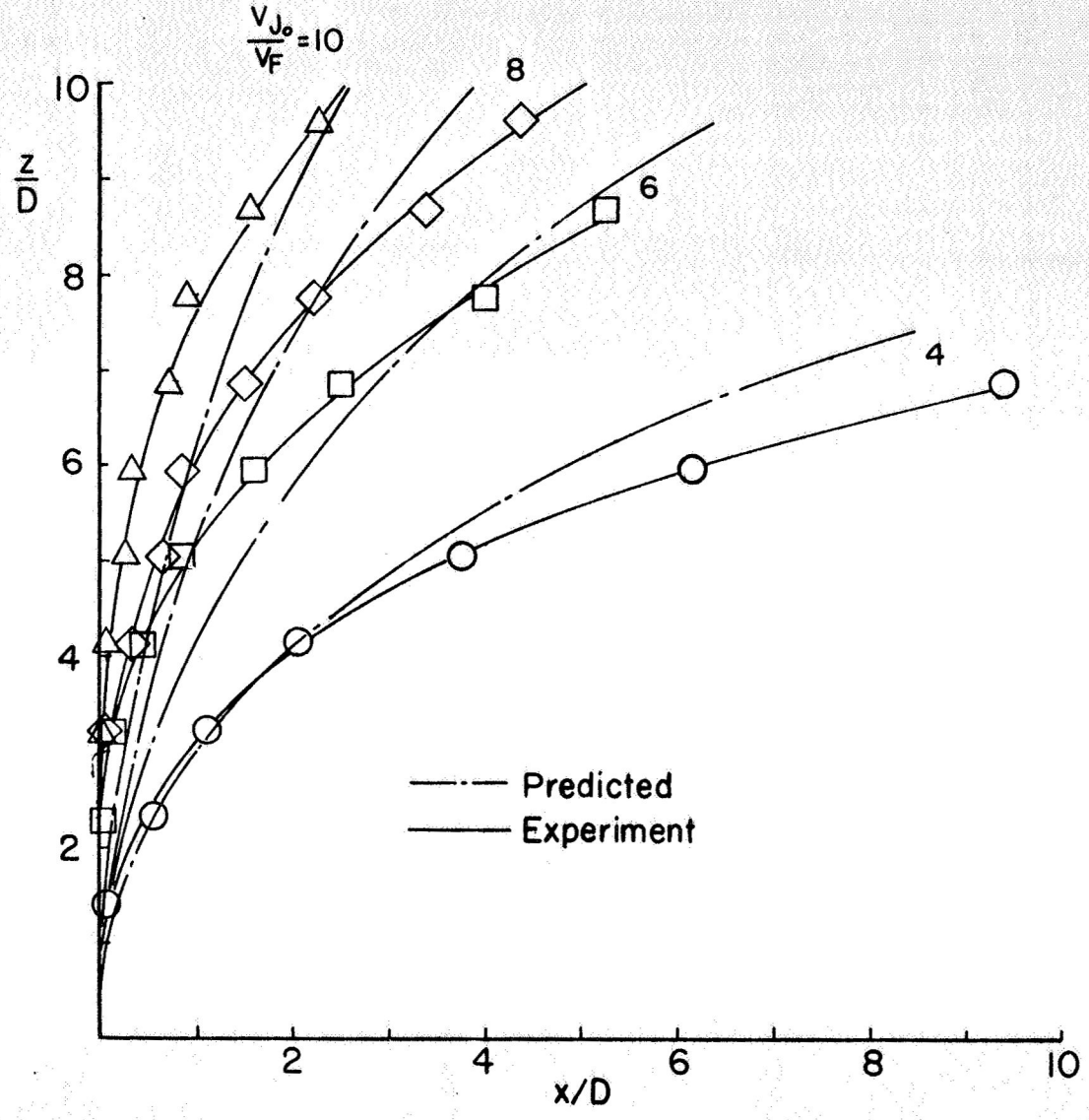

(a) Circular nozzle

FIGURE 3.12 - Jet paths

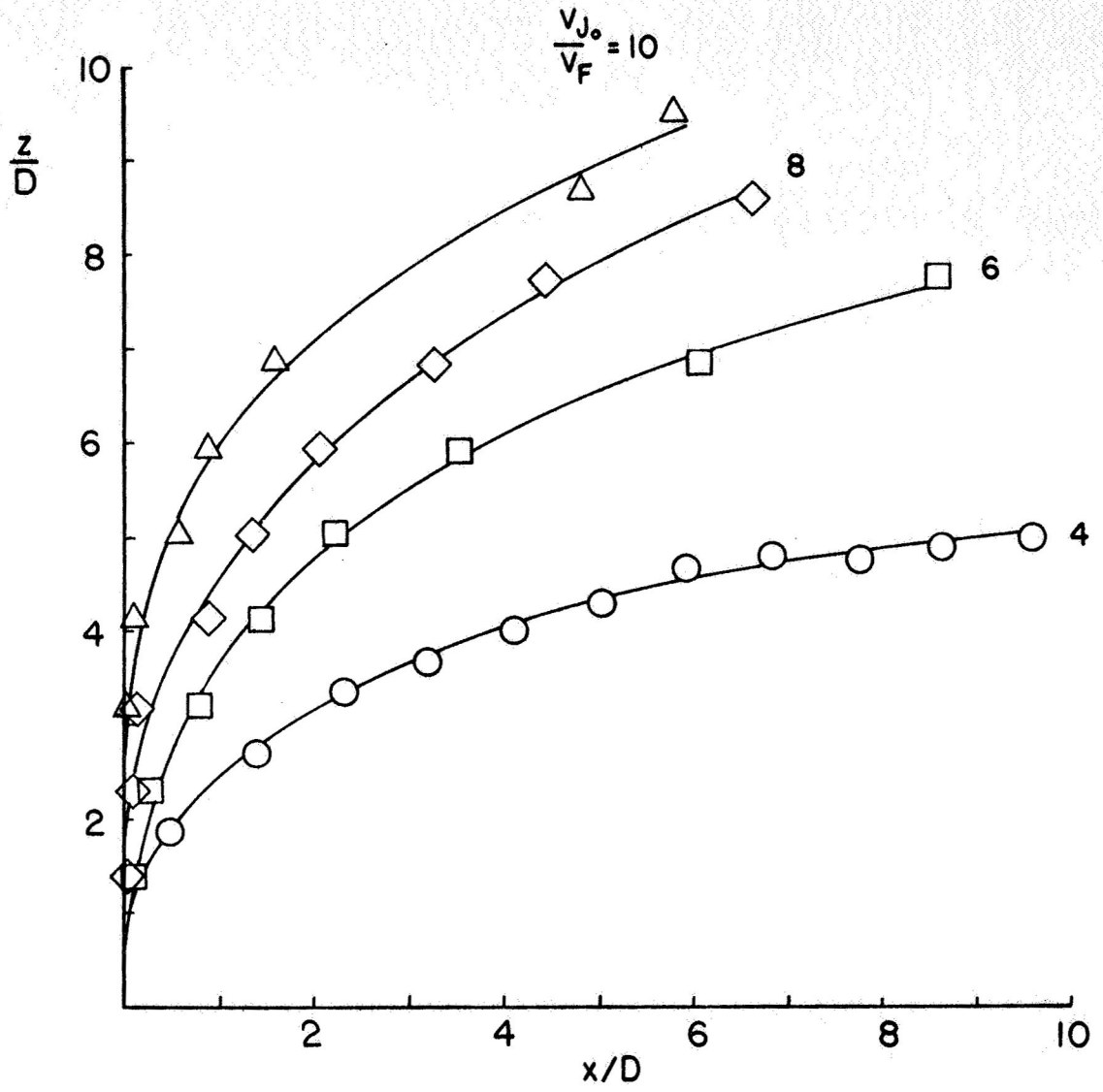

(b) Rectangular slot nozzle

FIGURE 3.12 - Concluded

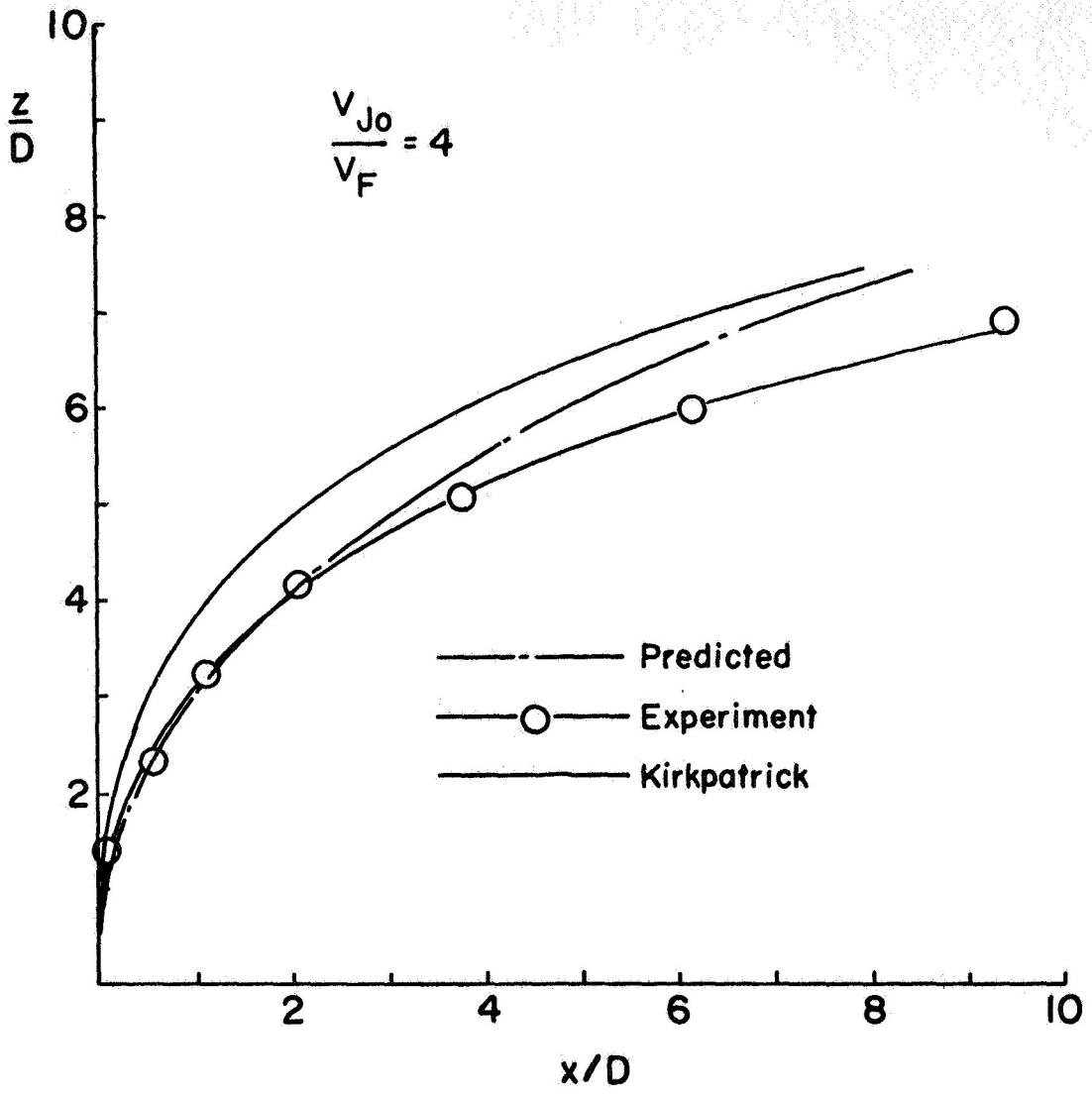

FIGURE 3.13 - Comparison of Kirkpatrick to experiment

revised analysis is far superior in predicting the path. Furthermore, there is no guarantee that the locus of maximum smoke density in the jet is the locus of the maximum velocity as was noted in the discussion of the validity of the results. Until velocity measurements are made within the jet itself, it cannot be concluded that the analysis is grossly in error.

In retrospect, the lack of agreement might be attributed to two factors not yet mentioned. First,in the analysis of the jet, no attempt was made to account for the presence of the boundary layer at the nozzle exit. Taking this factor into account would reduce the equivalent velocity at the orifice to some value less than unity. Secondly, the free jet investigations were conducted without the presence of a ground plate at the exit plane. Thus, mixing and spreading occurred sooner in the jet than if a ground plate had been used. Both of these factors influence the calculated jet paths. If accounted for in the calculations the effect would be to increase the penetration in the initial stages since the gradient of the equivalent jet velocity would be reduced. Also, as has been mentioned, the influence of the presence of the walls and ceiling of the tunnel on the jet curvature is not known and, therefore, cannot be introduced into the theoretical model or accounted for by means of corrections factors.

Figure 3.14 shows the jet as viewed from the top and side. These photographs are typical of the phenomena observed. A qualitative examination of the jet showed spreading behavior consistent

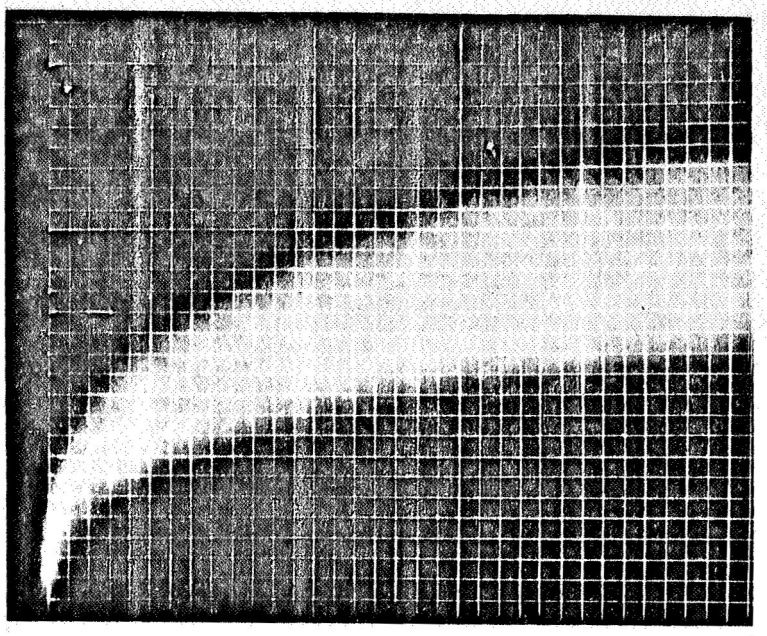

(a) Side view

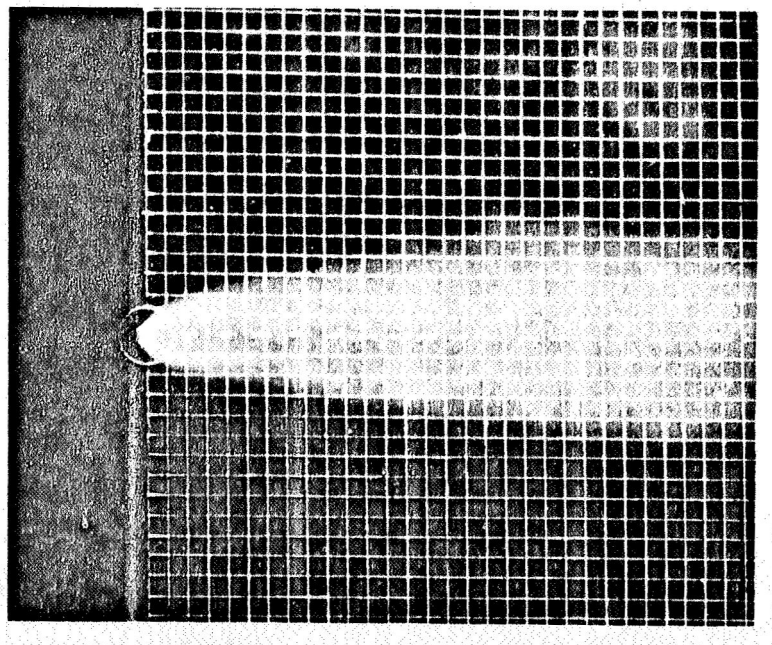

(b) Top view

FIGURE 3.14 - Typical slipstream for circular nozzle (initial jet velocity/free stream velocity = 8)

with Figure 2.8. The jet also exhibited the kidney-shaped cross-section; but this, unfortunately, could not be photographed during the scope of this investigation. A vortex sheet was also observed trailing from the jet's down stream edge. This sheet can be seen in the side view as an effective enlargement of the jet, but at reduced smoke density. The downstream edge of the jet made visible by the smoke is not the actual jet boundary but rather the lower edge of the trailing vortex sheet. The downstream jet boundary lies above this line near the leading edge of the jet slipstream.

CHAPTER IV

CONCLUSIONS & RECOMMENDATIONS

A simple, semi-empirical model of a three-dimensional, incompressible viscous jet issuing into a cross-wind has been developed. Examination of this mathematical model indicates that, for a particular initial jet to free stream velocity ratio, the primary influences on the penetration of the jet into the free stream are the centerline velocity decay and spreading characteristics of the free jet. Nozzles designed for downwash suppression (i.e., large degradations of dynamic pressure), therefore, would be expected to have less penetration than other nozzle configurations. The other primary influences on penetration are the velocity ratio and the initial inclination of the jet to the free stream. These, however, were discuss ed in detail by Kirkpatrick.

The experimental studies support the conclusions derived from the analysis. These studies also indicate the structure of the jet and present a guide to future analysis. It would seem that any future attempts to describe the jet theoretically should account for the vortex sheet by considering how such a vortex is generated through viscous action of the free-stream shearing on the jet boundary. Such an approach could lead to a better understanding of the mixing process and to an ability for predicting the spreading of the jet as well as its shape.

An experimental program should also be continued from the present one. Pressure measurements should be made within the test-section to check the results herein, to gain insight into the mechanisms which generate the vortex, and to investigate the effects of the walls on the slipstream. Free jet velocity decay measurements should also be made with a nozzle exit base plate. Swirl and compressibility effects should be examined, and the mixing process understood before the problem of predicting the jet characteristics can be considered in any sense solved.

The present study has offered just one approach to the analysis of non-parallel streams and has indicated the major influences on the jet penetration. Although restricted in scope, the analysis can be expanded quite easily to include compressibility, etc. The goals set forth in the Introduction have been attained. An improved understanding of the interaction of a jet in a cross-wind has been gained. It was pointed out that no single approach can include every type of situation that might arise; therefore the study of such problems should continue.

BIBLIOGRAPHY

1. Ackerberg, R. C. and Pal, A., "On the Interaction of a Two-Dimensional Jet with a Parallel Flow," Polytechnic Institute of Brooklyn Report 889, 1965.

2. Bradbury, L. J. S. and Wood, M. N., "The Static Pressure Distribution Around A Circular Jet Exhausting Normally from a Plane Wall into an Airstream," RAE Tech. Note Aero. 2978, 1964.

3. Callaghan, E. E. and Ruggeri, R. S., "Investigation of the Penetration of an Air Jet Directed Perpendicularly to an Air Stream," NACA TN 1615, 1948.

4. Callaghan, E. E. and Ruggeri, R. S. "A General Correlation of Temperature Profiles Downstream of a Heated-Air Jet Directed Perpendicularly to an Air Stream," NACA TN 2466, 1951.

5. Ehrich, F. F., "Penetration and Deflection of Jets Oblique to a General Stream," Journal of the Aeronautical Sciences, February, 1953.

6. Heyson, H. H., "Linearized Theory of Wind-Tunnel Jet-Boundary Corrections and Ground Effect for VTOL-STOL Aircraft," NASA TR R-124, 1962.

7. Higgens, C. C., Kelly, D. P., and Wainwright, T. W., "Exhaust Jet Wake and Thrust Characteristics of Several Nozzles. Designed for VTOL Downwash Suppression," NASA CR-373, 1966.

8. Higgens, C. C. and Wainwright, T. W., "Dynamic Pressure and Thrust Characteristics of Cold Jets Discharging from Several Exhaust Nozzles Designed for VTOL Downwash Suppression," NASA TN D-2263, 1964.

9. Jordinson, R., "Flow in a Jet Directed Normal to the Wind," Aeronautical Research Council, R. & M. No. 3074, 1958.

10. Keffer, J. F. and Baines, W. D., "The Round Turbulent Jet in a Cross Wind," Journal of Fluid Mechanics, Vol. 15, No. 4, 1962.

11. Kirkpatrick, D. L. I., "Wind Tunnel Corrections for V/STOL Model Testing," Unpublished Thesis, University of Virginia, 1962.

12. Lee, C. C., "A Review of Research on the Interaction of a Jet with an External Stream," Department of Defense Center TN R-184, 1966.

13. Olcott, J. W., "A Survey of V/STOL Wind Tunnel Corrections and Test Techniques," Princeton University Department of Aerospace Engineering Report 725, 1965.

14. Ruggeri, R. S., Callaghan, E. E., and Bowden, D. T., "Penetration of Air Jets Issuing from Circular, Square, and Elliptical Orifices Directed Perpendicularly to an Air Stream," NACA TN 2019, 1950.

15. Sforza, P M., Steiger M. H., and Trentacoste, N., "Studies on Three-Dimensional Viscous Jets" AIAA Journal, Vol 4, No. 5, 1966.

16. Storm, K. R., "Low Speed Wind Tunnel Investigation of a Jet Directed Normal to the Wind," Unpublished Thesis, University of Washington, 1965.

17. Warren, W. R., "An Analytical and Experimental Study of Compressible Free Jets," Princeton University Department of Aeronautical Engineering Report No. 381, 1957.

DISTRIBUTION LIST

Copy No.	
1-10	Scientific and Technical Information Division Code US National Aeronautics and Space Administration Washington, D. C. 20546 Attention: Winnie M. Morgan
11	A. R. Kuhlthau
12	R. A. Lowry
13-14	University Library, Attention: Dr. R. Frantz
15-20	G. B. Matthews
21-25	RLES Files